UNIVERSITÀ
DEGLI STUDI
FIRENZE

DOTTORATO DI RICERCA IN SCIENZE CHIMICHE

CICLO XXVIII

COORDINATORE Prof. ANDREA GOTI

SYNTHESIS OF NEW POLYAMINE RECEPTORS AND THEIR METAL COMPLEXES AS FLUORESCENCE CHEMOSENSORS FOR ANIONS.

Settore Scientifico Disciplinare CHIM/03

Dottorando
Dott. Francesco Bartoli

_____
(firma)

Tutore
Prof. Andrea Bencini

_____
(firma)

Coordinatore
Prof. Andrea Goti

_____
(firma)

Anni 2012/2015

1 Introduction

The supramolecular chemistry studies the adducts formed by two or more molecules that interact with each other via non-covalent type bonds, in particular hydrogen bonds, electrostatic interactions, Van der Waals forces, π-stacking, hydrophobic effect. These adducts have chemical and physico-chemical properties of its own, which are different from those of the molecules that compose them. These adducts are normally stable and their formation is reversible, since the multiplicity of non-covalent interactions established between the molecules counterbalances their lower strength with respect to the intramolecular covalent bonds. The beginning of modern supramolecular chemistry is generally traced to the work of Pedersen[1], who reported a series of cyclic polyethers, synthesized from reaction of aromatic vicinal diols with dihaloalkanes in presence of two equivalent of sodium hydroxide

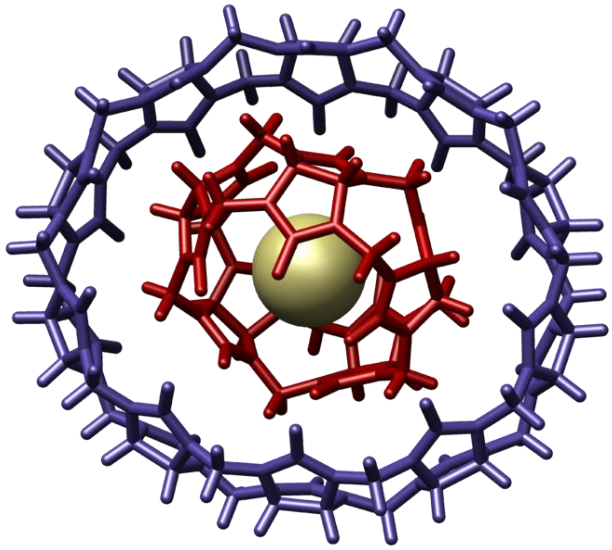

Figure 1.1 An example of supramolecular system. It features a chloride anion encapsulated in a cucurbit[5]Uril. The adduct is then further incorporated into a cucurbit[10]Uril. The complex was called a molecular 'gyroscope'. The host species is the chloride ion in the center.[2]

A supramolecular adduct is generally formed by two molecular species, the larger of which is called "receptor" (or "host"), while the smaller is called "substrate" (or "guest"). In order to obtain the formation of a stable adduct, the species should be

[1] Kenneth G. Caulton, Geoffrey Davies, Elizabeth M. Holt *Polyhedron*, **1990**, 9, 2319-2351.
[2] Anthony I. Day, Rodney J. Blanch, Alan P. Arnold, Susan Lorenzo, Gareth R. Lewis and Ian Dance, *Angew. Chem. Int.Edition,* **2002**, 41, 275-277

complementary from a structural point of view. In fact, the interactions that are formed in this case can lead to a selectivity of the recognition process.
Receptors can perform several functions:

- Substrate recognition;
- Substrate modification;
- Substrate transport: the receptor acts as a carrier and allows for substrate transfer through biological lipophilic membranes, in which it would not normally be soluble. This occurs normally in the case of receptor with lipophilic character.

1.1 Molecular recognition

Molecular recognition consists in the selective coordination of a particular chemical species in the presence of other species. This is generally due to the ability of the recognized species, the substrate, to form a large number of weak interactions.
The receptor should have two basic requirements to selectively coordinate a substrate:

- *Stereochemical complementarity of the coordination sites*: the receptor binding sites should have a spatial arrangement corresponding to the substrate binding sites, in order to achieve as large number of non-covalent interactions as possible and ensure the stability of the supramolecular adduct (called, in this case, "lock and key system").

- *Ligand pre-organization*: if a receptor already possesses, before the coordination process, a structural conformation similar to that assumed in the adduct, the energy required to achieve the final receptor conformation will be lower, the adduct formation will be faster, and the species formed more thermodynamically stable.

It is therefore necessary that the receptor has a contact surface with the substrate as high as possible, or should be able to "wrap" it, giving rise to numerous non-covalent interactions. In general the receptor should have a specific size, shape and architecture. A high degree of pre-arrangement of both receptor and substrate enhances the selectivity of the molecular recognition process.
The substrate types may be cationic (metal ions, systems containing ammonium groups), anionic (inorganic and organic anions) or neutral molecules.

1.1.1 Interactions between molecules in supramolecular adducts

The interactions established between the molecules forming a supramolecular adduct consist of a large number of weak bonds, whose overall strength is comparable to that of a covalent bond. The major difference resides in the energy required to break a single weak bond is greatly reduced compared to that required to

break a covalent bond. This necessarily implies that the supramolecular adduct possesses a geometric structure less rigid than that of the single molecule. This factor is responsible for the above cited reversibility observed for the formation of supramolecular adducts.
We will now give a short overview of the different types of interactions occurring between the species that form a supramolecular adduct.

1.1.1.1 Electrostatic interactions

Electrostatic interactions have major importance than the other weak forces, as they produce more stable contacts in host-guest adducts.
We can analyze this interaction approximating the charges to adimensional points. This model predicts that the interaction takes place along the line joining the charges, according to Coulomb's law:

$$F = k\frac{Q_1 Q_2}{r^2}$$

where Q_1 and Q_2 are the interacting point-like charges, r is the distance between them and k is Coulomb's constant, which in vacuum is approximately equal to $9 \cdot 10^9$ Nm^2C^{-2}. It is linked to the dielectric constant ε of the medium separating the interacting charges according to the relation:

$$k = \frac{1}{4\pi\varepsilon}$$

The role of dielectric constant is extremely relevant in the analysis of electrostatic interaction. A high dielectric constant corresponds to a polar environment, such as, for instance, water, and leads to a reduced electrostatic interaction. Conversely, a low dielectric constant corresponds to a non-polar or nearly non-polar environment, as occurs in a protein matrix, and has an amplifying effect on electrostatic interactions.

1.1.1.2 Hydrogen bond

The hydrogen bond interaction is a directional electrostatic interaction, in which the negative pole is constituted by an electronegative atom (e.g. fluorine, oxygen, nitrogen) and the positive pole is a hydrogen atom bound to an electronegative atom. Electronegative atoms (X, Y) feature a negative partial charge δ-, thus inducing a partial positive charge δ+ on the covalently bound hydrogen. A hydrogen bond between a species X-H and a species Y is represented as follows:

$$X^{\delta-} - H^{\delta+} \cdots Y^{\delta-}$$

Depending on the HX acidity and Y basicity, a partial or total transfer of the proton can occur. In the case of partial transfer, the interaction feature a proton shared between the X and Y atoms. However, when the Y species is more basic than X^-,

the proton transfer is complete and there is therefore the formation of the X^- and HY^+ species, interacting with each other through an ion pair formation.

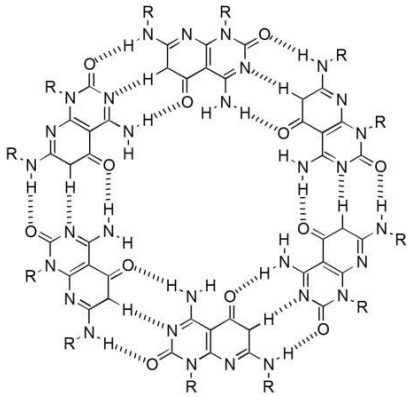

Figure 1.2 Structural representation of the cyclic hexamers assembled via hydrogen bonding.

The hydrogen bond strengths can be evaluated through the values enthalpy of binding.[3,4] Table 1.1 reports the binding enthalpy in the vapor phase.

Bond	Enthalpy energy (kJ/mol)
F – H ··· F	161.5
O – H ··· N	29
O – H ··· O	21
HO – H ··· OH	18
N – H ··· N	13
N – H ··· O	8

Table 1.1 Enthalpy of binding of some characteristics hydrogen bonds.

The hydrogen bond length depends on the bond strength, the temperature and the pressure. In turn, the bond strength also depends on the angle bond and the dielectric constant of the medium in which the interaction takes place. The typical hydrogen bond length in water is 1.97 Å. The ideal bond angle depends on the donor atom nature. The experimentally determined values of angles bond for the hydrogen bonds between the hydrogen fluoride and various substrates are reported in Table 1.2.

[3] J. W. Larson, T. B. McMahon, *Inorg. Chem.*, 23, 1984, 2029-2033.
[4] J. Emsley, *Chem. Soc. Rev.* 9, 1980, 91-124.

Bound	Geometry VSEPR	Bond angle (°)
HCN··· F	Linear	180
H_2CO··· F	Trigonal planar	110
H_2O··· F	Pyramidal	46
H_2S ··· F	Pyramidal	89
SO_2··· F	Trigonal	142

Table 1.2 Geometry and bond angles of some hydrogen bonds.

In the development of synthetic receptors, the hydrogen bonds directionality must be taken into account, in order to obtain an interaction as highest as possible between the receptor and the substrate. This allows to maximize the interactions energy and thus to achieve a better substrate complexation by the receptor.

1.1.1.3 Van der Waals interactions

They are produced by various types interactions:

- Dipole - dipole;
- Dipole - induced dipole (also called "London dispersion forces");
- Induced dipole - induced dipole.

The strength of these interactions depends on the dipole moments in the case of polar molecules, or by the polarizability in the case of apolar molecules. In any case, it decreases very quickly with distance and more quickly compared to the interaction between charged species. The interactions between the induced dipoles can be mathematically described by using the Lennard-Jones potential, expressed as follows:

$$U = \frac{A}{r^{12}} - \frac{B}{r^{6}}$$

The first term represents the repulsive contribution, while the second attractive one. The increase of polarizability of the interacting molecules enhances the bond energy.

1.1.1.4 Hydrophobic effect

This effect is the result of two contributions:

- *Enthalpy contribution:* the attractive Van der Waals interactions between non-polar solute and polar solvent are less intense than those between the molecules in the solvent mass phase, with a consequent enthalpy gain.
- *Entropic contribution:* the interaction between the two molecules, which occur between their surfaces implies desolvation, enhancing the overall entropy of the system.

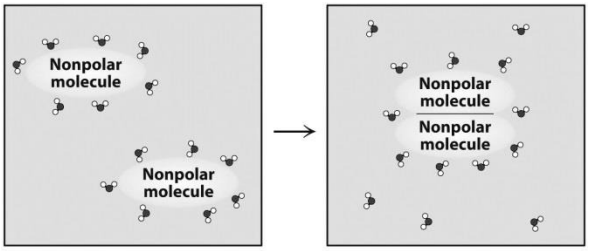

Figure 1.3 Aggregation via hydrophobic effect

1.1.1.5 π-stacking interactions

These interactions occur in the case of receptor and substrates containing aromatic rings in their structure. The interaction takes place between molecular orbitals of an electrons poor π system such as, for example, an aromatic ring substituted with an electron withdrawing group, and those of a π electron-rich species, such as an aromatic ring substituted with an electron donor group. The formed adduct is generally called "π complex". When the interaction induces a real charge transfer from the electron-rich system to the electrons poor one, the adduct is generally named "charge transfer complex".

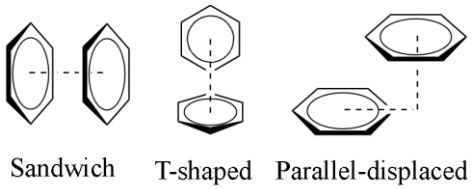

Figure 1.4 π-stacking interaction

1.1.2 Macrocyclic ligands

A macrocyclic ligand is a polidentate cyclic molecule that possesses a cavity containing at least three donor atoms that can function as binding sites for the substrate. Macrocyclic ligands can be efficient receptors for both anionic and cationic substrates.

The first systems of this type which were discovered and studied were "crown ethers". These ligands are cyclic compounds which contain ether groups, in which the oxygen atoms can behave as donors. The most common crown ethers are ethylene oxide oligomers, in which the $-CH_2CH_2O-$ group is the recurring unit. They are named by using two numbers: the first corresponds to the atoms number forming the cycle, while the second indicates the number of oxygen atoms. In the crown ether cycle other groups may also be present, such as, for example, aromatic rings. Figure 1.5 shows some structures among the most famous crown ethers.

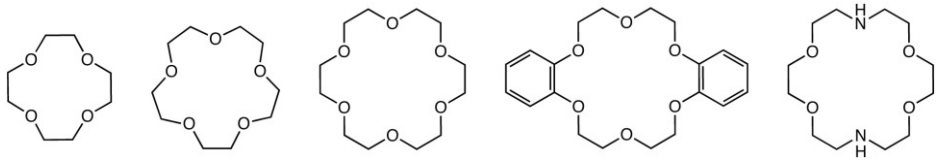

Figure 1.5 Structure of the most common crown ethers. Order: *12-crown-4, 15-crown-5, 18-crown-6, dibenzo-18-crown-6, diaza-18-crown-6.*

The crown ethers are good cationic receptors. In particular, they show a marked affinity for alkali and alkaline-earth metals cations. The affinity is strongly influenced by the size of their cavities. In fact, the 18-crown-6 strongly bound to the larger K^+ ion, while 15-crown-5 and 12-crown-4 show a greater affinity for Na^+ and Li^+, respectively.

Another famous class of macrocyclic ligands are polyazacycloalkane (figure 1.6), which possess a structure similar to that of the crown ethers but with nitrogen donor atoms replacing the oxygen donors. They give protonation equilibrium in aqueous media and form stable complexes with transition and post-transition metals. Furthermore, polyazamacrocycle can coordinate anions. In fact, their protonation in water afford polyammonium cations with high charge, capable of interacting with anions through hydrogen bonds and electrostatic interactions. Also in this case, appropriate functional groups can be introduced in the macrocyclic structure in order to enhance the interaction between the receptor and the substrate.

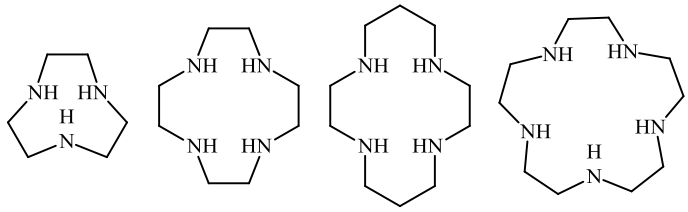

Figure 1.6 Structure of the smaller polyazacycloalkane. Order: 1,4,7-triazacyclononane (TACN); cyclen; cyclam; 1,4,7,10,13,16-esaazacycloottadecane.

The presence in nature of coordination compounds with macrocyclic ligands is related to the kinetic and thermodynamic stability of these complexes, which allows the coordinated ion to be strongly held in the macrocyclic cavity, thus ensuring a number of biological processes and functions. The ability to chemically synthesize ligands of this type, which can then be used as models for biological systems, has lead to a growing interest in the chemistry of macrocycles.

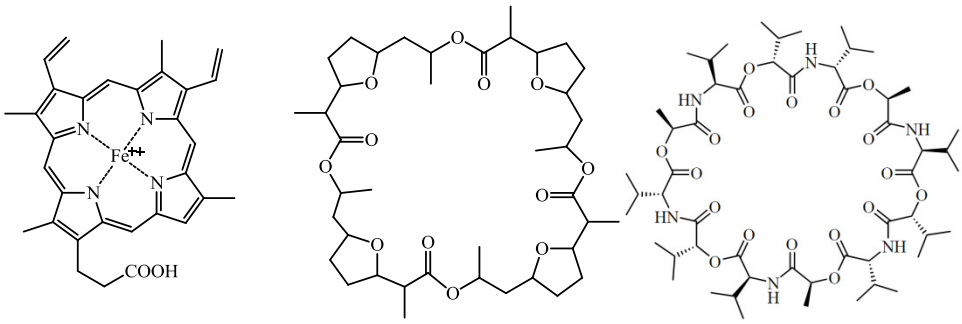

Figure 1.7 Examples of natural macrocycles.

1.2 Metal ion coordination

Heavy and transition metal cations possess a fundamental role in various biological processes and can have a deep impact on the environment[5]. The toxicity of mercury, cadmium and lead for most of the organisms, for example, it is well known. For this reason, there is a current interest in the development of new devices to determine the concentration of these analytes (separately or simultaneously), not only in samples of biological or clinic relevance, but also in situ. This has led to the development of fluorescent molecular sensors capable of quantitatively detecting these ions.

From the point of view of selectivity, measurements based on the increasing of a fluorescent emission signal originated by a sensor as a result of the substrate coordination are analytically favored with respect to those based on a fluorescence quenching. The first, in fact, have a signal to noise ratio greater and, above all, allow the observation of fluorescence transitions characterized by a life time of the excited state, often peculiar of the coordination of a targeted metal by the ligand, thus allowing the distinction between different metal cations. These advantages, however, are often in contrast with the experimental conditions: the cations of the transition metals and post-transition possess, indeed, properties which cause emission quenching in most organic fluorophores. Obviously, this increases the interest toward few devices that show different behaviors, e.g., fluorescence enhancement upon interaction with the metal[6]).

The changes observed in the absorption spectrum (ipso- or bathochromic shift) are similar for all the metal ions and the complexes bands often overlap[7]. This implies that the interaction between the analyte and the donor atoms of the receptor does not change much the absorption spectra of the ligand. Much to vary the analyte

[5] A. Müller, K. Schneider, H. Appel, W. Suer, C. Pohlmann, E. Diemann, W.-G. Thies, *Bioinorganic Chemistry*, **1997**, 725-740

[6] Yoon S, Miller EW, He Q, Do PH, Chang CJ., *Angew Chem Int*, **2007**, 46, 6658-61

[7] C. Bazzicalupi, A. Bencini, A. Bianchi, C. Giorgi, V. Fusi, B. Valtancoli, M. A. Bernardo, and F. Pina, *Inorg. Chem.*, **1999**, 38, 3806.

coordinated. The molar extinction coefficient of the free ligand and the complexes are often very similar.

In contrast to the scarce changes in the absorption characteristics, emission is subject to considerable variations as a result of metal ion complexation. There may be three situations, depending on electronic configuration of the target metal ion, the characteristics of the fluorogenic unit and the solvent:

- The complex is more fluorescent than the free ligand (CHEF effect, chelation enhancement of fluorescence): only diamagnetic transition metals, such as Zn^{2+}, give rise to this effect with most of the sensors.
- The complex is weakly fluorescent (partial CHEQ, e.g., partial chelation enhancement of quenching). It is typical case of diamagnetic ions, such as Hg^{2+} or Pb^{2+}, which may be considered "heavy metals" in terms of heavy atom effect[8] and that determine a more or less pronounced fluorescence quenching[9,10].
- The complex does not fluoresce (total CHEQ): it is typical of paramagnetic ions with an orbital d half-empty[11,12] as Cu^{2+} or Ni^{2+}.

While the quenching effects are substantially related to the metal ion nature, the increase in fluorescence may also arise from changes in the ligand geometry, induced by the ion coordination, as well as by the different availability, in the complex, of some functional groups involved in the free ligand deactivation processes. One example is the PET inhibition in a complex (see below). In the case of flexible ligand, coordination generally suppresses non-radiative decay processes of the excited state, such as for example torsional movements of the molecule[13].

1.3 Anion coordination

In the last few years, considerable attention has been focused on the design of synthetic receptors for the binding and detection of anions of relevance in environmental and biological fields.[14,15,16] Among these, receptors containing fluorogenic units capable to signal the binding event through quantifiable changes

[8] D. S. McClure, *J. Chem. Phys.*, **1952**, 20, 682.
[9] A. Harriman, *J. Chem. Soc. Faraday Trans.,* **1981**, 2, 77, 1281-1291
[10] H. Masuhara, *J. Phys. Chem.*,**1984**, 88, 5868.
[11] T.L. Banfield, *Trans. Faraday Soc.*, **1995**, 65, 1969.
[12] A.W. Varnes, *J. Am. Chem. Soc.*, **1972**, 94, 946.
[13] K. Rurack, *Eur. J. Inorg. Chem.,* **2000**, 2271.
[14] I. Stibor, *Anion Sensing* in *Top. Curr. Chem.*, Springer, **2005.**
[15] K. Bowman-James, *Supramolecular Chemistry of Anions*, Wiley-VCH, NY, **2012**.
[16] V. Amendola,*Coord. Chem. Rev.*, **2006**, 250, 1451.

of the emission are particularly attractive[17]. In fact, fluorescence sensing ensures low detection limits and avoids sample damages or destruction, an important added value in particular for the study of the metabolic role of anions in cells or tissues.
However, anion binding by synthetic receptors is particular difficult in aqueous medium, where both the receptor and the anion can be strongly solvated, making less favored the complexation process. A further drawback is the necessity to achieve fluorogenic sensors able to selectively coordinate a single targeted anion in complex matrices. This requires that the receptors possess many suitably organized binding sites in order to have a large number of interactions with the substrate, including charge-charge, H-bonding, hydrophobic and π-stacking interactions, and, in the case of metal complexes, anion-metal coordinative bonds[18].

1.3.1 Polyazacycloalkane based ligands

Ligands such as polyazacycloalkane[19] give protonation equilibria in aqueous solution, with production of species with high protonation degree even at neutral pH value. They have a high charge and can easily interact with anions. Several studies have shown that this interaction is caused mainly by electrostatic forces and by the hydrogen bond formation.
The coordination of dicarboxylic acids can be an exemplifying case. It was indeed found a particular selectivity in the coordination of $^{-}OOC\text{-}(CH_2)_n\text{-}COO^{-}$ dicarboxylates by polyamine ditopic receptors, in which the donor atoms are located in two opposite sides of the molecule, separated by aliphatic chains of different lengths. The structures of the receptor and substrate are shown in figure 1.8.

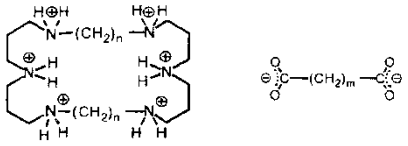

Figure 1.8 Example of receptor polyammonium for the coordination of dicarboxylic acids.

The selectivity earlier mentioned consists in molecular recognition based on the size of the receptor and substrate, and, in particular, on the values of the indices n and m in figure 1.8. In fact it has been observed that the receptor with n = 7 preferentially binds dicarboxylate anions with m = 2 or 3 (succinate, glutarate), while the one with n = 10 interacts more strongly with dicarboxylate anions having m = 4 or 5 (pimelate, adipate). This is due to the fact that in these cases there is an optimal fitting between the aliphatic chain length joining the two carboxyl groups (m) and

[17] J. L. Sessler, *Anion Receptor Chemistry, Royal Soc. of Chem.*, Cambridge, **2006**.
[18] C. Bazzicalupi, A. Bencini and V. Lippolis, *Chem. Soc. Rev.* 2010, **39**, 3709.
[19] G. A. Melson, *Coordin. Chem. of Macrociclyc Comp.*, Plenum Press, New York, **1979**.

the separation between the coordination sites of the polyamine binding agent (n). It is therefore clear that molecular recognition is attributable to the particular structural complementarity between receptor and substrate.

1.3.2 Characteristics of anions

The anion coordination to the receptor is based on the same rules that determine the selectivity in cation complexation. The characteristics of the anions are, however, different with respect to those of cations and, as explained below, this makes difficult to achieve anion binding by the receptor.

1.3.3 Effects due to the negative charge

Anions are negatively charged species that can exploit this characteristic to bind to positively charged species or polar groups *via* interactions of electrostatic nature. These interactions are generally rather weak, slightly directional and scarcely specific. The anions size influences the complexation mechanism with the ligand; the anions are larger than the cations, due to the increase of the atom and molecule sizes associated with the negative charge increase. The anions size has two main consequences on the recognition and interaction with the ligand: first, the receptor should possess a larger cavity to accommodate the anionic species; furthermore, an anion with the same electrons number of a cation has a greater spatial diffusion of charge and a consequent reduction of the ratio between charge and radius. This causes the establishment of less strong electrostatic interactions. However, the larger spatial diffusion of charges makes more polarizable the anionic species, thus facilitating weak interactions of Van der Waals type.

In table 1.3 we have reported the radius of both anionic and cationic species, to outline that the former result considerably larger.

Ion	Ionic radius (Å)	Ion	Ionic radius (Å)
F^-	1.33	$PdCl_6^{2-}$	3.19
Cl^-	1.81	Cs^-	3.50
Br^-	1.96	Li^+	0.76
I^-	2.20	NH^{4+}	1.48
Na^-	2.20	Na^+	1.02
ClO_4^-	2.50	K^+	1.38
NO_3^-	1.79	Cs^+	1.67
CO_3^{2-}	1.78	Ca^{2+}	1.00
SO_4^{2-}	2.30	Zn^{2+}	0.74
PO_4^{3-}	2.38	Al^{3+}	0.54
$H_2PO_4^-$	2.00	La^{3+}	1.03

Table 1.3 radius of the principal ionic species

1.3.4 Geometry of the anions

Another substantial difference between anions and metal cations is the fact that anions often feature characteristic geometries even for the simplest structures. Among these geometries, we can cite, beside the spherical structure of halide anions, the linear structure, characteristic of N_3^-, OCN^-, the trigonal planar structure peculiar of NO_3^- or R-CO_2^-, the tetrahedral structure of SO_4^{2-}, ClO_4^- and phosphates, and the octahedral structure of coordination compounds, such as $[M(CN)_6]^{n-}$. The large number of structures displayed by anions implies the development of receptors with particular arrangements of their binding sites, in order to establish a large number of non-covalent interactions. Therefore an accurate ligand design is a necessary requisite to synthesize receptors able to form stable complexes with specific anions.

1.3.5 Acid-base properties

It is usual to classify the anionic species as Lewis bases. Unlike cationic species they generally possess electrons pairs not interested in chemical bonds. The basicity of anions allows to acid groups to act as binding site, leading to the formation of highly directional acid-base interactions, which can therefore be exploited in the design of highly selective receptors.

Anionic species with weakly basic character, which do not so marked tendency to donate electrons, are able to establish with the receptor only weak interactions such as Wan der Waals forces, which are poorly directional and depend directly on the host-guest contact surface.

1.3.6 pH dependence

Interaction between anion and receptor is strongly influenced by the pH range in which complexation occurs. The electrostatic interaction and hydrogen bonds between receptor and anionic species are obviously favored by a positive charge gathered on the receptor, as occur in protonated polyamine compounds, while eventual protonation of the anionic species make less favorable the complexation process. In most cases a decrease of stability of the complexes is observed when protonation of the anion occurs in solution. Conversely, the complex stability increase with protonation of the ligand.

1.3.7 Solvation of anions

The water ability to solvate ionic species is due to its polarity. In particular, comparing the salvation energy of anions and cations for a given charge and size, anions show a ΔG^0 for hydration more negative compared to that found for metal cations. Water is a best solvating agent for anions than for cations. Binding of anions in water is consequently more difficult than the cations coordination.

Comparing different solvents, the stability of the complexes normally increases in the order:

H_2O <DMSO <CH_3CN <$CHCl_3$ <CCl_4

The Hofmeister series:

CO_3^{2-}> SO_4^{2-}> $S_2O_3^{2-}$> $H_2PO_4^-$> F^- >> Cl^-> Br^-> NO_3^-> I^-> ClO_4^-> SCN^-

The Hofmeister series, also said liotropic series, ranked ions according to their ability to effect salting in or salting out on proteins. It gives us an idea on hydrophobicity or hydrophilicity of an ion. These effects are more pronounced for anions that for the cations.

The ions leftmost in the series determine increase of the water order and a solubility decrease of nonpolar molecules (salting out), while the ions on the right cause an increase of the solubility of nonpolar molecules (salting in) and a decrease the order in water.

These properties are directly related to the interactions ion-solvent strength: the Hofmeister series thus provides a scale of ion hydration energy sorted by descending. The problem of the competition between the ligand and the solvent not easily eliminated: in fact even if we choose to operate in organic solvents (where the formation constants are greater) the low tendency of the apolar molecules or less polar solvent to interact with the ions would lead to the presence of the salt in solution in the ion pairs form. That is, the counter ion of the species in question is a very strong competitor against the receptor.

1.4 Chemosensors

The recognition and the quantitative determination of both cationic and anionic analytes, is of relevance in many human activities, including agriculture, food science, environmental protection and medicine. So the search for compounds whose physico-chemical properties can be changed with the presence of a target compound is a subject of wide and increasing interest, in particular in the last 20 years. From the point of view of supramolecular chemistry, a sensor is a molecule capable of operating a molecular recognition of a guest species and signaling the occurred coordination through the variation of a physical property relatively easy to measure.

To this purpose, researchers have commonly exploited changes in the spectrum of fluorescence emission (fluorimetric chemosensors) or color change (colorimetric chemosensors) or electrochemical properties, such as the reduction potential (electrochemical chemosensors).

In a chemosensors are always present at least two subunits:

- Binding subunit, e.g., a selective receptor unit for the substrate to be detected;

- Signaling subunit, e.g., a moiety able to signal the substrate presence.

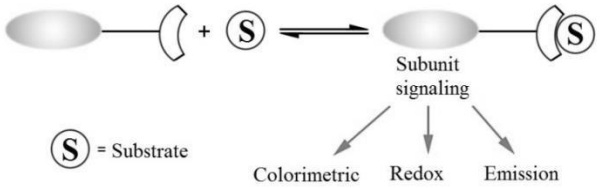

Figure 1.9 General chemosensor

In the design and optimization of a chemosensor, the receptor unit should possess some peculiar characteristics:

- high selectivity towards the substrate;
- easier detection of the signal emitted by the signaling subunits;
- high solubility in the medium and in the pH conditions in which the substrate should be coordinated. For example, in the case of anionic substrates of biological importance, the chemosensor should be soluble in water and should give a strong interaction with the substrate at neutral pH; a class of molecules particularly suitable for this purpose is those containing polyamine fragments.

1.4.1 Fluorimetric chemosensors

In this type of chemosensors, the signaling subunit is a fluorophore that converts the coordination of the substrate into an optical signal obtained thanks to the variation of its photophysical properties.

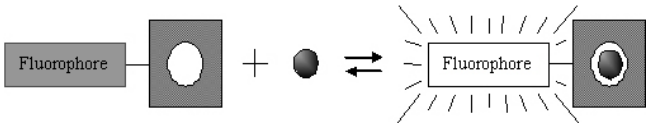

Figure 1.10 Generic fluorimetric chemosensor

In addition to those discussed in the previous paragraph, in the design of a fluorimetric chemosensor some additional factors should be considered:

- the range of emission wavelength of the fluorophore;
- the availability of adequate light sources, detectors and other optical components.

Fluorimetric chemosensors can be divided into three classes:

- Class 1: chemosensors consisting of fluorophores whose emission is turned off upon the collision with the substrate.

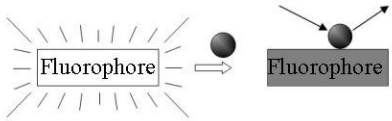

Figure 1.11 Class 1 chemosensor

- Class 2: chemosensors consisting of fluorophores which reversibly bind substrate. When the substrate is simply a proton, the chemosensor is called "fluorimetric pH indicators". The term "chelating fluorophore" is used in the case of metal ion recognition. A previously described, the coordination process can give either a CHEF or a CHEQ effect, as depicted in figure 1.12.

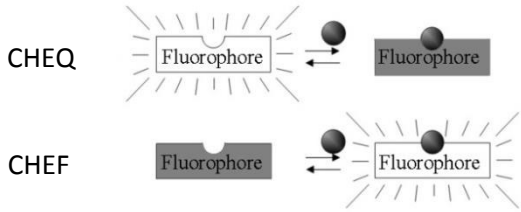

Figure 1.12 Class 2 chemosensors

- Class 3: chemosensors containing fluorophores linked to a receptor, directly ("integrated chemosensors") or *via* a molecular fragment acting as a spacer ("spaced chemosensors"). Usually the spacer, if present, is a chain formed by few carbon atoms that does not participate in the emission and absorption processes. In both cases, the coordination may results either in a CHEF or in a CHEQ effect.

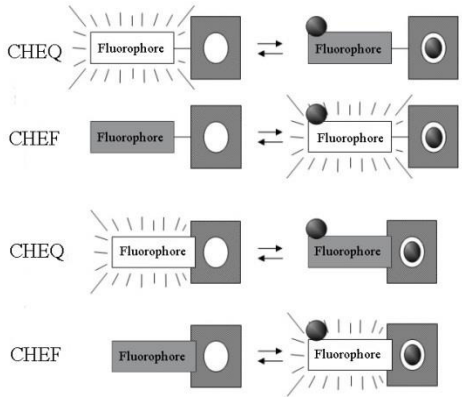

Figure 1.13 Class 3 chemosensors

1.4.1.1 Fluorescence modulation

The increase (CHEF) or decrease (CHEQ) of the fluorescence can be due to various types of mechanisms.

1.4.1.1.1 ICT, "Internal Charge Transfer"

ICT occurs in chemosensors containing an electron-donor group conjugated with an electron withdrawing group. In this case the incident radiation causes a real intramolecular charge transfer from the donor group to the acceptor unit, resulting in variation of the dipole moment, which produces a signals shift dependent on the fluorophore surroundings, named Stokes-Shift. The substrate can interact either with electron-donor group or with the electron withdrawing group. In the first case (indicated with 1 in the figure 1.14) the conjugation of the system decreases and there is therefore a shift to shorter wavelengths of the absorption spectrum ("blue shift") and a decrease of the molar absorption coefficient. In the second case (2 in figure 1.14), on the contrary, the spectrum shift towards longer wavelengths ("red shift") and the molar absorption coefficient increases. The fluorescence spectra shift in the same direction of the absorption spectra.

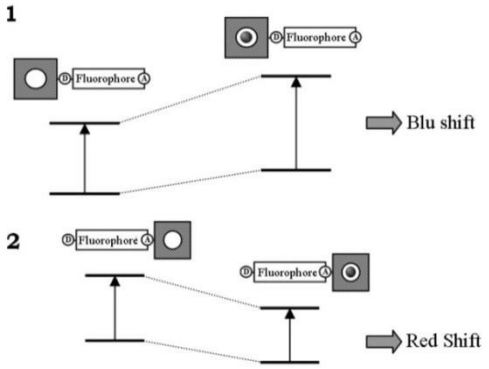

Figure 1.14 Charge transfer internal.

1.4.1.1.2 PET, "Photoinduced Electron Transfer"

The oxidative and reductive properties of a molecule in the excited state can be exploited to obtain electron transfer processes (PET) of oxidative or reductive type. In the reductive PET mechanism, for example, a fluorophore A is excited by radiation to the species A*, in which an electron is promoted from the highest occupied molecular orbital (HOMO) to the lowest unoccupied molecular orbital (LUMO). An electron is the transferred from the LUMO of the “electron rich” quencher to the HOMO of the fluorophore. This decaying mode quenches the emission of fluorescence (Figure 1.15). Most of the PET sensors are constituted by a fluorophore connected to a polyamine residue by one methylene spacer. The amine groups constitute electron donors groups able to give photoinduced electron transfer processes, leading to fluorescence quenching. When the amine groups are

protonated or interact with metal cation, the PET process is inhibited and a marked fluorescence increase is often observed.

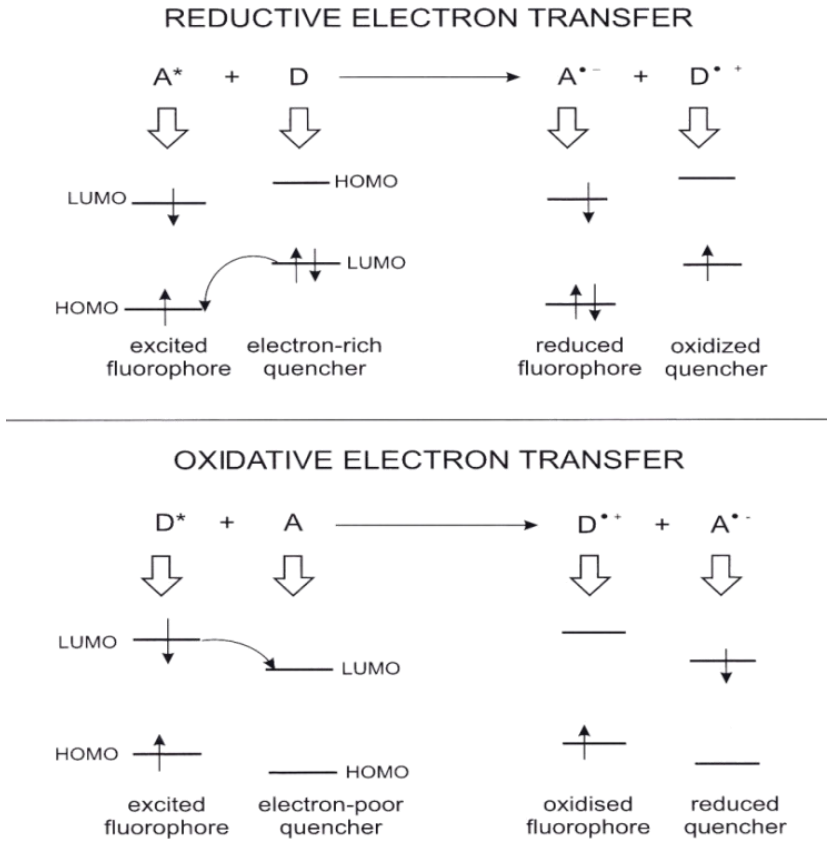

Figure 1.15 Photoinduced electron transfer

In this case, in fact, the redox potential of the donor increases and its LUMO has a lower energy than the HOMO of the fluorophore and the PET process cannot occur. The quenching is inhibited and the fluorescence increases.

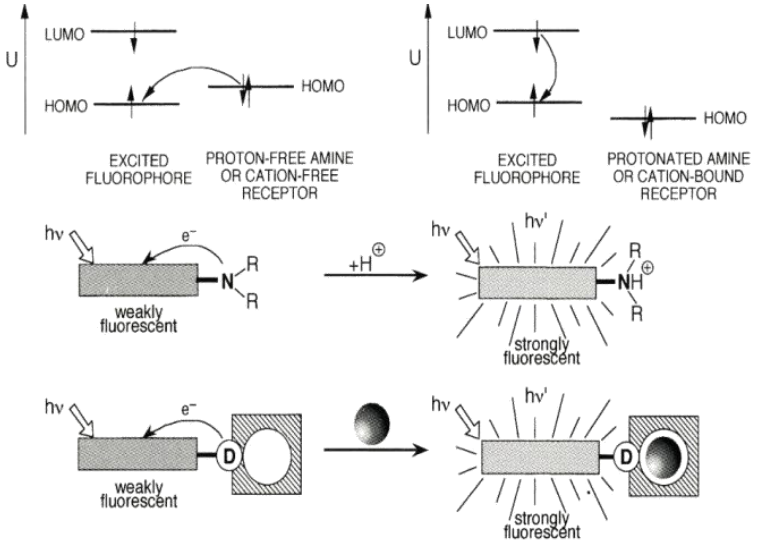

Figure 1.16 PET for a fluorimetric sensor

1.4.1.1.3 EET: "Electron Energy Transfer"

Electron energy transfer occurs if both the HOMO and LUMO of the receptor have an intermediate energy between the HOMO and LUMO of the fluorophore. In this case, upon excitation of the fluorophore, an electron is transferred from the LUMO of the fluorophore to the LUMO of the receptor. A second electron simultaneously moves from the HOMO of the receptor to the HOMO of the fluorophore, restoring the ground state of the fluorophore. If these electronic transitions take place according to radiationless processes, the fluorescence emission is turned off. Subsequently, an electron transfer process from the LUMO to the HOMO of the receptor restores the initial state of the system.

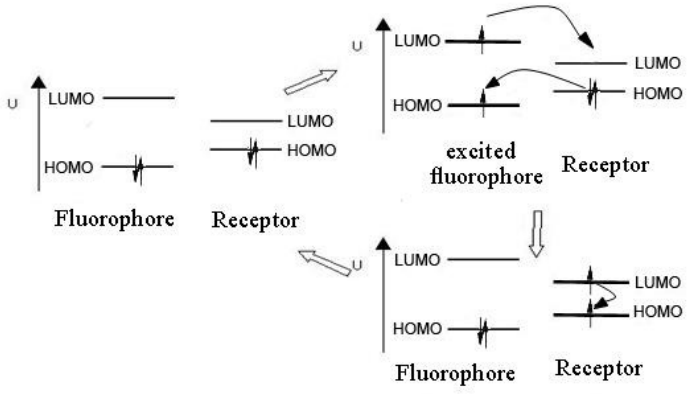

Figure 1.17 Electronic energy transfer

1.4.1.1.4 Formation of excimer

An excimer is a complex formed by the interaction of two equal fluorogenic units, the first in the excited state and the second in the ground state.

$$\mathbf{M^* + M \rightarrow (MM)^*}$$

The excimer fluorescence emission band is shifted to longer wavelengths compared to the single fluorophore (figure 1.18) and generally its formation is accompanied by the disappearance of the emission band of the monomeric species. In the case of coordination of substrate involving the formation or disruption of an excimer complex, the binding process can be monitored by following the excimer emission band intensity variation.

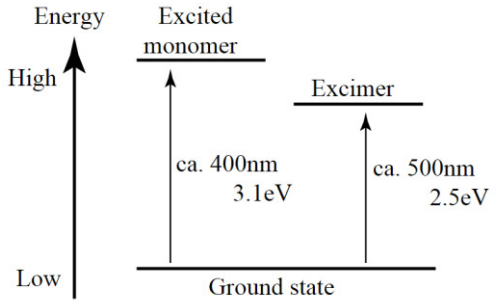

Figure 1.18 Difference between the energy of the ground state and the excimer.

1.4.1.1.5 Formation of exciplex

An exciplex is a complex formed by the interaction of two different fluorogenic units, the first in the excited state and the second in the ground state.

$$\mathbf{M^* + F \rightarrow (MF)^*}$$

The exciplexes behavior is similar to that of the excimer.

1.4.2 Colorimetric chemosensors

Among the various types of chemosensors, colorimetric ones are of particular interest because they allow the qualitative naked eye substrate determination, without the use of expensive equipment.

The colorimetric chemosensors are formed by a receptor specific for a targeted substrate, and by a chromophore. Bathochromic or ipsochromic shifts of the bands are observed in the UV-visible absorption spectrum of the chromophore upon substrate binding and they can be accompanied by variation of the molar absorbance. These spectral changes are produced by an increase (bathochromic shift) or a decrease (shift ipsochromic) of the electron density on the signaling unit upon substrate coordination by the receptor[20].

[20]N. Kaur, S. Kumar , *Tetrahedron*, **2011**, 67**,** 9233 – 9264

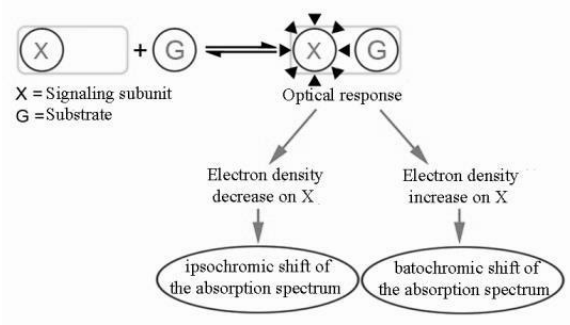

Figure 1.19 Colorimetric chemosensor general scheme.

Charged substrates can be colorimetrically determined much more easily than neutral ones. In fact, the former are capable of inducing a higher electron density variation on the chromophore, thanks to their charge. Therefore, many colorimetric chemosensors are available for anionic or cationic substrates and not for neutral substrates.

Another method for obtaining a colorimetric chemosensor consists in the use, together with the receptor, of a dye that meets the following requirements[21]:

- In the absence of substrate, a significant amount of dye is bound to the receptor;
- The dye possesses optical properties different depending on the fact that it is coordinated or uncoordinated;
- The substrate addition in solution causes a partial or total dye replacement by the substrate in the complex with the receptor, leading to a change in color of the solution, easily visible and quantifiable, in order to efficiently monitor the coordination of the substrate to be determined.

The mechanism of competition between the dye and the substrate is shown in Figure 1.20.

Figure 1.20 Competition between the dye (D) and substrate.

1.5 The synthesis of polyamine based chemosensors. The bis-aminal method.

In recent years, there has been a growing interest in the development of techniques to achieve synthetic macrocyclic systems containing one or more functional groups, linked to the cyclic structure by a suitable spacer. The synthetic procedures are indeed numerous and we will give only a brief description of the procedure based

[21] Kay Severin, *Current Opinion in Chemical Biology*, **2010**, 14, 737–742.

on the use of bis-aminals, largely exploited in the course of this work to introduce one or more fluorogenic functional groups on tetraazamacrocyclic structures.
Tetraazamacrocyclic bis-aminals have resulted to be excellent tools for the synthesis of symmetrical, dissymmetrical or functionalized bis-tetraazamacrocycles. The key feature of the process is the separation of insoluble mono- or bis-quaternary ammonium salts from solution during the course of the alkylation reaction. Macrocyclic bis-aminals, synthesized from the condensation of glyoxal with tetraazamacrocycles such as cyclen, cyclam or homocyclam, have been known for more than twenty years. When the reaction is carried out in methanol, compounds 1, 2 and 3 are obtained quantitatively (Scheme 1.1).

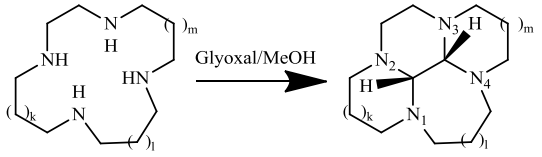

k = l = m = 0 Cyclen **1**
k = m = 1 ; t = 0 Cyclam **2**
k = l = m = 1 Homocyclam **3**

Scheme 1.1

Their respective structures are characterized by a maximum of six-membered fused rings and the *cis* configuration of the central two-carbon bridge is revealed by the temperature-dependent ^{13}C NMR spectrum. The *cis* isomers are indeed known to exhibit exchange phenomena whereas the more rigid trans isomers do not allow such a process.[22,23]
This procedure allows selective monoalkylation or 1,3 dialkylation of cyclic tetraamine bis-aminals, producing a variety a molecular architectures. In fact, the bis-aminal structure orients the non-bonding doublets of the other two amino groups in 2,4 positions toward the center of the cavity, and this inhibits their reactivity. This condition makes the nucleophilic substitution reactions stereoselective for the isomer substituted in position 1,7. This methodology has been used for the synthesis of fluorescent systems through the introduction of one or two fluorogenic group appended to a single macrocyclic structure or as well as *via* the insertion of one or two fluorescent groups bridging two macrocyclic systems. After removing the bis-aminal protection, tetraazamacrocycles with a single or two (equal or different) functional groups (**1** and **2**, respectively, in Scheme 1.2) or two macrocycles

[22] R.A. Kolinski, F.G. Riddell, *Tetrahedron Lett*., **1981**, 22, 2217
[23] F. G. Riddel, P. Murray-Rust, R. Kolinski and P. Gluzinski, *Tetrahedron Lett.* , **1982**, 38, 673.

separated by a single or a double bridge (**3** and **4**, respectively, in Scheme 1.2) have been obtained.

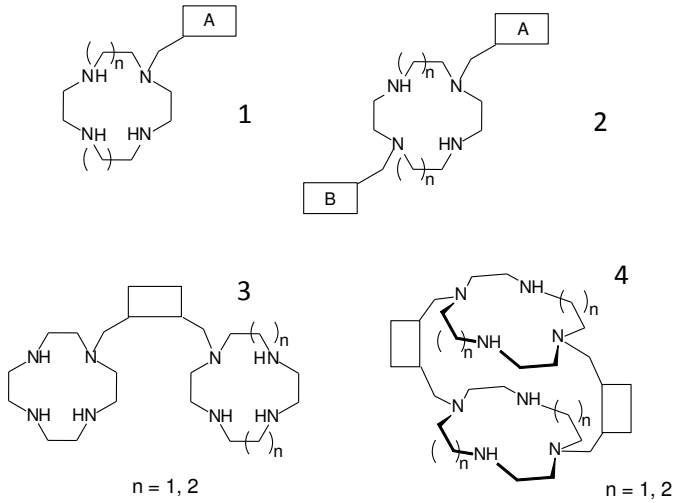

Scheme 1.2

Although this procedure is known it has not yet been used to introduce fluorogenic side arms or bridges between macrocyclic units, producing mono- or polycyclic structures containing one or two fluorophores.

1.6 Used fluorophores

The fluorescence intensity of heterocycles containing nitrogen depends on the interactions via hydrogen bonding with the solvent. The explanation of this phenomenon lies in the fact that the singlet excited state at lower energy is n,π * in polar solvents, whereas in hydrogen bond donor solvents is π,π *. The decay from the singlet state n,π* to the ground state is forbidden by symmetry. This inhibits radiative decay processes. Therefore, in polar solvents the return to the ground state takes place preferentially via non radiative processes as intersystem crossing and/or internal conversion, rather than radiative emission, can easily occur.

1.6.1 Quinoline

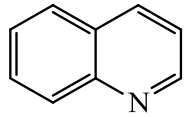

Figure 1.21 Quinoline

Quinoline is a heterocyclic aromatic compound, whose structure is depicted in Figure 1.21. It has a very high fluorescence quantum yield, therefore, is highly suitable as a fluorescent unit for the achievement of fluorimetric chemosensors. In addition, the aromatic nitrogen atom has a doublet on the molecule nodal plane and

it is therefore available for interactions with metal cations. This nitrogen atom can also be protonated affording the quinolinium ion, with pK_a value of 4.79 log units.

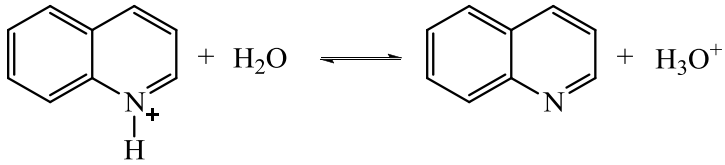

Figure 1.22 Quinoline acid-base equilibrium

The quinoline UV-V spectrum presents a broad band with a maximum at 318 nm, while the cation quinolinium, derived from the protonation of the heteroaromatic nitrogen atom presents a structured band with a maximum at 305 nm (figure 1.23).

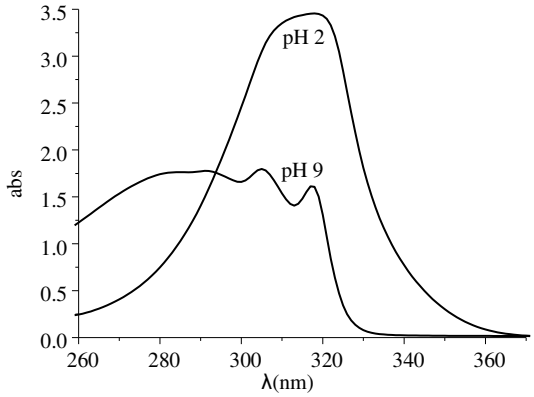

Figure 1.23 pH dependence of quinoline UV spectra

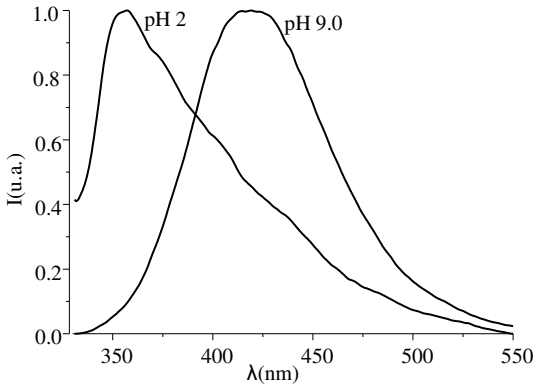

Figure 1.24 pH dependence of quinoline emission spectra

The fluorescence emission spectrums of the two form (the protonated and non-protonated), recorded by exciting at 315 nm, are substantially different. In fact, the

quinoline presents an emission band with a maximum at about 425 nm, while the band of the quinolinium cation is shifted to shorter wavelengths, about 350 nm, as can be seen in figure 1.24.

1.6.2 8-hydroxyquinoline[24]

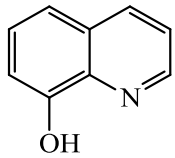

Figure 1.25 8-hydroxyquinoline

It is a derivative of quinoline, which is obtained by substitution of the hydrogen in position 8 with a hydroxyl group. This fluorophore also has a good quantum yield, but with an emission band red-shifted with respect to quinoline.

It is a bifunctional hydrogen-bonding molecule, which in aqueous or alcohol solution simultaneously act as an H-donor at the OH site and as acceptor at the N-atom. Upon photoexcitation, the acid/base properties of this molecule significantly change at the both the sites, rendering OH group more acidic and the N-atom more basic. The 8-hydroxyquinoline also behaves as a bidentate chelating agent, using both the hydroxyl group and the nitrogen atom in the process of metal coordination. In recent years, metal chelates of 8-hydroxyquinoline (often simply named 8-HQ) have played an important role in the field of organic electroluminescence (OEL), and these complexes were widely introduced in OEL cell as emission layer.

In aqueous solution 8-HQ has two acid-base equilibria, the first involves the nitrogen atom heteroaromatic, with a pK_a = 5.13, while the second involves the hydroxyl oxygen atom, with a pK_a = 9.89. The main species formed in 8-HQ solution consist of neutral, cationic and anionic, the relative contributions being dependent on the degree of acidic and basic character of the medium. It is established that the zwitterions form though predominant in the excited state is known to be non-fluorescent in most of the solvents. In all the pure solvents, H-bonded complexes have been reported to be the main emitting species and the low quantum yield of their fluorescence has been attributed to either to hydrogen bonding or to the prototropic equilibrium between excited states of two ionic species.

[24] L. R. Naik and N. N. Math, *Indian Journal of Pure & Applied Physics*, **2005**, 43, 743-749

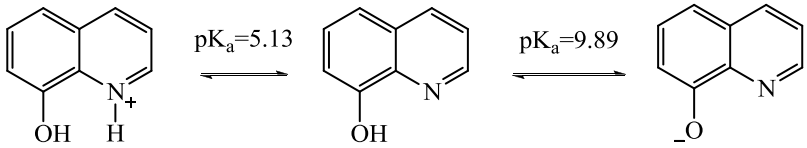

Figure 1.26 8-hydroxyquinoline acid-base equilibrium

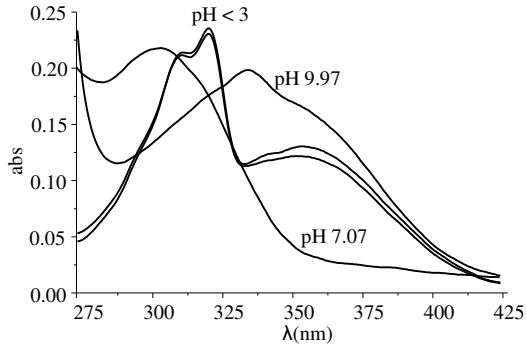

Figure 1.27 pH dependence of 8-HQ UV spectra

Considering the absorption characteristics of UV/Vis of 8-hydroxyquinoline, figure 1.27, in very acid environment, where it is present in aqueous solution the cation 8-hydroxy quinolinium, the spectra are characterized by two bands with maximum at 321 and 354 nm, respectively. By increasing pH, the band at 354 nm disappears and the spectra recorded at neutral pH feature a single band at 303 nm, attributable to the neutral 8-hydroxyquinoline form, containing an -OH group and a not protonated nitrogen atom. At alkaline pH values, this band undergoes a red shift to give an absorption maximum at 334 nm, typical of the anionic species of 8-hydroxyquinoline.

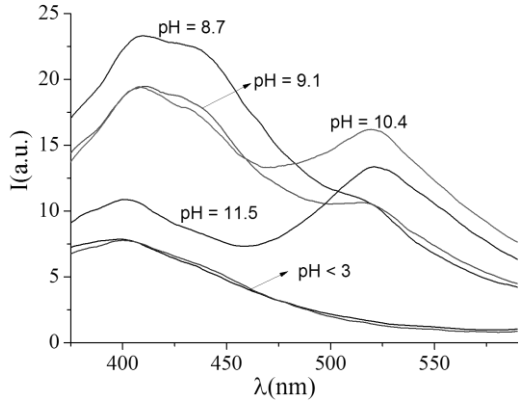

Figure 1.28 pH dependence of 8-HQ emission spectra

The 8-hydroxyquinoline fluorescence emission spectra, shown in figure 1.28, are recorded at various pH values. At acidic pH value (pH=2.85), when the fluorophore is in its cationic monoprotonated form, the emission spectrum features a very weak band at *ca* 400 nm. By increasing pH, the band shape changes and presents an emission maximum at 410 nm, whose intensity increases up to pH 8.6. This spectral features are typical of the neutral form of 8-HQ. A more alkaline pH values, the emission intensity at 410 nm decreases and simultaneously a second band appears at 520 nm, due to the formation of the monoanionic form of 8-HQ. Acridine[25,26]

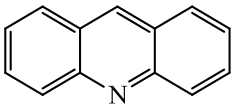

Figure 1.29 Acridine

Acridine is an important aza-aromatic compound also used as a staining dye for biological tissues. Its derivatives have significant antibacterial and potential antiviral activity and have been widely used in pharmacology. Acridine derivatives also have been used as ligands for heavy metals in different areas of inorganic chemistry Similarly to pyridine and quinoline, acridine is a weak base basic, with $pK_a = 5.6$.

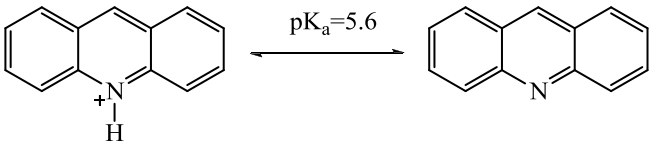

Figure 1.30 Acridine acid-base equilibrium

It was shown that in this molecule the nitrogen of acridine cycle is a protonation site. The changes in the acridine absorption spectra in acidified solutions show an extremely specific pattern. In parallel with the emergence of a band in the long-wavelength edge of acridine absorption around 400 nm, there is also an increase in the intensity of the long-wavelength acridine absorption band at ~ 350 nm (figure 1.31a). The cationic form of acridine, unlike the neutral one, exhibits moderate fluorescence. For a hydrochloric acid concentration as low as 10^{-5} M in solution, there is intense fluorescence around 479 nm along with weak fluorescence belonging to the neutral form around 415 nm. The fluorescence spectra of acridine and those of its protonated form are shown in figure 1.31b. The fluorescence

[25]Ò. Rubio-Pons, L. Serrano-Andrés and M. Merchán, *J. Phys. Chem.,* **2001**, 105, 9664-9673

[26] N.I. Selivanov, L.G. Samsonova, T.N. Kopylova et al*., High Energ. Chem.,* **2009**, 105 No2, 43.

maximum of protonated form considerably shifted in the red region and a fluorescence quantum yield increased up to 0.27 (for neutral form it is equal 0.03).

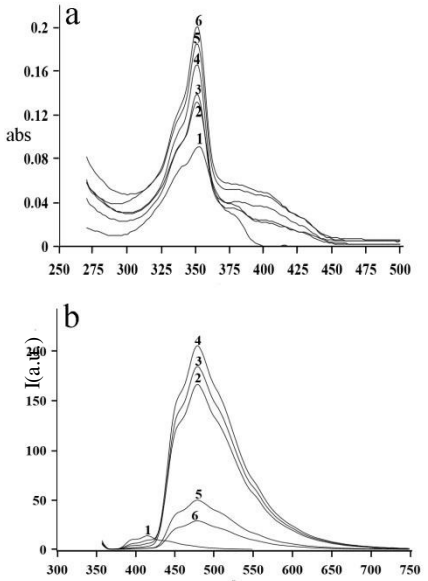

Figure 1.31 Absorption (a) and fluorescence spectra of acridine in ethanol (b) for $C_{HCl} = 0$ (1), 10^{-5} (2), 10^{-4} (3), 10^{-3} (4), 10^{-2} (5), and 10^{-1} M (6)

1.6.3 Terpyridine[27]

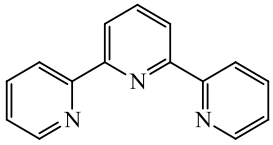

Figure 1.32 Terpyridine

2,2';6',2"-terpyridine compound is a well-known tridentate ligand largely used in coordination chemistry. Until 1990s it has been recognized as a pivotal component for the construction of molecular devices and supramolecular assemblies. The interest in terpyridine has increased continuously, thanks to the design and the synthesis of a variety of sophisticated derivatives tailored for a wide range of applications.

[27] C. Bazzicalupi, A. Bencini, A. Bianchi, A. Danesi, E. Faggi, C. Giorgi, S. Santarelli, B. Valtancoli, *Coordination Chemistry Reviews*, **2008**, 252, 1052–1068

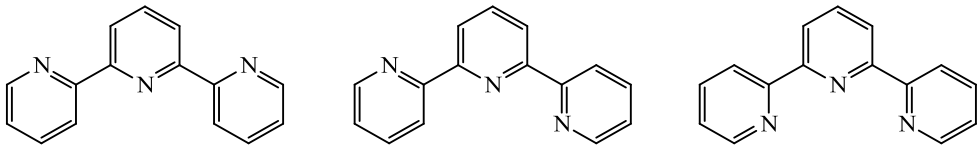

Figure 1.33 The three possible conformations of terpyridine.

Terpyridine undergoes protonation in moderately acidic solution giving rise to $[Htpy]^+$ and $[H_2tpy]^{2+}$ species, the successive protonation constants in water being pKa = 4.7 and pKa = 3.5, respectively. Depending on the protonation site and the molecular conformation, seven structures are possible for $[Htpy]^+$ and for $[H_2tpy]^{2+}$ has a *cis,cis* conformation, with the two acidic protons on the lateral pyridine groups, leading to the formation of two intramolecular hydrogen bonds.

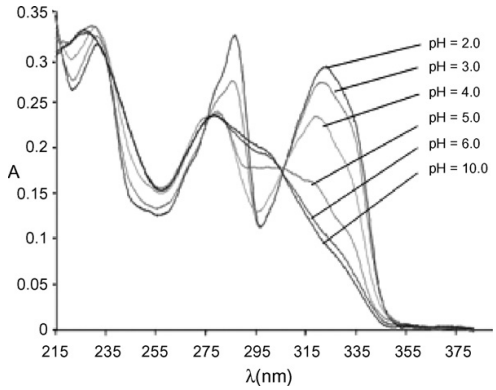

Figure 1.34 UV spectra of terpyridine at different pH values.

The ultraviolet spectrum of terpyridine in aqueous solution is strongly pH dependent (figure 1.34). In alkaline solution, where terpyridine is present as a free base in the *trans,trans* conformation, the spectrum consists of two bands at 285 and 235 nm (respectively, at pH 12) and is very similar to those in organic solvents. As the solution pH is decreased to intermediate values, a new spectrum consisting of three bands at ca. 320, 279 and 232 nm (respectively, at pH 4) appears, corresponding to the formation of the monoprotonated *cis,trans* $[Htpy]^+$ species, occurring at intermediate pH values. Further protonation, leading to the formation of the cis,cis $[H_2tpy]^{2+}$ species in more acidic solution, gives rise to some modifications of the spectrum observed at an intermediate pH. Although the three bands undergo only modest wavelength shifts to ca. 325, 285 and 230 nm, their molar extinction coefficients increase appreciably (respectively, at pH 2.0) and the 325 and 285 nm bands show poorly resolved fine structure.

The fluorescence spectrum of terpyridine is also markedly pH dependent. In alkaline solution the emission spectra are characterized by a band resulting from the overlapping of two peaks at 337 and 350 nm. This band becomes more intense and

is red-shifted on lowering the solution pH, as the $[Htpy]^+$ and $[H_2tpy]^{2+}$ species are formed.

1.6.4 2,2'-Bipyridine

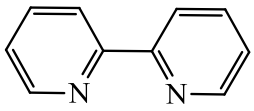

Figure 1.35 2,2'-Bipyridine

Aromatic N-heterocycle compounds, such as 2,2'- bipyridine (bipy), provide an opportunity to examine the effects of varying molecular structure on the energetics and reactivities of the excited states. The nitrogen heteroatom is an intimate part of the aromatic structure and, being a Lewis base, is subject to protonation and coordination to metal ions. These latter processes, as well as substitution on the aromatic system are expected to have a significant effect on the excited states and their observed photochemistry and photophysics. Bipy is a bidentate chelating ligand, forming complexes with many transition metals. Ruthenium complex and platinum complexes of bipyridine exhibit intense luminescence, which may have practical applications. Bipy is a weak base with a pK_a relative to the dipyridyl protonation of 5.3 log units.

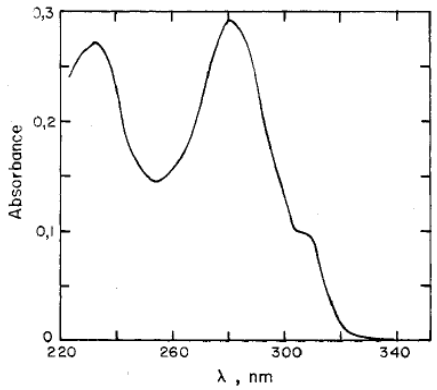

Figure 1.36 UV-Vis spectra of 2,2'-dipyridyl in aqueous solution, pH 6.5.

The absorption spectrum shows two bands at 282 and 235 nm, which are typical of non-protonated form of the molecule, figure 1.36. A spectrum of its protonated form shows a marked red-shift, with peaks repositioned to 301 and 241 nm.
Even in the emission spectrum is observed a substantial pH-dependent band shift, due to the protonation equilibrium. This bands shift is due to the different conformation that the 2,2'-dipyridyl assumes at different pH values. Below pH 5.3, dipyridyl is in its protonated form and the acidic proton, is shared by the two nitrogens via hydrogen bonding, thus stabilizing the cis conformer of the molecule;

in neutral or basic solution, bipy is not protonated and the trans conformer is energetically favored.

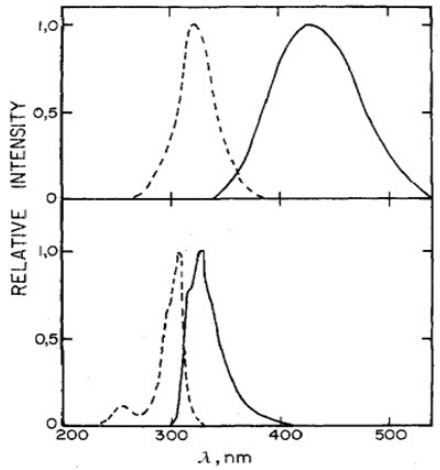

Figure 1.37 2,2'-dipyridyl emission spectrum (continuous line) and absorption (dotted line) in aqueous solution. Above: pH 1.7. Below pH 8.2. The fluorescence and absorption intensities are reported in arbitrary units.

1.7 Project objectives

This project will be devoted to design and synthesis of new fluorescence molecular sensors (chemosensors) for anions in aqueous solution. The targeted species will be inorganic anions of environmental importance, such as halides, phosphates, nitrates, arsenate, etc., or biological substrates having anionic or easy ionizable functions, such as aliphatic and aromatic carboxylic acids, nucleosides and nucleotides. In this respect, we will synthesize new fluorescent polyamine systems, whose protonated forms can be able to bind anions in water, as well as their metal complexes. Both polyammonium and metal based receptors will be tested as selective binding and signaling agents for anionic substrates; this aim is reached when the coordination of the guest changes the fluorescence emission properties of the chemosensor. Selective binding can be achieved by synthesizing receptors containing suitably constructed cleft or cavities to host the anion, in order to maximize the receptor-anion interaction.

In the course of the development of new metal-based chemosensors for anions, we have in particular investigated the fluorescence emission properties of Zn(II) complexes, whose ability to adapt its coordination environment to bind exogenous substrates is well known. This has lead to the synthesis and characterization of selective fluorescence chemosensors for the recognition of the ion Zn(II). This goal may be also of relevance. Zinc(II) is in fact an essential trace element in all forms of life. Despite its crucial importance in the basic functions maintenance such as proliferation and cell growth, the knowledge of the biological mechanisms

involving Zn(II) at a cellular and sub-cellular level are not completely clarified and Zn(II) chemosensors may represent new efficient tools for the analysis of its role in biological processes.

1.7.1 The ligands analyzed in the course of this work

1.7.1.1 Cyclen based ligands

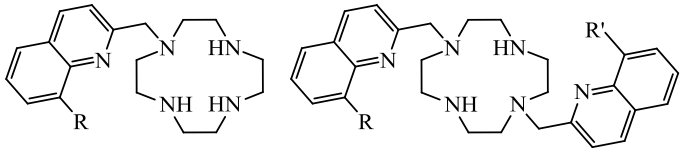

R= H **L1**
R= OH **L2**

R= H R'= OH **HL3**
R= R'= OH **H_2L4**
R= R' = H **L5**

Figure 1.38 Cyclen based ligands

Ligands **L1**-**L5**, figure 1.37, are [12]aneN_4-based ([12]aneN_4 = 1,4,7,10-tetraazacyclododecane, also named cyclen) ligands containing one or two quinoline or hydroxyquinoline units as side arms. These receptors are expected to form stable 1:1 complexes with transition metal cations. We have synthesized these ligands and analyzed the coordination of four metal ions: Zn (II) and Cd (II), the coordination of which generally tends to increase the chemosensors fluorescence emission and Cu(II) and Pb(II), which instead tend to turn off the emission of fluorescence, due to their paramagnetic and 'heavy' characteristics, respectively.

1.7.1.2 1,4,7-triazonane-based ligands

There is intense interest in the development of molecular systems capable of binding phosphate anions, due to the relevance of these anions in areas as diverse as biology, medicine, catalysis and environment.[28] In this context, we have studied 1,4,7-triazonane ([9]aneN_3) based systems composed by two macrocyclic moieties linked by a fluorogenic unit, such as acridine (**L6**) and terpyridine (**L7**) (figure 1.39). In particular we have analyzed their binding features toward inorganic phosphate anions, such as mono-, di- and triphosphate.

[28] A. K. H. Hirsch, F. R. Fischer and F. Diederich, *Angew. Chem., Int. Ed.*, **2007**, 46, 338–352

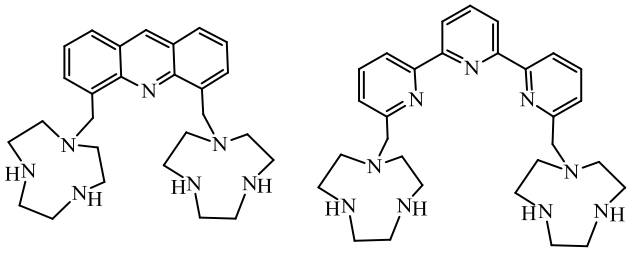

L6 **L7**

Figure 1.39

1.7.1.3 Pentaamine chain linking the 6,6' positions of bipyridine

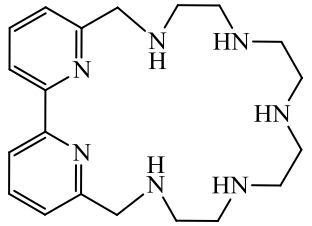

L8

Figure 1.40

Selective binding of nucleobases and nucleosides is involved in a number of biological processes including protein synthesis, genome duplication, and signal transduction[29]. Nucleobases/nucleosides derivatives can also be potent pharmacological agents. They actually play a crucial role in the current treatment of cancer and viral infections as the primary components of highly active anti-retroviral therapy. As a consequence, there is a current interest in the design and synthesis of new receptors able to recognize specific, isolated, nucleobases.

Receptor **L8** (figure 1.40) contains a pentaamine chain linking the 6,6' positions of bipyridine. It was shown that ligand **L8** forms a stable dizinc complex in aqueous solution, the two metals being enclosed within the macrocyclic cavity at short distance one another. Therefore, both metal cations feature a coordination environment not saturated by the ligand donor atoms, and therefore, there are promising binding sites for exogenous substrates, including nucleobases, nucleosides and nucleobases derivatives of pharmacological interest. The ability of the Zn(II) complex with **L8** to bind these substrates has been studied in the course of this thesis work.

[29] C. Bazzicalupi, A. Bencini, L. Bussotti, E. Berni, S. Biagini, E. Faggi, P. Foggi, C. Giorgi, A. Lapini, A. Marcelli, B. Valtancoli, *Chem. Commun,* **2008**, 1230-1232.

1.7.1.4 H_2L9

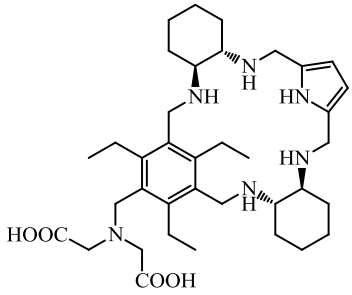

H_2L9

Figure 1.41

We have also investigated the binding properties of a new synthetic receptor (**H_2L9**, figure 1.41) for phosphate anions receptor is obtained by assembling an iminodiacetic (IDA) fragment, as a Zn(II) binding site, with a polyamine macrocyclic portion containing two trans-1,2-diaminocyclohexane (DAC) units and a pyrrole ring, as a binding site for anions, into an adaptive structure appropriately spanning the length of di- and tridentate phosphates.

1.7.1.5 xylyl-tetracyclam

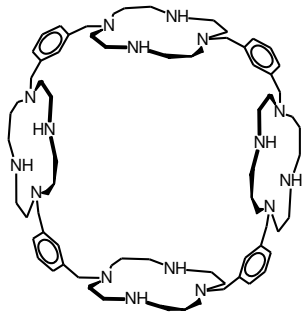

L10

Figure 1.42 xylyl-tetracyclam

Macrocycles **L10** featuring a large cavity can encapsulate molecules or ions of large dimensions. To this purpose we chose the receptor shown in figure 1.42, synthesized by the research group of Prof. Raphael Tripier (University of Brest, France), called "xylyl-tetracyclam". This receptor has a cavity capable, in principle, to accommodate large molecules, such as some pH indicators. In particular, it is logical to expect the formation of species with a high degree of protonation in aqueous solution, capable of forming stable complexes with anionic species, such as colorimetric pH indicators.

2 Experimental Details

2.1 Synthesis

2.1.1 L1

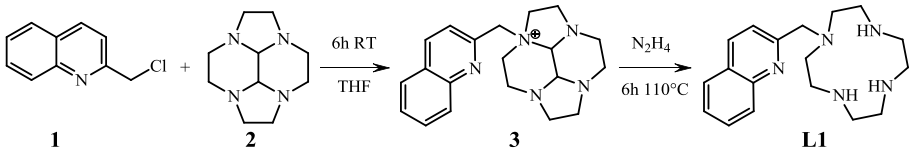

1 2 3 L1

Scheme 2.1

A solution of 2-(chloromethyl)quinoline (**1**, 800 mg, 4.50 mmol) in THF (10 mL) was added drop wise to a stirred solution of **2** (800 mg, 4.10 mmol) in THF (10 mL). The solution was stirred at room temperature for six hours. In the course the reaction, a light yellow precipitate is formed, which was filtered off and washed with THF, obtaining product **3.** Deprotection of **3** was performed with hydrazine (N_2H_4). 1.3g of **3** were dissolved in 25ml of N_2H_4 and 5 ml of EtOH, the mixture was stirred at 110 °C for 6h. The resulting solution was cooled at room temperature and quenched by addition of a 5 M NaOH aqueous solution (15 mL). The resulting solution was extracted with chloroform (5x50 mL). The organic layer was dried over Na_2SO_4 and evaporated under reduce pressure. The crude product was dissolved in ethanol and transformed in its hydrobromide salt by adding concentrated HBr. Upon addition of HBr, a solid compound precipitated, which was filtered off to give the compound **L1** as a light yellow powder.

(1.88 g, 73%). *d*H (500 MHz, D_2O pD ≤ 2.4): 8.62(d, 1 H), 8.10(t, 2 H) , 7.93(t, 1 H), 7.76(t, 1 H), 7.66 (d, 1 H), 4.28 (s, 2 H), 3.28 (t, 4 H), 3.23 (t, 4 H), 3.12 (m, 8 H); *d*C (125 MHz, D_2O pD ≤ 2): 154.31, 148.46, 139.10, 136.15, 130.76, 129.81, 129.10, 123.34, 120.77, 55.60, 48.87, 45.11, 42.53, 42.11. (CHN) Anal. Calc. C, 33.93; H, 4.90; N, 10.99. Found C, 34.11; H, 4.77; N, 11.09.
[CuL1]$(ClO_4)_2 \cdot 2H_2O$. Crystals suitable for X-ray analysis of the dihydrate salt **[CuL1]**$(ClO_4)_2 \cdot 2H_2O$ were prepared in 75% yield by slow evaporation at room temperature of an aqueous solution of **L1** (0.01 M) with one equivalent of Cu(II), acidified with 1 M $HClO_4$ up to pH 5, in the presence of a twenty-fold excess of $NaClO_4$. (CHN) Anal. Found. C, 34.33; H, 5.11; N, 11.43.

2.1.2 HL2

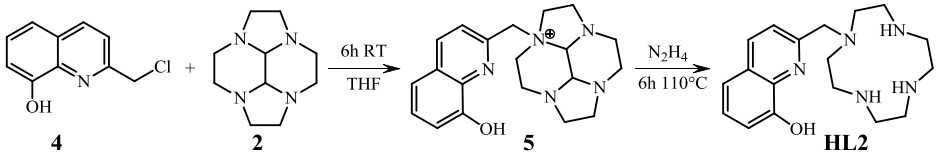

Scheme 2.2

A solution of 2-(chloromethyl)quinolin-8-ol (**4**, 850 mg, 4.32 mmol) in THF (10mL) was added drop wise to a stirred solution of **2** (750 mg, 3.86 mmol) in THF (10mL). Compound **HL2** was obtained by using the same procedure reported for **L1**. The compound was isolated as a yellow powder
(1.97 g, 78%). *d*H (500 MHz, D_2O pD ≤ 2): 8.84(d, 1 H), 7.89(d, 1 H), 7.64(d, 1 H), 7.63(s, 1 H), 7.38 (dd, 1 H), 4.32 (s, 2 H), 3.23 (t, 4 H), 3.12 (t, 4 H), 2.95 (m, 8 H); *d*C (125 MHz, D_2O, pD ≤ 2): 154.62, 148.43, 146.44, 131.93, 130.76, 130.06, 123.30, 120.14, 117.02, 55.73, 49.17, 45.00, 42.60, 42.27. (CHN) Anal. Calc. C, 33.10; H, 4.78; N, 10.72. Found C, 33.11; H, 4.77; N, 11.09.

2.1.3 HL3

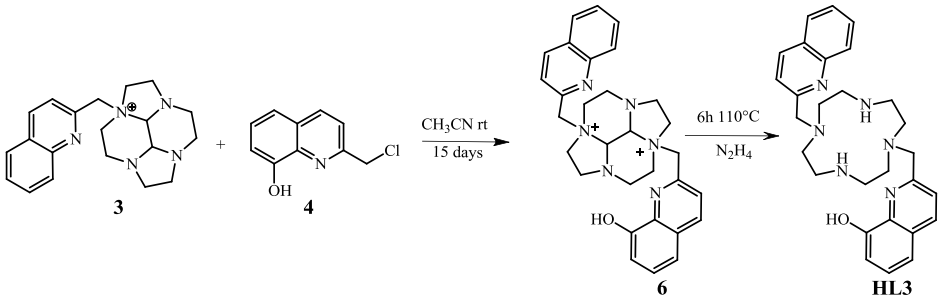

Scheme 2.3

A solution of 8-(hydroxy)-2-(chloromethyl)-quinoline (**4**, 600 mg, 3.1 mmol) in CH_3CN (10 mL) was added drop wise to a stirred solution of **3** (820 mg, 2.2 mmol) in CH_3CN (10 mL). The solution was stirred at room temperature for 15 days. In the course the reaction, a yellow precipitate is formed, which was filtered off and washed with CH_3CN thus obtaining the product 6. Deprotection of **6** was obtained with hydrazine (N_2H_4). 1.1g of **6** is dissolved in 25 ml of N_2H_4 and 5 ml of EtOH, and the mixture was stirred at 110 °C for 6h. The resulting solution was cooled at room temperature and quenched by addition of a 5 M NaOH aqueous solution (15 mL). The resulting suspension was extracted with chloroform (8x50 mL). The organic layer was dried over Na_2SO_4 and evaporated under reduce pressure. The crude product was dissolved in ethanol and transformed in its hydrobromide salt by

adding concentrated HBr. Upon addition of HBr, a solid compound precipitated, which was filtered off to give compound **HL3** as a light yellow powder.
(1.75 g, 73%). dH (500 MHz, D2O pD ≤ 2.4): 8.27(d, 1H), 7.89 (m, 3H), 7.76 (d, 1H), 7.68 (d, 2H), 7.41 (d, 1H), 7.36 (d, 1H), 7.13 (t, 1H), 6.69 (d, 1H), 4.35 (s, 2H), 4.28 (s, 2H), 3.42 (m, 4H), 3.35 (m, 4H), 3.10 (m, 8H); dC (125 MHz, D_2O, pD ≤ 2.4): 157.5, 155.3, 146.54, 139.32, 135.59, 130.24, 129.53, 128.01, 122.18, 121.25, 120.94, 120.31, 113.64, 56.88, 56.02, 49.56, 43.43, 43.24. (CHN) Anal. Calc. C, 42.34; H, 4.82; N, 10.82. Found C, 42.11; H, 4.95; N, 10.77.

2.1.4 H_2L4

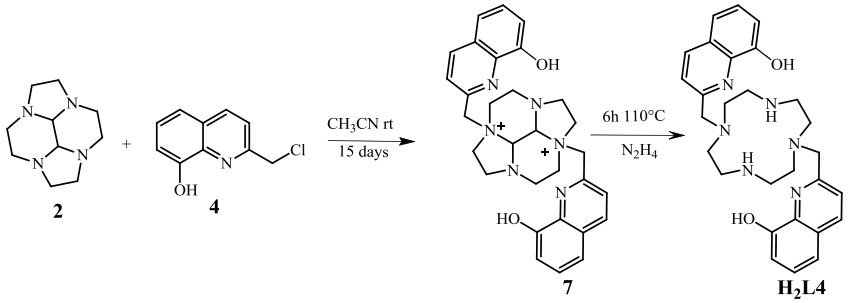

Scheme 2.4

A solution of 8-(hydroxy)-2-(chloromethyl)-quinoline (600mg, 3.1mmol) in CH_3CN (10 mL) was added drop wise to a stirred solution of **3** (820mg, 2.2mmol) in CH_3CN (10 mL). Compound **H_2L4** was obtained by using the same procedure reported for **HL3**.
(1.88 g, 73%). dH (500 MHz, D2O pD ≤ 2.4): 7.80(d, 2 H), 7.24 (d, 2 H), 7.14(t, 2 H), 7.03 (d, 2 H), 6.75 (d, 2 H), 4.25(s, 4 H) , 3.41(m, 4 H) , 3.36 (m, 4 H) , 3.18(m, 4 H), 3.00(m, 4 H); dC (125 MHz, D_2O, pD ≤ 2.4): 156.36, 149.36, 139.44, 134.18, 128.17, 127.28, 120.56, 119.35, 113.31, 55.66, 49.12, 42.73. (CHN) Anal. Calc. C, 38.12; H, 5.25; N, 9.52. Found C, 9.54; H, 5.42; N, 9.54.
[ZnH_2L4]$(ClO_4)_2 \cdot H_2O$. Crystals suitable for X-ray analysis of the monohydrate salt **[ZnH_2L4]**$(ClO_4)_2 \cdot H_2O$ were prepared in 68% yield by slow evaporation at room temperature of an aqueous solution of **H_2L4** (0.01 M) with one equivalent of Zn(II), acidified with 1 M $HClO_4$ up to pH 5, in the presence of a twenty-fold excess of $NaClO_4$. (CHN) Anal. Found. C, 43.33; H, 4.87; N, 9.20.
[CdH_2L4]$(ClO_4)_2 \cdot H_2O$. Crystals suitable for X-ray analysis of the monohydrate salt **[CdH_2L4]**$(ClO_4)_2 \cdot$ obtained following the same procedure of the Zn(II) complex, 72% yield. (CHN) Anal. Found. C, 43.33; H, 4.87; N, 9.20.
[PbHL4]$(ClO_4) \cdot H_2O$. Crystals suitable for X-ray analysis of the monohydrate salt **[PbHL4]**$(ClO_4) \cdot H_2O$ obtained following the same procedure of the Zn(II) complex, 60% yield (CHN) Anal. Found. C, 41.33; H, 4.54; N, 10.27.

2.1.5 L5

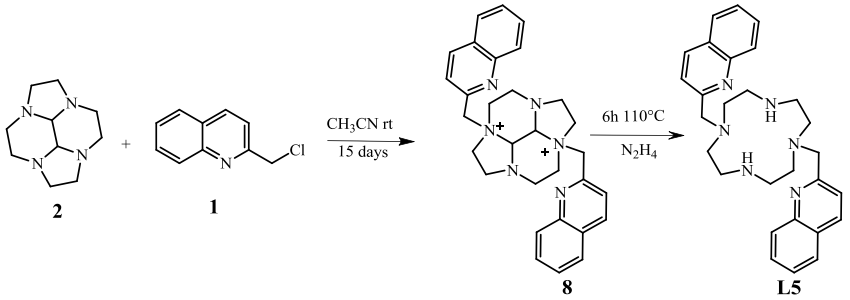

Scheme 2.5

A solution of 2-(chloromethyl)quinoline (1.2 g, 6.75 mmol) in CH_3CN (15 mL) was added drop wise to a stirred solution of 2 (525 mg, 4.10 mmol) in CH_3CN (20 mL). Compound **L5** was obtained by using the same procedure reported for **L1**.
(1.97 g, 78%). dH (500 MHz, D2O pD ≤ 2.4): 8.04 (d, 2 H), 7.70 (d, 2 H), 7.56 (t, 2 H), 7.45 (t, 2 H), 7.33 (d, 2 H), 4.35(s, 4 H), 3.45(m, 8 H), 3.12(m, 8 H); dC (125 MHz, D_2O, pD ≤ 2.4): 157.50, 144.02, 140.46, 132.00, 128.94, 127.86, 124.93, 121.36, 56.64, 49.68, 43.30. (CHN) Anal. Calc. C, 43.21; H, 4.92; N, 10.80. Found C, 43.45; H, 4.98; N, 10.77.
[ZnL5]$(ClO_4)_2 \cdot 1/2H_2O$. Crystals suitable for X-ray analysis of the hydrate salt [**ZnL5**]$(ClO_4)_2 \cdot 1/2H_2O$ were prepared in 48% yield by slow evaporation at room temperature of an aqueous solution of **L5** (0.01 M) with one equivalent of Zn(II), acidified with $HClO_4$ 1M up to pH 5, in the presence of a twenty-fold excess of $NaClO_4$. (CHN) Anal. Found. C, 46.58; H, 4.89; N, 9.56.
[CdL5]$(ClO_4)_2 \cdot H_2O$. Crystals suitable for X-ray analysis of the hydrate salt [**CdL5**]$(ClO_4)_2 \cdot$ obtained following the same procedure of the Zn(II) complex, 79% yield (CHN) Anal. Found. C, 42.58; H, 4.73; N, 10.70.

2.2 Physico-chemical techniques

2.2.1 Potentiometric

The potentiometric measures have been performed with a potentiometric system consisting of:

- Potentiometric system Metrohm 713 pH-meter
- 1 mL automatic burettes Metrohm 665 Dosimat
- Mechanical shaker Metrohm 728 Stirrer
- Thermostatic cells with capacity of 25 cm^3 and thermo-regulated by water circulation.
- Combined Hamilton Liq-Glass Glass electrode
- Personal computer

The solutions used during the measurements were prepared with MilliQ water, which was desaerated by boiling and subsequently cooled under N_2 flux.

The solutions of NaOH, HCl and NaCl were prepared using commercial products of high purity and their concentrations were determined by standard analytical procedures.

The measurements were carried out at a temperature of 298.1 K. The temperature of the potentiometric cell was maintained at this temperature by means of a water circulation bath. During the measurements N_2 was insufflated into the cell in order to avoid carbonation of the solutions. All measurements were conducted at constant ionic strength using solutions of NaCl 0.1 M.

During the titrations, computer-controlled volumes of the titrant solutions were added to the starting solution. The potential was read at fixed times.

The characteristics of the acquisition are chosen by setting seven parameters:

1. Maximum number of readings.
2. Time interval between two measures.
3. Tolerance on the standard deviation.
4. Tolerance on the drift.
5. Volume of titrant initially added.
6. Total volume of titrant to be added.
7. Increase of volume of titrant.

The data obtained are then processed with the calculation program HYPERQUAD[30].

[30] P. Gans, A. Sabatini, A. Vacca, *Talanta*, **1996**, 43,1739-1753.

2.2.1.1 Calculation methods

When you have to determine the equilibrium constants of the species present in a solution it is not possible to use methods of direct measurement. However, the concentration of one of the components is often in relation with the equilibrium constants and the initial concentrations of the system.

The measurement can be carried out by potentiometric through the calculation of the potential difference between a reference electrode and a working electrode. The reference electrode potential is obtained experimentally, while that of the working electrode is a function of the concentration of the targeted species.

In the case of complexation equilibria involving a protonable ligand, the targeted species for the determination of the equilibrium constants is the hydrogen ion, whose concentration is measured by a glass electrode.

The dependence of the measured potential by the hydrogen ion concentration is brought out by the Nernst equation:

$$E = E^0 + \frac{RT}{F} ln[H^+]$$

E^0 is experimentally determined in the specific conditions required by potentiometric measurements.

The calibration of the reference electrode is performed by titration of a known amount of strong acid (HCl) with a strong base (NaOH). This allows obtaining the values of both E^0 and ionic product of water.

The equivalent point in the titration was determined by the Gran's method.

In aqueous solution the formation of a metal ion complex with a protonable ligand L can be expressed by the equation:

$$pM + qL + rH = M_pL_qH_r$$

Where M, L and H are the metal, the protonable ligand and the hydrogen ion, while p, q and r represent the stoichiometry coefficients.

For each complex species we can define a formation constant:

$$\beta_{pqr} = \left[M_pL_qH_r\right] \Big/ [M]^p[L]^q[H]^r$$

In hydroxylated complexes, the constant βpqr is related to the equation:

$$pM + qL + rH_2O = M_pL_q(OH)_r + rH$$

β_{pqr} is in relation with β' the constant:

$$\beta' = \left[M_pL_q(OH)_r\right] \Big/ [M]^p[L]^q[OH]^r$$

The two constants are related by the water ionic product:

$$\beta_{pqr} = \beta'(K_W)^r$$

In addition, the ligand may undergo processes of protonation independently by the presence of the metal:

$$L + jH = H_jL$$

and we can define a corresponding protonation constants:

$$\beta_{01j} = \left[H_JL\right] \Big/ [L][H]^j$$

In the study of a metal-ligand interaction, the first step is therefore the determination by potentiometry of the protonation constants of the free ligand, by titrating the free ligand with a strong base starting form a known acidic pH value (generally raging between 2 and 2.5). The second step consists in a titration of a solution containing both metal and ligand, once again using a strong base as titrant a starting form a known acidic pH value.

The total concentrations of metal, ligand and protons are defined by the equations:

$$T_M = [M] + \sum\nolimits_{pqr} p\left[M_pL_qH_r\right]$$

$$T_L = [L] + \sum\nolimits_{pqr} q\left[M_pL_qH_r\right] + \sum\nolimits_{j} \left[H_JL\right]$$

$$T_H = [H] + \sum\nolimits_{pqr} r\left[M_pL_qH_r\right] + \sum\nolimits_{j} \left[H_JL\right] - [OH]$$

Substituting the expressions for β_{pqr} and β':

$$T_M = [M] + \sum\nolimits_{pqr} p\beta_{pqr}[M]^p[L]^q[H]^r$$

$$T_L = [L] + \sum\nolimits_{pqr} q\beta_{pqr}[M]^p[L]^q[H]^r + \sum\nolimits_{j} \beta_{01j}[L][H]^j$$

$$T_H = [H] + \sum\nolimits_{pqr} r\beta_{pqr}[M]^p[L]^q[H]^r + \sum\nolimits_{j} \beta_{01j}[L][H]^j - [OH]$$

The formation of a complex in aqueous solution resulting from the interaction of a protonable anion A^{n-} with a protonable ligand L^{m+} can be expressed by the following equation, in which the charges have been omitted for simplicity:

$$pA + qL + rH = A_pL_qH_r$$

In this system anion-ligand-proton can form a large number of complexes, each featuring different combination of the three coefficients p, q and r. For each one we can define a formation constant:

$$\beta_{pqr} = \left[A_pL_qH_r\right] \Big/ [A]^p[L]^q[H]^r$$

The anion and the ligand may undergo processes of protonation and thus we have to consider also the equilibria:

$$A + iH = H_iL$$
$$L + jH = H_jL$$

and the corresponding stability constants:

$$\beta_{10i} = {[H_iA]}/{[A][H]^i}$$

$$\beta_{01j} = {[H_jL]}/{[L][H]^j}$$

In the study of a particular anion-receptor system, the procedure generally followed implies first the determination of the basicity constants of the anion and the ligand via separated potentiometric titration. The second step is the titration of a solution containing both anion and ligand in known concentrations. The titration is usually carried out by starting at a known acidic pH and titrating with a strong base (NaOH).

The total concentration of the species involved in complex formation is defined by:

$$T_A = [A] + \sum_{pqr} p[A_pL_qH_r] + \sum_i [A_iL]$$

$$T_L = [L] + \sum_{pqr} q[M_pL_qH_r] + \sum_j [H_iL]$$

$$T_H = [H] + \sum_{pqr} r[A_pL_qH_r] + \sum_i i[A_iL] + j\sum_j j[H_iL] - [OH]$$

Substituting the expressions for β_{pqr} and β':

$$T_A = [A] + \sum_{pqr} p\beta_{pqr}[A]^p[L]^q[H]^r + \sum_i \beta_{10i}[A][H]^i$$

$$T_L = [L] + \sum_{pqr} q\beta_{pqr}[M]^p[L]^q[H]^r + \sum_j \beta_{01j}[L][H]^j$$

$$T_H = [H] + \sum_{pqr} r\beta_{pqr}[M]^p[L]^q[H]^r + \sum_i i\beta_{10i}[A][H]^i + \sum_j j\beta_{01j}[L][H]^j - [OH]$$

In all cases, the titration curve is obtained plotting the electrode potential as a function of the volume of titrant added. This allows determining the proton concentration. Knowing the initial concentrations of metal and ligand, they are obtained distribution curves of the species present in solution. Each experimental point corresponds to a system of equations in n+2 variables (where n is the number of formed species), e. g. the n stability constants, and concentrations of ligand and free metal cation. For N experimental points we obtain a system of 3N equations in n + 2N variables.

Given the complexity of the mathematical treatment of the data, an iterative calculation method is used. In our case, the data were treated with the HYPERQUAD program, which determines the stability constants of the complexes by exploiting the method of nonlinear least squares. During calculation a variable U

is minimized. U depends on experimental data and it is mainly related to the electrode potential and errors on the same measures and on the volume of titrant added.

$$U = \sum_i w_i [E_i(calc) - E_i(exp)]^2$$

The coefficient w that appears in the equation takes into account the statistical weight of each experimental point and it is inversely proportional to σ_i^2:

$$\sigma_i{}^2 = \sigma_e{}^2 + \left({}^{dE_i}/_{dV} \right)^2 \sigma_v{}^2$$

This equation contains the estimated variances on the read potential and on the reagent volume added, as well as the derivative dE/dV which represents the titration curve slope.

The slope has a high value in proximity of the equivalence point. Consequently the coefficient weigh assigned to the points collected in this part of the potentiometric curve are generally small, while the weight is larger for the data points collected in the buffer zone.

U also depends on E_i(exp) and E_i(calc), e.g. the measured potential and the experimentally calculated potential, respectively. E_i(calc) is obtained from the experimental parameters (concentration, E^0, K_w) and form the equilibrium constants of the system studied.

The program solves the matrix equation:

$$A^T\ W\ A\ s = A^T\ W\ e$$

where W is the matrix of the statistical weights, A is the partial derivatives matrix of the potential respect to the parameters to refine, A^T is its transposed and the discard vector on potential [E(calc)-E(exp)], s is the vector deviations to be applied to the parameters to be refined. The latter values are those to be determined in the process of refining to obtain the minimization of U.

The best refinement possible with the available experimental data is achieved when a group of self-consistent values is obtained.

The calculation program provides two statistical parameters to verify the quality of refinement.

The first is the value of standard deviations, defined as:

$$\sigma = \left({}^{e^T\ W\ e}/_{m-n} \right)^{1/2}$$

where m is the number of points and n the number of parameters to be refined.

The best value of σ is 1, but, as suggested by the program authors, all values of σ less than 3 can be acceptable.

The second statistical parameter, χ^2, measures the distribution of the differences. If $\chi^2 = 12.6$, the weighed errors are distributed statistically around $\sigma = 0$; in this case there are no systematic errors in the treatment.
Considering the number of points and variables to be refined, the program distributes the points in eight different classes depending on how the errors are distributed around $\sigma = 0$, in order to set a value with $\sigma = 0$.
Each class is defined by assuming a normal distribution of errors and that each class contains an equal number of points.
Based on the difference between the number of experimental points and number of theoretical points, χ^2 is calculated for each class by the expression:

$$\chi^2 = \sum_i \chi^2 \qquad \text{where} \qquad \chi_i{}^2 = {}^{8(m/8 - m_i)^2}/_{m}$$

with m the total number of points in the system and m_i number of experimental points of the i^{th}-class.
If the value of χ^2 is greater than 12.6, the differences do not possess a normal distribution, and this can be due either to systematic errors or to very small.
With a value of 12.6 corresponds to a χ^2 distribution with seven degrees of freedom (the number of classes minus one) and the reliability level is 95%.
The potentiometric titrations can be used for the determination of stability constants only in the absence of unstable species in the range of time necessary to perform the measurement.

2.2.2 Nuclear magnetic resonance

The instrument used for the characterization of the compounds is the Brüker Ultrasheald 400 MHz spectrometer.
The pH of the solutions thus obtained was varied by additions of DCI or NaOD.
pH and pD are related by the following equation: pH = pD – 0.4[31].

2.2.3 Electron spectroscopy UV-Visible

The UV-Visible spectrophotometric measurements were performed by using a Shimadzu UV-2101PC spectrophotometer. Working solutions of ligands and complexes were obtained by appropriate dilution of stock solutions, prepared by direct weigh directly in MilliQ water.
In the case of pH titrations, the solutions were placed in quartz cuvettes with an optical path of 1 cm. The pH was varied by small volumes additions of HCl and NaOH solutions in order to consider negligible the variation in volume of the sample.

[31] D. J. Cram, *Angew. Chem. Int. Ed Eng.*, **1986**, 25, 1039.

2.2.4 Fluorescence emission spectroscopy

The fluorescence measurements were obtained with a PerkinElmer Lumiscence Spectrofotometer LS 55 spectrofluorimeter. The working solutions of ligand and complexes were obtained by appropriate dilution of stock solutions, prepared by direct weigh in MilliQ water.

The solutions were placed in a quartz fluorescence cuvette with an optical path of 1 cm and a volume of 3ml.

Titrations were conducted by direct addition into the cuvette of known volumes of titrant solutions. After each addition the pH was adjusted by adding small volumes of concentrated solutions of HCl and NaOH, in order to neglect the volume variation.

3 Discussion

3.1 Cyclen derivates

3.1.1 Ligands synthesis

Considering ligand synthesis, several ligands has been obtained by using the bis-aminal procedure. The functionalization of macrocycles such as cyclam and cyclen protected with glyoxal is already known and reported in the literature[32]. We have modified the already known methods, in order to obtain a synthetic route well suited for monofunctional and bifunctional of cyclen with fluorogenic units[33]. Starting from the commercial product 8-hydroxy-quinolin-2-carboxy aldehyde, we have reduced the carbonyl group using $NaBH_4$. The resulting alcohol transformed in its corresponding dichloro derivative by nucleophilic substitution with thionyl chloride, to finally obtain 8-hydroxy-2-chloromethyl-quinoline (scheme 3.1).

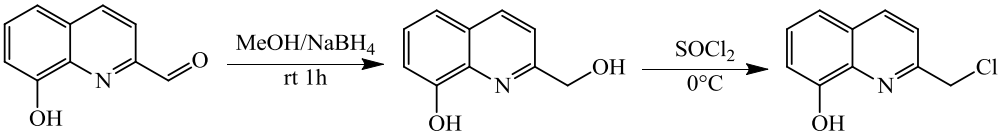

Scheme 3.1

The use of protected cyclen with glyoxal, i.e. the bis-aminal cyclen derivative is the key point of this synthetic procedure. In this bis-aminal compound, only two of four amino groups present in the macrocycle (in 1,7 position, i.e. in trans position) are reactive toward nucleophilic reagents. In fact, the two remaining amino groups have their non-bonding electron pairs oriented towards the center of the cavity and this inhibits their reactivity. In consequence, the nucleophilic substitution reactions of amino groups stereoselectively occur in 1,7 position.

Furthermore, the functionalization of the first nitrogen atom is typically much faster than the nucleophilic substitution on the second amino group. This may allow the isolation of the product mono-functionalized before the formation of the bifunctionalized compound. In our case, we have observed that the cationic monofunctionalized product appears poorly soluble in some solvents, making even easier to isolate the mono-functionalized product. For this reason, we chosen for the synthesis of mono-functionalized products, THF as solvent. In fact, our mono-functionalized products are poorly soluble in this solvent and they can therefore easily removed away from the reaction mixture by filtration, thereby preventing the formation of further substituted compounds. For the synthesis of bi-functionalized

[32] M. Le Baccon, F. Chuburu, L. Toupet, H. Handel, M. Soibinet, I. Déchamps-Olivier, J. Barbier and M. Aplincourt, *New J. Chem*., **2001**, 25, 1168-1174

[33] F. Rizzo, F. Meinardi, R. Tubino, R. Pagliarin, G. Dellepiane, A. Papagni, *Synthetic Metals,* **2009,** 159, 356–360

products, we carried out the functionalization of the bis-aminals in CH_3CN, where the monofunctionalized intermediate is soluble while the bifunctionalized product show a scarce solubility and it can be separated at the end of the reaction by filtration. We can conclude that the exploitation of the peculiar reactivity of the cyclen bis-aminal and the solvent choice are decisive to direct the functionalization in precise positions with excellent selectivity. This synthetic method can also be of interest to synthesize not-symmetrical products, e.g., to insert two different functional groups within the macrocyclic structure, simply by using a two steps procedure. In fact, we can isolate mono-functionalized a bis aminal product, which can then, be used as the starting reagent to obtain a bi-functionalized product with two different substituents. (Scheme 3.2)

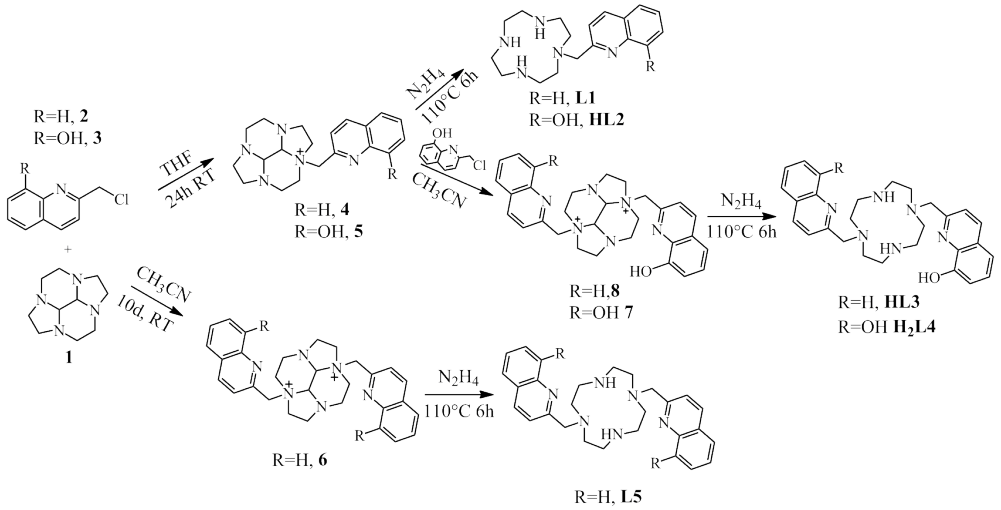

Scheme 3.2

3.1.2 Ligand acid-base properties

In aqueous solution the amino groups of the synthesized ligands give acid-base equilibria that compete with metal ions coordination. Furthermore, ligand protonation can affect the fluorescence emission intensity. The five ligands **L1-L5** are water soluble and the acid-base characteristics have been studied by potentiometric and spectroscopic (UV-visible absorption and fluorescence emission) measurements.

Potentiometric titrations show that the ligands **L1** and **L5** can bind up to three protons in aqueous solution in the pH range investigated. Conversely, H**L2**, H**L3** and H_2**L4** give rise to a larger number of acid-base equilibria, four in the case of H**L2** and H**L3** and five in the case of H_2**L4**, due to the presence of the hydroxyl groups, which may undergo deprotonation reactions. Tables 3.1-3.5 report the protonation equilibria observed in potentiometric measurements and the corresponding constants, determined in aqueous solution for the five ligands. Due to

known slow kinetics in the metal coordination by the cyclen we performed the potentiometric measures at 308.1°K.

Equilibrium	**L1**
$L + H^+ = [LH]^+$	10.71(5)
$[LH]^+ + H^+ = [LH_2]^{2+}$	8.90(7)
$[LH_2]^{2+} + H^+ = [LH_3]^{3+}$	2.3(1)

Table 3.1 Protonation constants of **L1**, standard deviation in parentheses (308.1K, NaCl = 0.1 M).

Equilibrium	**HL2**
$L^- + H^+ = [LH]$	11.06(6)
$[LH] + H^+ = [LH_2]^+$	10.54(5)
$[LH_2]^+ + H^+ = [LH_3]^{2+}$	8.85(5)
$[LH_3]^{2+} + H^+ = [LH_4]^{3+}$	2.88(7)

Table 3.2 Protonation constants of H**L2**, standard deviation in parentheses (308.1K, NaCl = 0.1 M).

Equilibrium	**HL3**
$[L]^- + H^+ = [LH]$	11.08(2)
$[LH] + H^+ = [LH_2]^+$	9.35(4)
$[LH_2]^+ + H^+ = [LH_3]^{2+}$	8.79(6)
$[LH_3]^{2+} + H^+ = [LH_4]^{3+}$	2.3 (1)

Table 3.3 protonation constants of H**L3**, standard deviation in parentheses (308.1K, NaCl = 0.1 M).

Equilibrium	**H_2L4**
$L^{2-} + H^+ = [LH]^-$	10.66(4)
$[LH]^- + H^+ = [LH_2]$	11.01(7)
$[LH_2] + H^+ = [LH_3]^+$	9.90(6)
$[LH_3]^+ + H^+ = [LH_4]^{2+}$	9.2(1)
$[LH_4]^{2+} + H^+ = [LH_5]^{3+}$	3.9(1)

Table 3.4 Protonation constants of H_2**L4**, standard deviation in parentheses (308.1K, NaCl = 0.1 M).

Equilibrium	**L5**
$L + H^+ = [LH]^+$	10.54(4)
$[LH]^+ + H^+ = [LH_2]^{2+}$	8.72(6)
$[LH_2]^{2+} + H^+ = [LH_3]^{3+}$	2.74(8)

Table 3.5 Protonation constants of **L5**, standard deviation in parentheses (308.1K, NaCl = 0.1 M).

From the data in tables 3.1-3.5 we can calculate the species distribution diagrams that are shown below in figures 3.1.

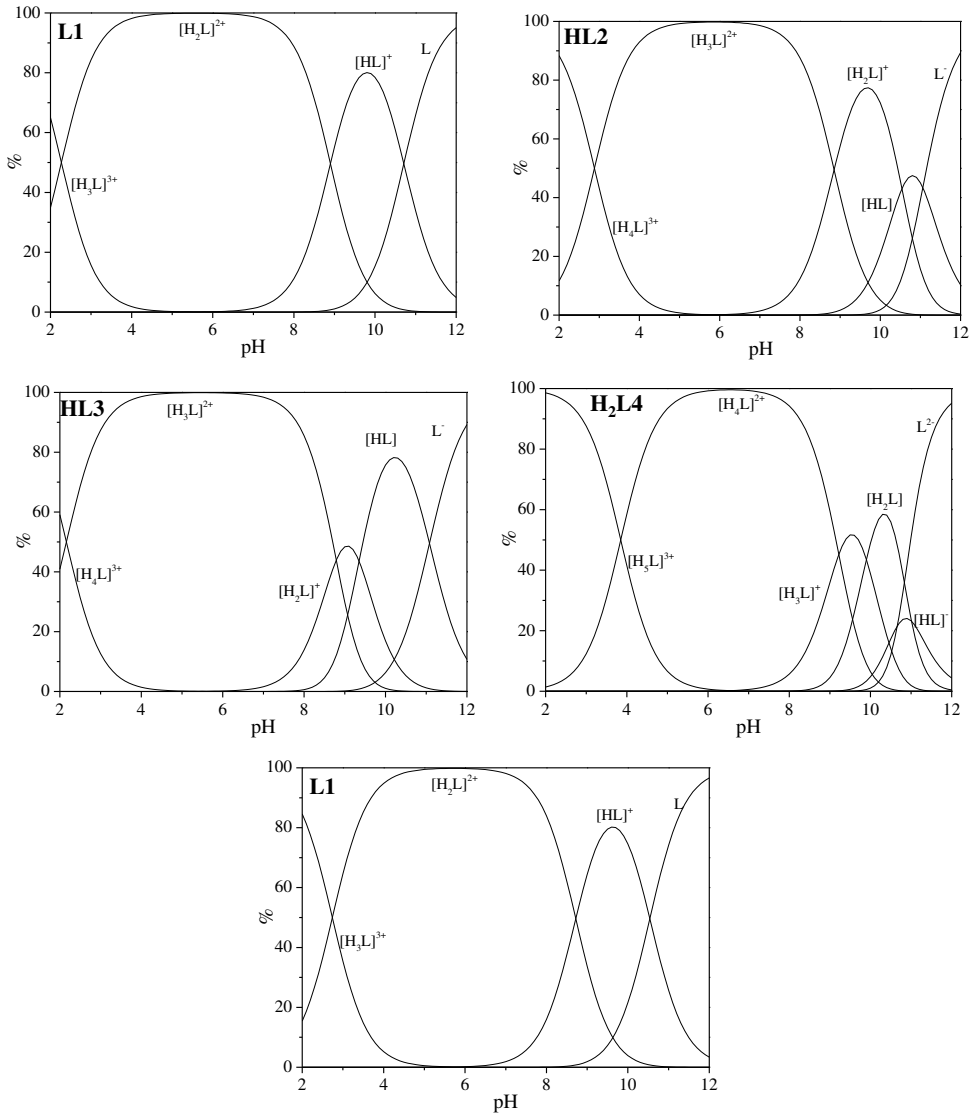

Figure 3.1 Distribution diagrams calculated by using the protonation constants for the ligands **L1**-**L5** ([L]=10^{-3} M 308.1K, NaCl = 0.1 M).

The ligands **L1** and **L5**, containing one or two quinoline units give rise to nearly equal distribution diagrams, as expected considering the protonation constants are very similar. At pH values lower than 4 only a tri-protonated species is formed in solution. **L1** and **L5** are in their fully deprotonated neutral form at strongly alkaline pH (pH >10), while at pH 10 the prevalent species is $[LH]^+$. At neutral pH value, we find the almost exclusive presence of the species $[LH_2]^{2+}$.

For ligands H**L2**, H**L3** and H_2**L4** we have to consider that the -OH groups quinoline ring can deprotonate. It is known as the quinoline nitrogen atom has scarce basic characteristics (log K_a < 3), while the hydroxyl group unit 8-hydroxyquinoline has

poor acid characteristics (log K_a > 9). Conversely, cyclen has marked basic characteristics, at least in its two first protonation equilibria (pK_{a1}=11.27; pK_{a2}=9.96). The first two protonation equilibria can involve either the cyclen nitrogen atoms or 8-hydroxyquinoline phenol groups, having similar basic characteristics. Finally the acid-base equilibria that take place at low pH values may involve either the cyclen amino groups, or the nitrogen atom of the heteroaromatic system.

To clarify these issues we have performed UV-visible spectrophotometric measurements at different pH values on solutions the different ligands. Considering the UV-vis spectra, their determined by fluorogenic units appended to cyclen. In consequence **L1** and H**L2** display spectral features similar to **L5** and H_2**L4,** respectively, while the absorption characteristics of H**L3**, which contains two different fluorophores, are peculiar of this ligand.

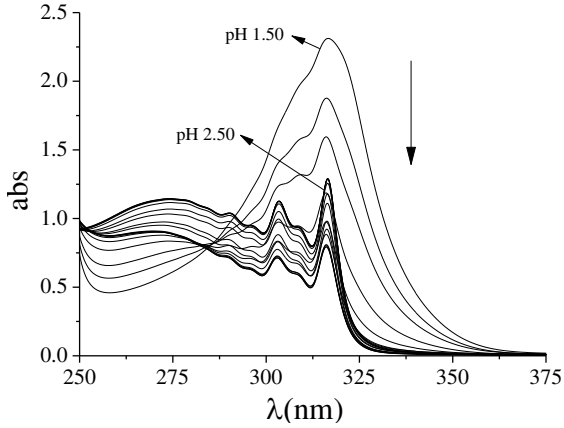

Figure 3.2 Absorption spectra of **L5** at different pH values ([**L5**] = $5 \cdot 10^{-4}$ M)

L1 and **L5** possess the typical absorption spectrum of quinoline and it is not much influenced by pH. In Figure 3.2 we reported the **L5** absorption spectra at different pH values. We can see that the absorption spectrum of **L5**, characterized by a structured band with a maximum at 316 nm, is scarcely pH-dependent in the pH region 2.5-12.5. It is to be noted, however, that the spectral characteristics remarkably change below pH 2.5, where a substantial absorbance increase at 316 nm can be observed, in agreement with protonation of the quinoline unit at very acid pH. To clarify this aspect we have plotted the absorption intensity at 316 nm as a function of pH superimposed on the ligand protonated species distribution diagram of the **L5** (Figure 3.2) .The behavior of the ligand **L1** is similar.

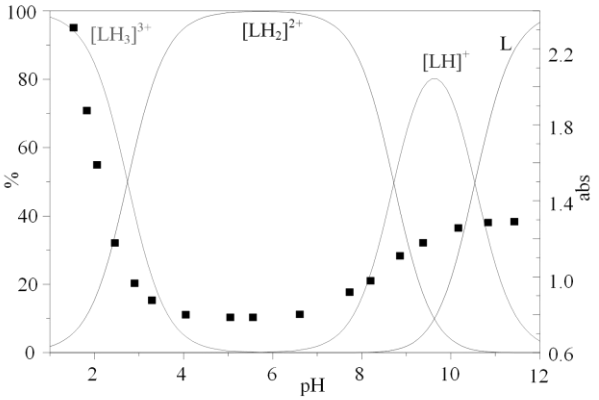

Figure 3.3 Absorbance at 316 nm superimposed on the distribution diagram of the protonated species.

Figure 3.3 clearly shows that the absorbance increase at 316 nm takes place with the formation of the $[H_3L]^{3+}$ species. This suggests that the formation of this species is accompanied by protonation of the quinoline nitrogen atom. The pH dependence of the H**L2** and H_2**L4** spectral characteristics (figure 3.4) has a different trend from that found for **L1** and **L5**. In figure 3.4 we have reported the UV-vis spectra of H_2**L4** at various pH values. H**L2** shows a quite similar behavior.

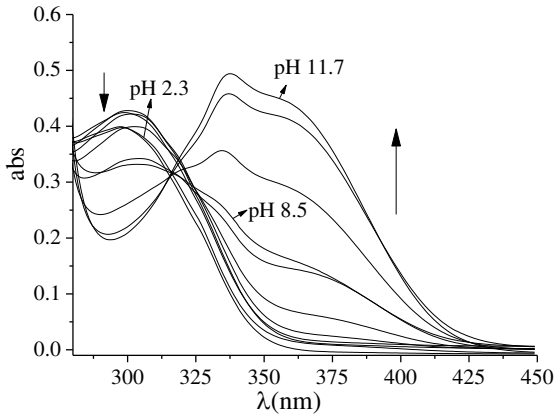

Figure 3.4 Absorption spectra of H_2**L4** at different pH values ([H_2**L4**] = $9 \cdot 10^{-6}$ M)

Figure 3.4 clearly shows the presence of a single band that marked red-shifts form 300 nm to 352 nm as the pH increases. In particular, the ligand is characterized by a band with a maximum at 300 nm at acidic pH values, the intensity of which decreases at alkaline pH, where it can be noted the formation of a new band with a maximum at 352 nm. This behavior can be evidenced reporting the absorption intensity at 300 nm and at 352 nm as a pH function, superimposed on the species distribution diagram. In figure 3.5 we can note that the absorption intensity at 300 nm and 352 nm are almost constant form acidic to neutral pH value, e.g., in the pH region in which the species $[H_5L]^{3+}$ and $[H_4L]^{2+}$ prevails in solution. The $[H_3L]^{+}$

formation at alkaline pH leads to an absorbance increase at 352 nm and a simultaneous absorbance decrease at 300 nm. This suggests that at alkaline pH deprotonation of the 8-hydroxy-quinoline occurs in solution.

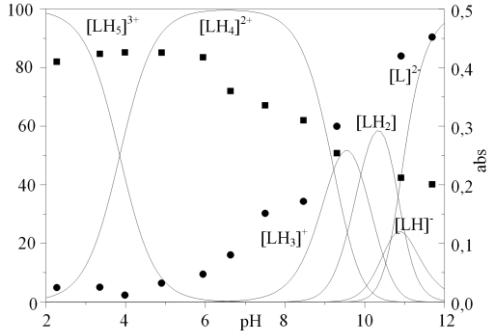

Figure 3.5 Absorbance at 300 (■) and 352 (●) superimposed on the distribution diagram of the protonated species for **H_2L4**.

In particular, this leads us to suggest that depronation of $[H_4\mathbf{L}]^{2+}$ to give $[H_3\mathbf{L}]^{+}$ corresponds to the deprotonation of the fluorophore phenolic OH group, to give a classic band absorption red-shift normally observed for deprotonation of phenol and phenol derivatives. Ligand H**L3**, figure 3.6, shows spectral features similar to those of **L1** at pH values lower than 8.1. However, a higher pH values the formation of a new absorption band is observed in the spectra, attributable to deprotonation of the OH group.

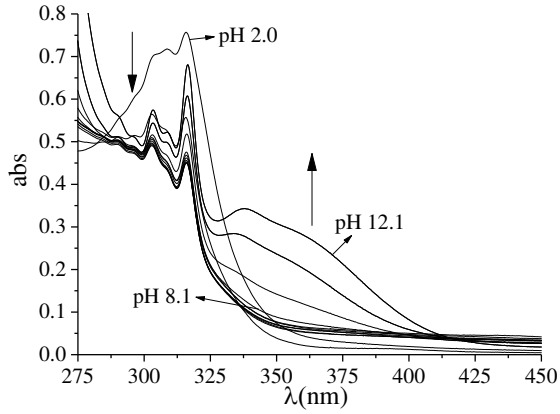

Figure 3.6 Absorption spectra of H**L3** at different pH values ([H**L3**] = $3.6\cdot10^{-5}$ M)

We have subsequently analyzed the fluorescence emission dependence on pH, recording the emission spectra for different pH values with an excitation wavelength of 316 nm. Their emission properties depend on their protonation degree, the most emissive being the species with higher protonation degrees. The not protonated or scarcely protonated species are normally almost not emissive, due

to a photoinduced electron tranfer process from the not protonated amine groups to the fluorophore.

In figure 3.7 we reported the emission spectra recorded at various pH values of ligand **L1**, while Figure 3.8 shows the emission intensity at 400 nm as a function of pH compared with the species diagram formed in solution. **L5** shows a similar pH dependence of emission spectra.

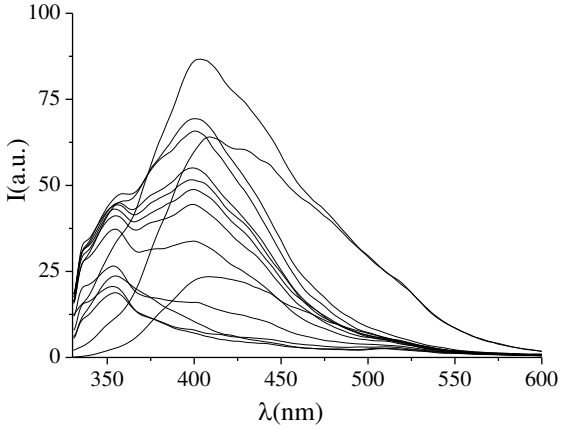

Figure 3.7 Emission spectra of **L1** at different pH values ([**L1**] = $5 \cdot 10^{-4}$M)

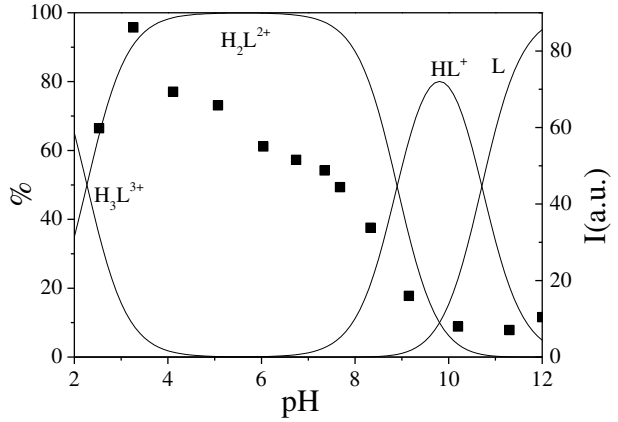

Figure 3.8 L1 Emission intensity at 400 nm pH function superimposed on the **L1** species distribution diagram.

For pH greater than 10, where the ligand is present in fully deprotonated form, the system is very weakly emissive. Once again, this effect is likely to be determined by a fluorescence quenching through a photoinduced electron transfer effect (PET) to the fluorophore in its excited state. The formation of protonated species inhibits this process leading to an emission intensity increase for pH values lower than 10, up to a maximum at pH 3.

For ligands H**L2** and H_2**L4** the fluorescence emission spectra display different pH dependence. In particular, the ligands feature a band at about 405 nm in the acidic

region, while at alkaline pH values both H**L2** and H_2**L4** are characterized by a band at higher wavelengths (465 nm and 524 nm, respectively). The emission spectra of H**L2** and the pH dependence of the emission intensity at 405 and 465 nm are reported in Figures 3.9 and 3.10, respectively. H_2**L4** shows an almost equal pH dependence of its spectral features.

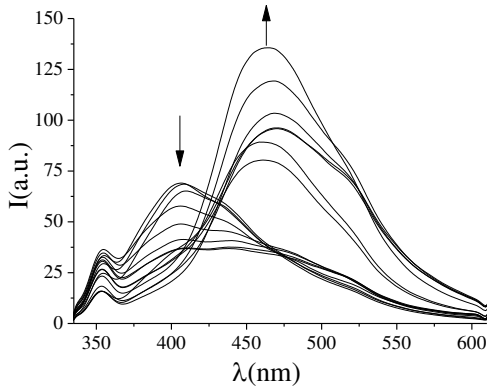

Figure 3.9 H**L2** emission spectra at different pH values ([H**L2**] = $4.8 \cdot 10^{-4}$M).

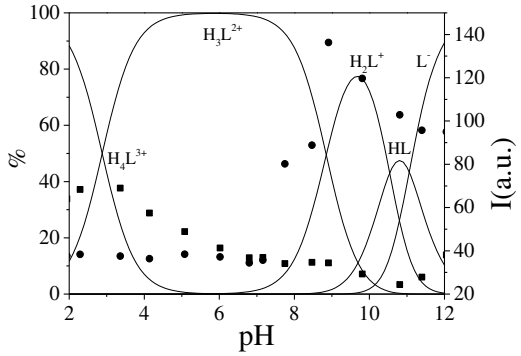

Figure 3.10 Fluorescence emission intensity at 406 (■) and 465 (●) superimposed on the distribution diagram of the protonated species for H**L2**.

As shown in figures 3.9 and 3.10, the emission band at 406 nm, which characterizes the spectra for pH lower than 4, decreases progressively from pH 4 to pH 6. These spectral changes can be associated to the deprotonation of the species $[\mathbf{L}H_4]^{3+}$ to give the species $[\mathbf{L}H_3]^{2+}$. Conversely, at alkaline pH values, the formation of a new emission band at 465 can be observed, the intensity of which increases from pH 7 to pH 10. The latter changes are attributable to deprotonation of the 8-hydroxyquinoline -OH group, and occurs upon deprotonation of the $[\mathbf{L}H_3]^{2+}$ species to give the $[\mathbf{L}H_2]^{+}$ form (Figure 3.10).

3.1.3 Metal ions coordination in aqueous solution

To analyze the coordination properties of ligands **L1-L5** towards metal cations, we have carried out potentiometric, spectrophotometric and fluorescence emission measurements in aqueous solution. The metal cations studied were Zn(II), Cd(II), Pb(II) and Cu(II). We have studied these four metals because Zn(II) and Cd(II) are able to inhibit the PET effect, often giving fluorescent complexes. Conversely, Pb(II) is an example of heavy metal and Cu(II) is an example of paramagnetic metal and normally quench the emission of the ligand. Potentiometric measurements have allowed us to determine the complexes formed and their stability constants. We have then recorded UV-vis absorption spectra at different pH values in order to analyze, where possible, the spectral features of each species. Finally, we have analyzed the effect of metal coordination on the ligands fluorescence emission properties, to verify whether these systems can be considered fluorescence chemosensors for the investigated metal cations.

Potentiometric titrations in aqueous solution point out that all receptors form mononuclear complexes with Zn(II), Cu(II), Cd(II) and Pb(II). The stability constants of the complexes determined through potentiometric measurements are reported in Tables 3.6-3.10.

Equilibrium	Zn(II)	Pb(II)	Cu(II)	Cd(II)
$L + M^{2+} = [LM]^{2+}$	16.37 (3)	15.78 (4)	20.3 (1)	15.19 (2)
$[LM]^{2+} + H^{+} = [MLH]^{3+}$	3.77 (3)	3.73 (8)	-	3.59 (9)
$[LM]^{2+} + OH^{-} = [ML(OH)]^{+}$	2.27 (6)	-	-	1.8 (1)
$[ML(OH)]^{+} + OH^{-} = [ML(OH)_2]$	4.80 (4)	-	-	-

Table 3.6 Stability constants of the **L1** complexes with Zn(II), Pb(II), Cu(II) and Cd(II), standard deviation in parentheses. (308.1 K, 0.1 M NaCl).

Equilibrium	Zn(II)	Pb(II)	Cu(II)	Cd(II)
$L^{-} + M^{2+} = [LM]^{+}$	18.76 (6)	16.6 (1)	25.4 (1)	-
$[LM]^{+} + H^{+} = [MLH]^{2+}$	10.23 (4)	10.02 (5)	5.6 (1)	-
$L^{-} + H^{+} + M^{2+} = [MLH]^{2+}$	-	-	-	27.95 (1)
$[MLH]^{2+} + H^{+} = [MLH_2]^{3+}$	3.26 (6)	4.21 (9)	-	4.48 (3)

Table 3.7 Stability constants of the **HL2** complexes Zn(II), Pb(II), Cu(II) and Cd(II), standard deviation in parentheses. (308.1 K, 0.1 M NaCl).

Equilibrium	Zn(II)	Pb(II)	Cu(II)	Cd(II)
$[L]^{-} + M^{2+} = [LM]^{+}$	15.5 (1)	-	15.5 (1)	9.9 (1)
$[ML]^{+} + H^{+} = [HML]^{2+}$	10.21 (6)	-	10.4 (1)	11.0 (1)
$[ML]^{+} + OH^{-} = [ML(OH)]$	2.59 (9)	-	-	-

Table 3.8 Stability constants of the H**L3** complexes with Zn(II), Pb(II), Cu(II) and Cd(II). standard deviation in parentheses. (308.1 K, 0.1 M NaCl).

Equilibrium	Zn(II)	Pb(II)	Cu(II)	Cd(II)
$L^{2-} + M^{2+} = [LM]$	18.2 (1)	15.1 (2)	21.1 (5)	-
$[LM] + H^{+} = [MLH]^{+}$	-	10.6 (3)	11.3 (4)	-
$[MLH]^{+} + H^{+} = [MLH_2]^{2+}$	-	9.3 (2)	9.3 (2)	-
$L^{2-} + 2H^{+} + M^{2+} = [MLH_2]^{2+}$	-	-	-	42.35 (6)

Table 3.9 Stability constants of the H_2**L4** complexes with Zn(II), Pb(II), Cu(II) and Cd(II), standard deviation in parentheses. (308.1 K, 0.1 M NaCl).

Equilibrium	Zn(II)	Pb(II)	Cu(II)	Cd(II)
$L + M^{2+} = [LM]^{2+}$	16.74 (9)	13.77 (4)	18.67 (6)	17.10 (4)
$[LM]^{2+} + H^{+} = [MLH]^{3+}$	5.65 (7)	4.0 (2)	2.4 (1)	3.58 (5)

Table 3.10 Stability constants of the **L5** complexes with Zn(II), Pb(II), Cu(II) and Cd(II), standard deviation in parentheses. (308.1 K, 0.1 M NaCl).

In all cases, the complexes with the Cu(II) ion are the most stable, as expected considering the stabilization due to the ligand field for a d^9 ion. However, it should be observed that the Zn(II) and Cd(II) also form particularly stable complexes. In particular, all the complexes are much more stable than those with the simple non-functionalized cyclen (e.g. Log K=15.3 for the formation of the $[Zn(cyclen)]^{2+}$ complex). This is probably due to the involvement of the quinoline nitrogen in metal ion coordination, which leads to an overall complex stabilization. This hypothesis is confirmed by the single crystal X-ray crystal structures of the complexes (see section 3.1.4).

From the data in tables 3.6-3.10, we can calculate the distribution diagrams of the species that are shown below in figures 3.11-3.16.

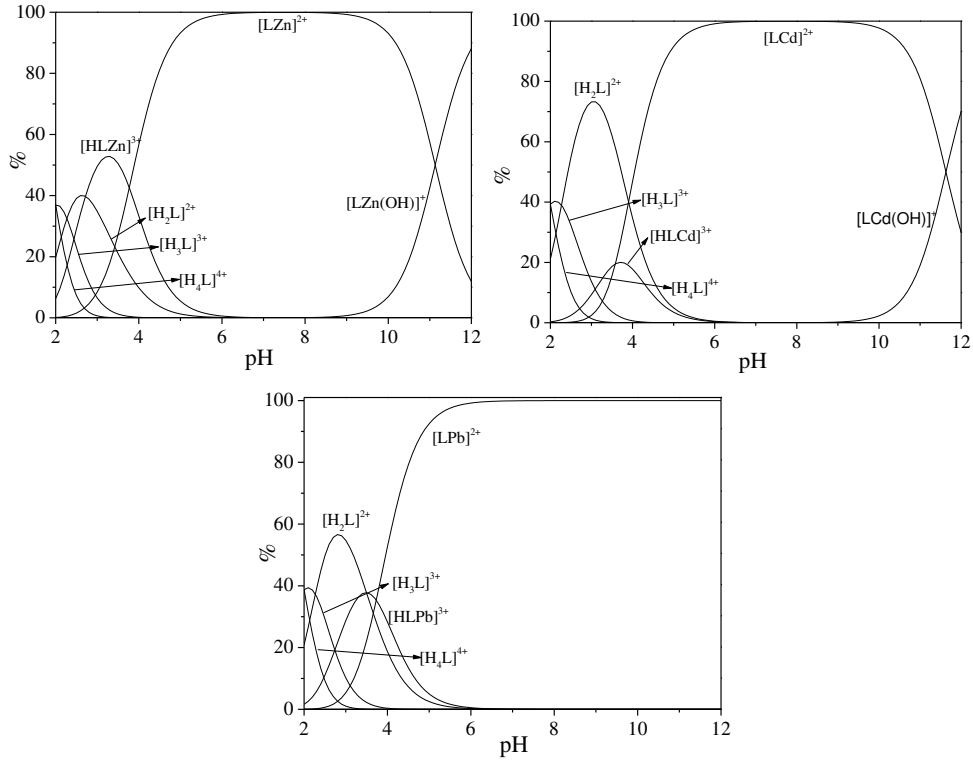

Figure 3.11 Distribution diagrams calculated by using the formation constant of the complex of **L1** with different M(II). ([**L1**]=[M]=10^{-3} M 308.1K, NaCl = 0.1 M).

L1 is able to form complexes with Zn(II) in a wide pH range, figure 3.11, and in fact already at pH > 4 over 50% ligand is involved in the metal coordination. Between pH 5 and 10 the complex $[ZnL]^{2+}$ is almost the only species in solution whereas at alkaline pH the mono-hydroxylated species $[LZnOH]^{+}$ is prevalent in solution. The distribution diagram for the Cd(II) and Pb(II) complex is almost similar, except for the absence of hydroxylated species for Pb(II), while the Cu(II) complex have only one specie and is already completely formed at pH 3

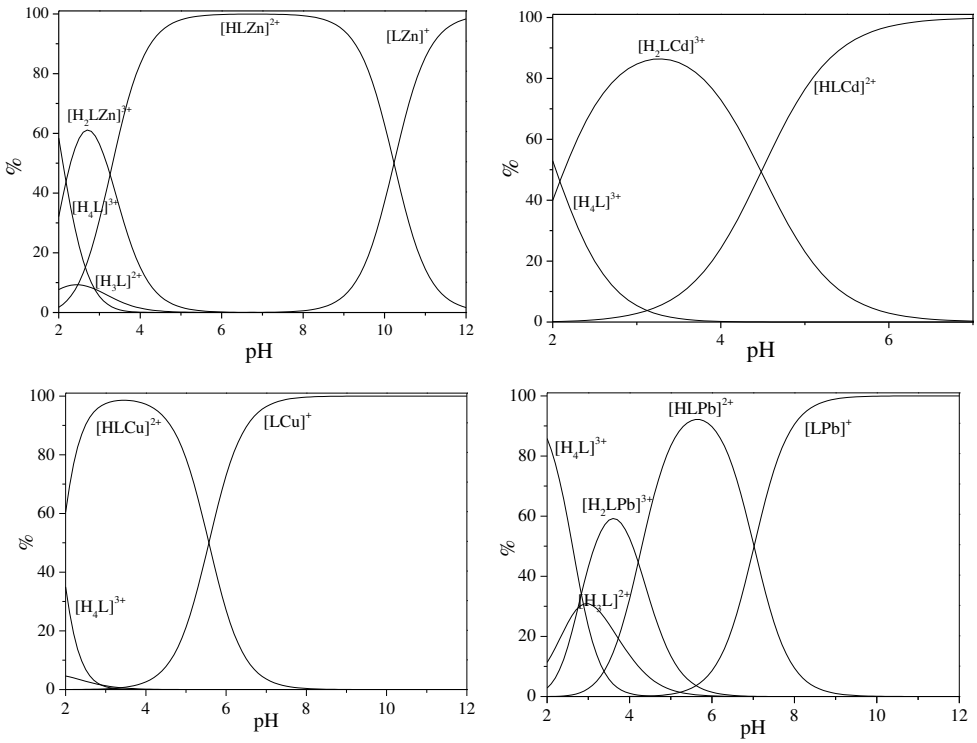

Figure 3.12 Distribution diagrams of the complex with H**L2** with different metal cations. ([H**L2**]=[M]=10^{-3} M 308.1K, NaCl = 0.1 M).

The ligands H**L2**, H**L3** and H_2**L4** have different characteristics in aqueous solution. In particular, H**L2** and H**L3** form stable complexes their mono-anionic **L2**$^-$ and **L3**$^-$ forms, the quinoline group being in its deprotonated form. In a similar manner, H_2**L4** form neutral complexes containing two deprotonated quinoline groups. These complexes are more stable than the corresponding complexes with **L1** and **L5**, probably due to stabilizing electrostatic interactions between the deprotonated phenol functions and the metal cations. In the case of H**L2** and H_2**L4** in the presence of Cd(II) complex precipitation is observed in aqueous solution above pH 7, making not possible to determine the species formed in alkaline environment.

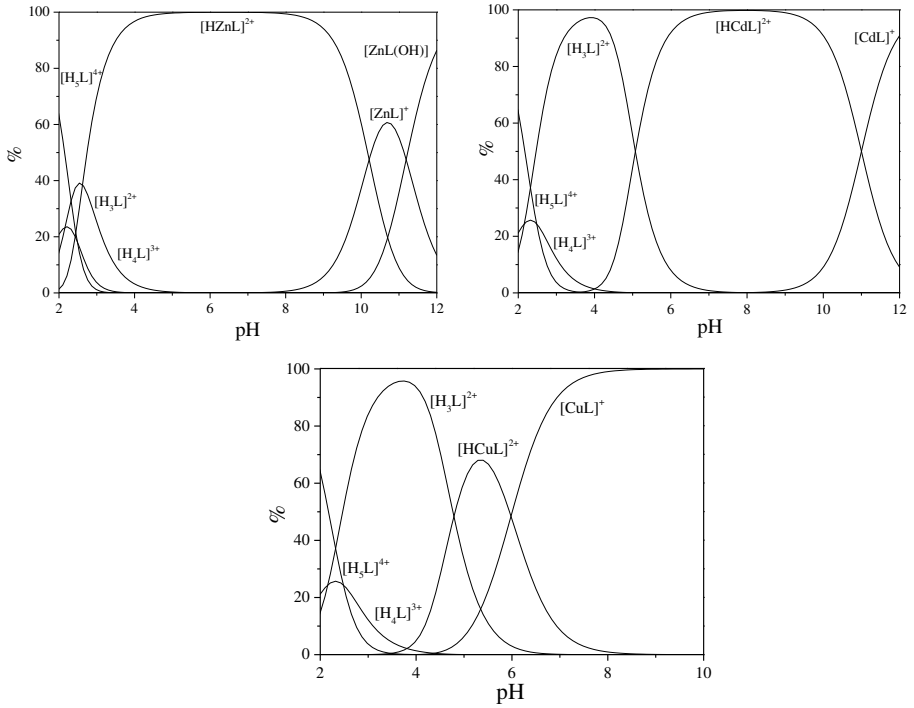

Figure 3.13 Distribution diagrams calculated by using the formation constant of the complex of H**L3** with different M(II). ([H**L3**]=[M]=10^{-3} M 308.1K, NaCl = 0.1 M).

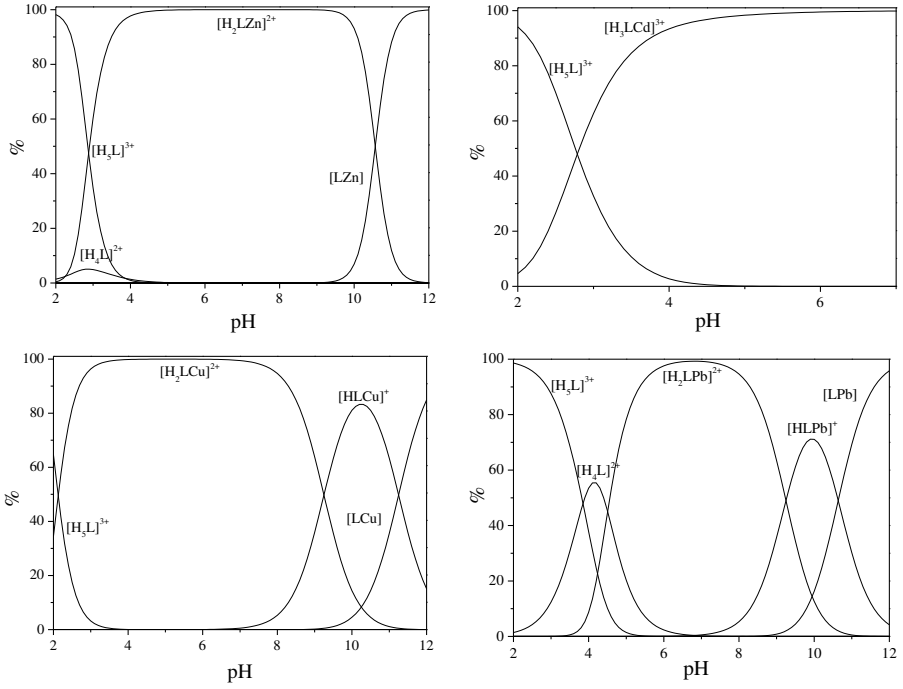

Figure 3.14 Distribution diagrams calculated by using the formation constant of the complex of H_2**L4** with different M(II). ([H_2**L4**]=[M]=10^{-3} M 308.1K, NaCl = 0.1 M).

The distribution diagrams of the **L5** complexes are similar to **L1**, with the only exception of the absence of hydroxylated species at alkaline pH values. This can be attributed to a more saturated coordination sphere of the metal ions by ligand donor atoms compared to **L1**. This leads us to hypothesize that both quinoline units are involved in the coordination of the metal ions under investigation. This hypothesis is confirmed by crystal structures to the chapter 3.1.4

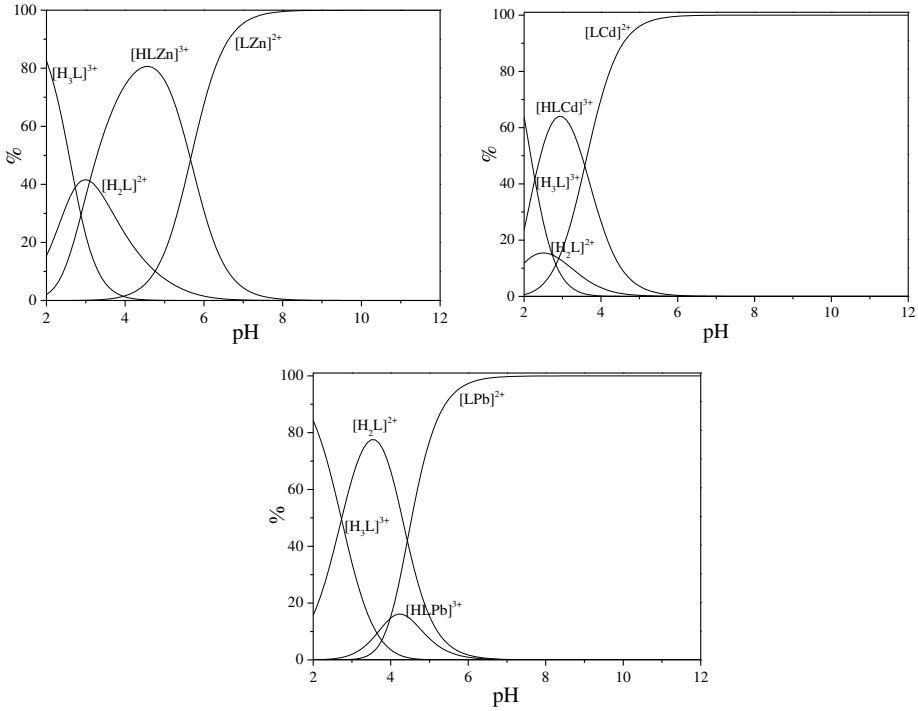

Figure 3.15 Distribution diagrams calculated by using the formation constant of the complex of **L5** with different M(II). ([**L5**]=[M]=10^{-3} M 308.1K, NaCl = 0.1 M).

3.1.4 Crystal structures of metal complexes.

In the course of this work we isolated crystals of the complexes and the crystal structures of the $[Cu\mathbf{L1}]^{2+}$, $[Cd\mathbf{L5}]^{2+}$, $[Zn\mathbf{L5}]^{2+}$, $[HPb\mathbf{L4}]^{+}$, $[H_2Zn\mathbf{L4}]^{2+}$and $[H_2Cd\mathbf{L4}]^{2+}$ complexes were solved

Representations of the $[Cu\mathbf{L1}]^{2+}$, $[Cd\mathbf{L5}]^{2+}$, $[Zn\mathbf{L5}]^{2+}$, $[HPb\mathbf{L4}]^{+}$, $[H_2Zn\mathbf{L4}]^{2+}$and $[H_2Cd\mathbf{L4}]^{2+}$ complexes are shown in figure 3.16-3.17

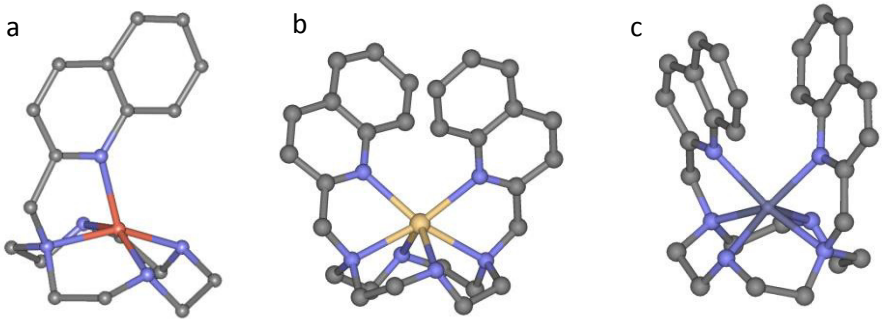

Figure 3.16 a) $[[Cu\mathbf{L1}](ClO_4)_2(H_2O)]$; b) $[[Cd\mathbf{L5}](ClO_4)_2(H_2O)]$; c) $[[Zn\mathbf{L5}](ClO_4)_2 1/2(H_2O)]$.

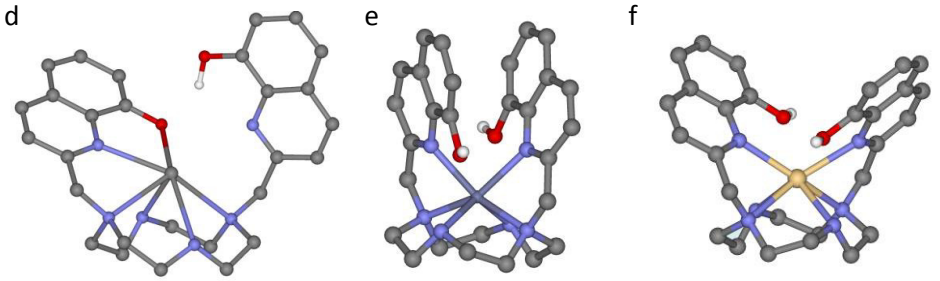

Figure 3.17 d) $[[PbH\mathbf{L4}](ClO_4)(H_2O)]$; e) $[[ZnH_2\mathbf{L4}](ClO_4)_2(H_2O)]$; f) $[[CdH_2\mathbf{L4}](ClO_4)_2(H_2O)]$.

X-ray characterization of the complexes may lead to relevant information on the ligands properties. The crystal structures of the $[Cu\mathbf{L1}]^{2+}$, $[Cd\mathbf{L5}]^{2+}$, $[Zn\mathbf{L5}]^{2+}$, $[HPb\mathbf{L4}]^{+}$, $[H_2Zn\mathbf{L4}]^{2+}$and $[H_2Cd\mathbf{L4}]^{2+}$, solved in collaboration with Prof. C. Bazzicalupi, Dr. E. Macedi, Dr. P. Rossi and Prof. P. Paoli.

3.1.4.1 Crystal structures of L1 metal complexes.

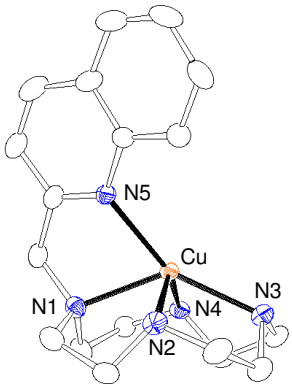

Cu - N4	2.06 (4)
Cu - N3	2.01 (4)
Cu - N5	2.14 (4)
Cu - N1	2.00 (5)
Cu - N1	2.03 (5)

N4 - Cu - N3	86.1 (2)
N4 - Cu - N5	81.2 (2)
N4 - Cu - N1	86.9 (2)
N4 - Cu - N2	151.8 (2)
N3 - Cu - N5	102.3 (2)
N3 - Cu - N1	147.3 (2)
N3 - Cu - N2	85.2 (2)
N5 - Cu - N1	108.1 (2)
N5 - Cu - N2	127.0 (2)
N1 - Cu - N2	86.0 (2)

Figure 3.18 ORTEP-3 view of complex [Cd**L1**]$^{2+}$. Hydrogen atoms have been omitted for clarity, bond distances in **L1**-Cu.

The structure shows that the metal ion is pentacoordinated by the five nitrogen atoms of the ligand with a distorted square-pyramidal geometry. The four atoms of the macrocyclic system constitute the basal plane, while the nitrogen atom of the quinoline unit occupies the apical position. The metal ion lies at approximately 0.15 Å above the plane defined by the four nitrogen atoms of cyclen unit, shifted toward the nitrogen atom in apical position. Distances Zn-N are *ca* 2 Å (only the nitrogen atom heteroaromatic is at a slightly greater distance), reflecting the formation of Cu-N bonds particularly stable.

3.1.4.2 Crystal structures of H_2L4 metal complexes.

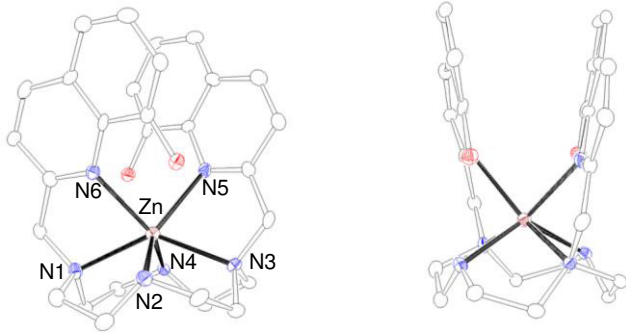

Figure 3.19 ORTEP-3 view of complex [Zn**L4**]$^{2+}$. Hydrogen atoms have been omitted for clarity.

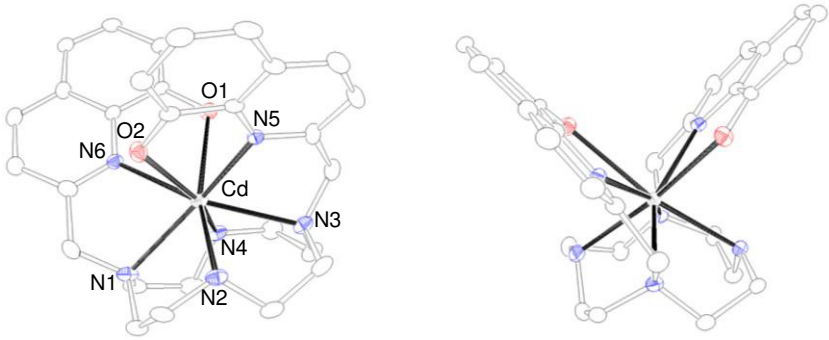

Figure 3.20 ORTEP-3 view of complex $[Cd\mathbf{L4}]^{2+}$. Hydrogen atoms have been omitted for clarity.

Concerning the coordination of the two metal cations, Cd(II) is octacoordinated, being the donor atoms the six nitrogen atoms and the two oxygen atoms provided by the ligand $H_2\mathbf{L4}$ (see table 3.11-3.12 for bond distances and angles). The resulting coordination geometry may be described as a distorted square anti-prism, being the square faces defined by N1, N2, N3,N4 and N5, N6, O1, O2 (the angle between the mean planes defined by these atoms is 1.21(2)°).

Zn(II) is hexacoordinated by the six nitrogen atoms of $H_2\mathbf{L4}$ (see table 3.11-3.12 for bond distances and angles). The resulting coordination polyhedron is a distorted trigonal prism being the trigonal faces those defined by N3, N4, N6 and N1, N2, N5 (the angle between the mean planes defined by these atoms is 4.5(3)°)

The two side arms of the ligand $H_2\mathbf{L4}$ point toward the ligand macrocyclic ring, the angles between the mean planes defined by the non-hydrogen atoms of the two aromatic rings and the mean planes defined by the nitrogen atoms of the macrocyclic base are 50.3(2) and 45.0(2)° the angle between the aromatic rings is 85.8(2)° in $[CdH_2\mathbf{L4}]^{2+}$ and 66.9(2) and 79.5(2)°, the angle between the aromatic rings is 37.7(1)°]in $[ZnH_2\mathbf{L4}]^{2+}$.

The conformation taken by the macrocyclic base is the usual [3,3,3,3]-C corner.

In both structures an OH group of $H_2\mathbf{L4}$ interacts with a perchlorate anion while the other gives place to an H-bond with a water molecule (O2-H2O···O1w). In addition one water molecule bridges together two perchlorate anions.

Bond	**L4-Cd**	**L4-Zn**
M-N1	2.392(7)	2.2390(1)
M-N2	2.438(7)	2.1636(1)
M-N3	2.354(8)	2.2339(1)
M-N4	2.492(8)	2.1708(1)
M-N5	2.413(7)	2.2462(1)
M-N6	2.370(7)	2.2302(1)
M-O1	2.707(6)	
M-O2	2.622(6)	

Table 3.11 Bond distances in $[ZnH_2\mathbf{L4}](ClO_4)_2(H_2O)$ and $[CdH_2\mathbf{L4}](ClO_4)_2(H_2O)$.

	L4-Cd	L4-Zn
N1-M-N2	73.3(2)	80.3(2)
N1-M-N3	111.8(3)	134.0(1)
N1-M-N4	73.9(3)	78.9(4)
N1-M-N5	132.0(2)	74.5(1)
N1-M-N6	84.9(3)	146.4(3)
N2-M-O2	80.5(2)	
N2-M-N3	75.8(3)	78.9(2)
N2-M-N4	120.4(3)	124.4(1)
N2-M-N5	69.0(2)	93.1(2)
N2-M-N6	150.7(2)	131.2(1)
N2-M-O2	92.5(3)	
N3-M-N4	72.4(3)	79.8(3)
N3-M-N5	86.5(3)	146.9(1)
N3-M-N6	131.8(3)	74.2(2)
N3-M-O1	163.3(2)	
N3-M-O2	158.9(2)	
N4-M-N5	152.3(2)	128.9(1)
N4-M-N6	69.7(3)	89.9(1)
N4-M-O1	94.0(2)	
N4-M-O2	128.5(2)	
N5-M-N6	116.2(2)	88.1(1)
N5-M-O1	163.3(2)	
N5-M-O2	72.9(2)	
N6-M-O1	80.0(2)	
N6-M-O2	64.2(2)	

Table 3.12 Bond angles in $[ZnH_2\mathbf{L4}](ClO_4)_2(H_2O)$ and $[CdH_2\mathbf{L4}](ClO_4)_2(H_2O)$;

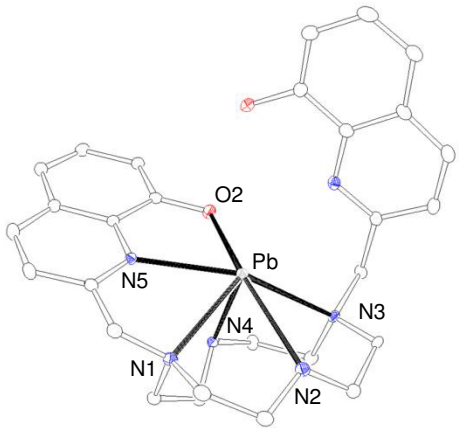

Figure 3.21 Ortep-3 view of $[[PbH\mathbf{L4}](ClO_4)(H_2O)]$.
Hydrogen atoms have been omitted for clarity.

The asymmetric unit of $[PbH\mathbf{L4}](ClO_4)(H_2O)$; contain one $[ML]^{2+}$ cation, one perchlorate anion and one water molecule. In figure 3.21 an ORTEP-3 view of the $[PbH\mathbf{L4}]^{+}$ complex is reported. The Pb(II) metal cation is hexacoordinated being the donor atoms the four nitrogen atoms of the macrocyclic base and one nitrogen atom and one oxygen atom of a quinoline side arm (see table 3.13-3.14 for bond distances and angles).

Pb-N1	2.767(4)
Pb-N2	2.741(4)
Pb-N3	2.393(4)
Pb-N4	2.712(4)
Pb-N6	2.566(3)
Pb-O2	2.492(3)

Table 3.13 Bond distances in [[PbH**L4**](ClO_4)(H_2O)].

N1-Pb-N2	64.1(1)
N1-Pb-N3	86.3(1)
N1-Pb-N4	64.6(1)
N1-Pb-N6	126.8(1)
N1-Pb-O2	158.2(1)
N2-Pb-N3	69.1(1)
N2-Pb-N4	114.9(1)
N2-Pb-N6	144.0(1)
N2-Pb-O2	95.6(1)
N3-Pb-N4	70.4(1)
N3-Pb-N6	77.2(1)
N3-Pb-O2	78.5(1)
N4-Pb-N6	62.3(1)
N4-Pb-O2	122.9(1)
N6-Pb-O2	65.0(1)

Table 3.14 Bond angles in [[PbH**L4**](ClO_4)(H_2O)];.

All the six donor atoms are located on one side of the lead atom, suggesting the presence of a stereochemically active alone pair.
Concerning the relative disposition of the two side arms the mean planes defined by the not-hydrogen atoms of the two aromatic moieties for an angle of 75.45(7)°. In addition, the one containing the donor atoms O2 and N5 form an angle of 31.7(1)° whit the mean plane defined by the four nitrogen atoms of the macrocyclic base, with the "not interacting" one for an angle of 80.5(1)°. The conformation taken by the macrocyclic base is [3,3,2,4]-C corner.

3.1.4.3 Crystal structures of L5 metal complexes.

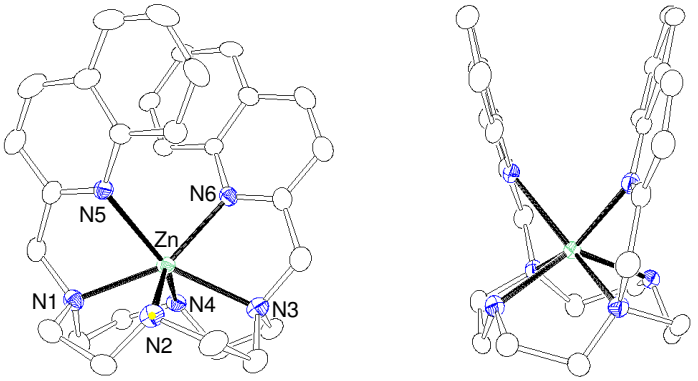

Figure 3.22 ORTEP-3 view of complex [[Zn**L5**](ClO_4)$_2$(1/2H_2O)]. Hydrogen atoms have been omitted for clarity.

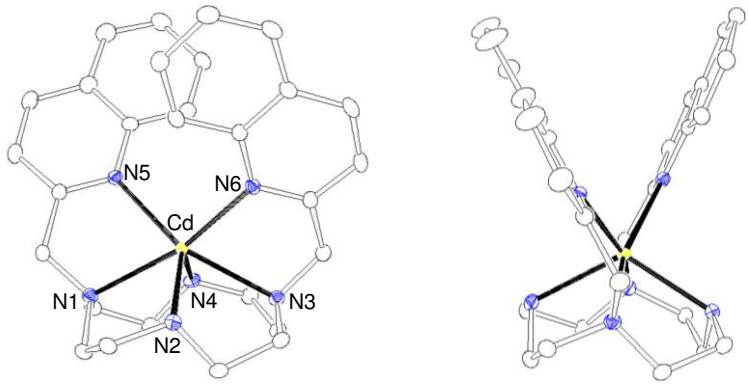

Figure 3.23 ORTEP-3 view of complex [[Cd**L5**]$(ClO_4)_2(H_2O)$]. Hydrogen atoms have been omitted for clarity

The Asymmetric units of [[Cd**L5**]$(ClO_4)_2(H_2O)$] and [[Zn**L5**]$(ClO_4)_2(1/2H_2O)$]; contain one $[ML]^{2+}$ cation and two perchlorate anion, in addition in [[Cd**L5**]$(ClO_4)_2(H_2O)$] one water molecule is present, while in [[Zn**L5**]$(ClO_4)_2(1/2H_2O)$] there is just one half water molecule. The complex cation $[ML]^{2+}$ in all the two structures has a similar conformation, as evidenced in figure 3.24 where the superimposition of $[Cd\mathbf{L5}]^{2+}$ and $[Zn\mathbf{L5}]^{2+}$ is reported.

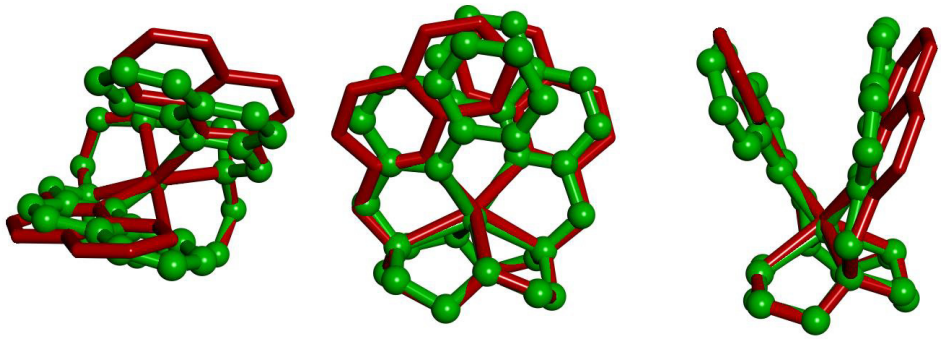

Figure 3.24 Superimposition of $[Cd\mathbf{L5}]^{2+}$ (stick) and $[Zn\mathbf{L5}]^{2+}$ (ball and stick).

Both metal cations, *i.e.* Zn(II) and Cd(II), are hexacoordinated, being the donor atoms the six nitrogen atom provided by the ligand **L5**. The resulting coordination geometry may be described as a distorted trigonal prism, being the trigonal faces those defined by N1, N2, N5 and N3, N4, N6 (the angle between the mean planes defined by these atoms is 10.06(6)°) in [Cd**L5**]$(ClO_4)_2(H_2O)$, and N1, N4, N6 and N2, N3, N5 (the angle between the mean planes defined by these atoms is 2.9(1)°)in [ZnL5]$(ClO_4)_2(1/2H_2O)$. The two side arms of the ligand **L5** point toward the ligand macrocyclic ring, the angles between the mean planes defined by the non-hydrogen

atoms of the two aromatic rings and the mean planes defined by the nitrogen atoms of the macrocyclic base are 59.21(5)° and 69.16(4)°, the angle between the aromatic rings is 51.63(4)° in $[CdL]^{2+}$ and 77.77(8)° and 71.89(9)°, the angle between the aromatic rings is 30.46(8)° in $[ZnL]^{2+}$. The conformation taken by the macrocyclic base is the usual [3,3,3,3]-C corner.

Bond	**L5-Cd**	**L5-Zn**
M-N1	2.352(7)	2.2199(1)
M-N2	2.408(7)	2.1538(1)
M-N3	2.324(8)	2.2236(1)
M-N4	2.392(8)	2.1504(1)
M-N5	2.431(7)	2.2163(1)
M-N6	2.380(7)	2.2001(1)

Table 3.15 Bond distances in **L5**-Cd and **L5**-Zn.

3.1.5 UV-vis absorption spectra in the presence of Zn(II)

The UV-vis spectra of L1 and **L5** (see figure 3.25 for **L1**), in water pH 7 in the presence of increasing amounts of Zn(II) show a marked increase of the quinoline absorption band at 316 nm upon Zn(II) addition.

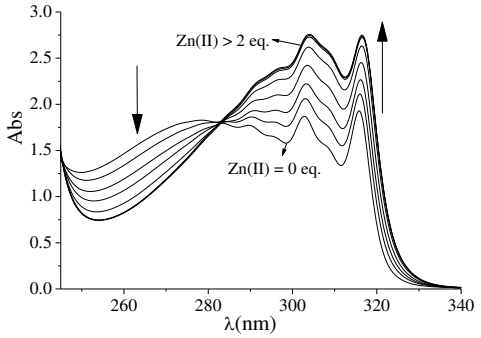

Figure 3.25 UV-vis spectra of **L1** in water pH 7 in the presence of increasing amounts of Zn(II) ([**L1**=$1.4 \cdot 10^{-4}$ M])

As shown in figure 3.26, the absorption intensity at 316 nm increase linearly with Zn(II) concentrations up to a ligand/Zn (II) 1:1 molar ratio and then assumes a constant value, to indicate the formation of stable 1:1 complexes in solution.

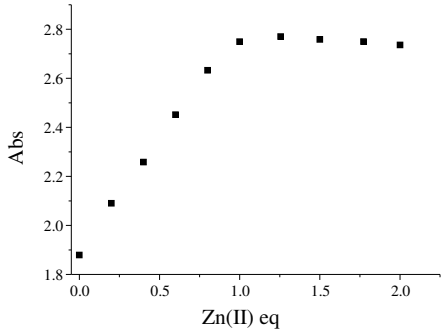

Figure 3.26 Absorbance of **L1** at 316 nm in the presence of increasing amounts of Zn(II)

In the case of H**L2** and H_2**L4** (see Figure 3.27 for H**L2**), the UV-Vis spectra in water at pH 7 the presence of increasing amounts of Zn(II) that the 8-hydroxy-quinoline absorption band at 303 nm undergoes a marked red-shift as the metal quantity increases from 0 to 1 equivalent, in keeping with deprotonation of the -OH function(s) upon metal coordination.

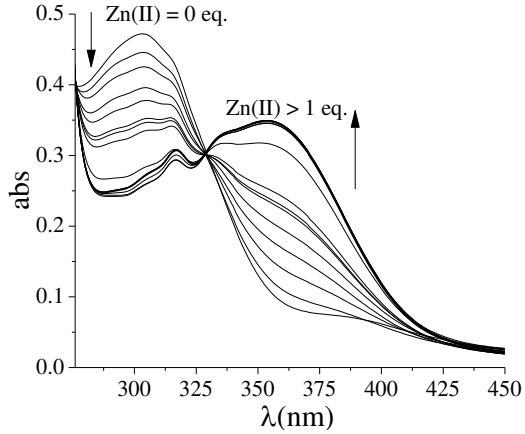

Figure 3.27 UV-vis spectra of H**L2** in water pH 7 in the presence of increasing amounts of Zn(II) ([H**L2**=$5.2 \cdot 10^{-5}$ M])

Figure 3.28 reports the absorbance at 354 nm and at 303 nm as a function of the Zn(II) equivalents added. Once again, there is a linear decrease of the absorbance at 303 nm and simultaneously a linear increase at 354 nm up to the addition of 1 equivalent of metal. Further addition of metal does not change the spectral feature, indicating the formation of a 1:1 complex in solution. The most interesting finding, however, resides in the fact that metal coordination in solution implies deprotonation of the hydroxyl group of 8-hydroxyquinoline, at least in aqueous solution.

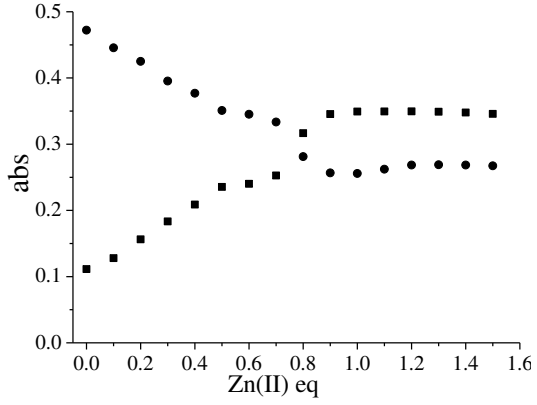

Figure 3.28 Absorbance of H**L2** at 354 (■) and 303 (●) nm in the presence of increasing amounts of Zn(II).

3.1.6 Fluorescence emission characteristics of the complexes

After studying acid-base and coordination properties of the ligands by potentiometric and spectrophotometric measurements, we analyzed the emission properties of the ligands in order to verify their ability as fluorescence chemosensors for metal ions. This was done by recording fluorescence emission spectra of ligand solutions in the presence of each metal ion in order to check the possible variation in the emission intensity. The experiments were carried out at fixed pH values in the presence of increasing amount of the metal cations as well as at different pH values on solutions containing a single metal and each. As a first step were recorded ligands emission spectra with one equivalent of M(II) in aqueous solution at pH 7. In this way we were able to define the emission characteristics of the various complex species formed by each metal ion.
Let's see more in detail the possible fluorescence chemosensors.

3.1.6.1 Fluorescence emission properties of the complexes with L1

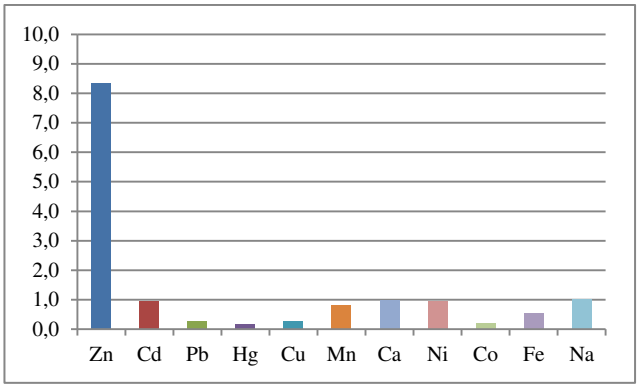

Figure 3.29 I/I_0 values for **L1** in the presence of one equivalent of different metal ions. I is the emission intensity in the presence of one equivalent of metal ion and I_0 the intensity of the free ligand.

In a preliminary experiments, we recorded the emission spectra of **L1** in the presence of 1 eq. of several metal cations (Zn(II), Cd(II), Pb(II), Hg(II), Cu(II), Mn(II), Ca(II), Ni(II), Co(II), Fe(II), Na(I)) at neutral pH, figure 3.29. This experiments showed that the fluorescence intensity increases more than eight-fold in the presence of Zn(II), while with the other metal ions there are only minor intensity variations. In particular, in the presence of Pb(II), Hg(II), Cu(II), Fe(II), Mn(II) and Co(II) is an intensity decrease, due to the heavy atom effect in the case of Pb(II) and Hg(II) and paramagnetic effect in the case of Cu(II), Mn(II), Fe(II) and Co(II). Based on these results, we investigated the coordination effects of Zn(II) on the **L1** emission properties, in particular by recording the **L1** emission spectra at different pH values in the presence of one equivalent of Zn(II) (Figure 3.30).

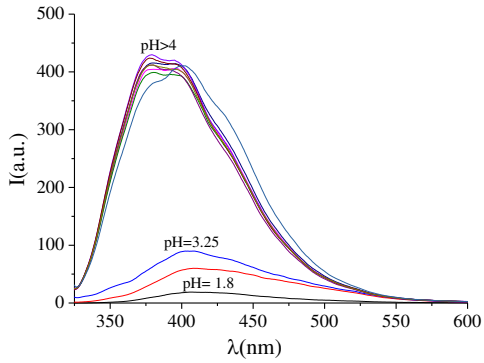

Figure 3.30 Fluorescence emission spectra of complex [**L1**Zn] at different pH values. ([L1] = [Zn(II)] = $5 \cdot 10^{-4}$M).

Figure 3.30 shows that the fluorescence intensity increases from pH 2 to pH 4, pH at which the Zn(II) complex is fully formed in solution. The complex formation is also accompanied by a slight shift toward the blue (about 10 nm). The emission then does not change to the higher pH of 4. They were also recorded **L1** spectra in the presence of increasing amounts of Zn(II) at pH 7.

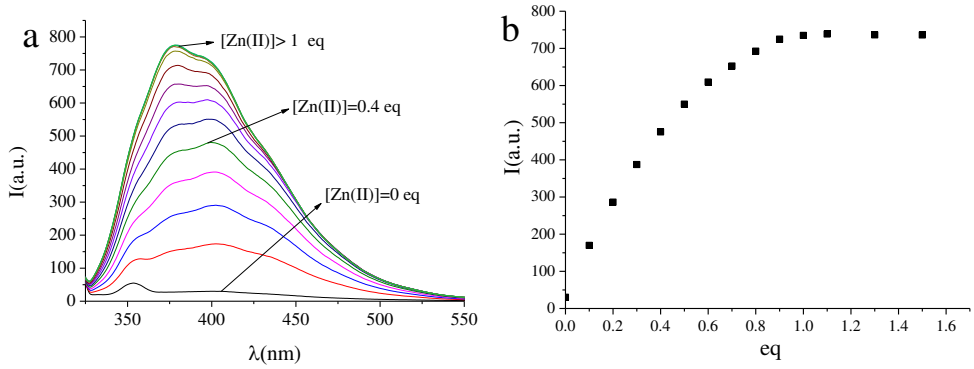

Figure 3.31 a) Emission spectra of **L1** in water at pH 7 in the presence on increasing amounts of Zn(II). **b)** Fluorescence emission intensity of L1 at 390 nm in water at pH 7in the presence on increasing amounts of Zn(II). ([**L1**] = $5 \cdot 10^{-4}$M).

These spectra are shown in figure 3.31a), while in figure 3.31b we reported the emission intensity at 390 nm as a function of the Zn(II) added equivalents. It is clear that the metal ion coordination leads to an almost linear emission intensity increase up to the addition of approximately one equivalent of Zn(II). The addition of higher amounts of Zn(II) does not induce additional spectral variations. This results further confirms the **L1** ability to "reveal" the Zn(II) ion thanks to a good CHEF effect as well as the formation of complexes with stoichiometry 1:1 in aqueous solution.

3.1.6.2 Fluorescence emission properties of the complexes with HL2

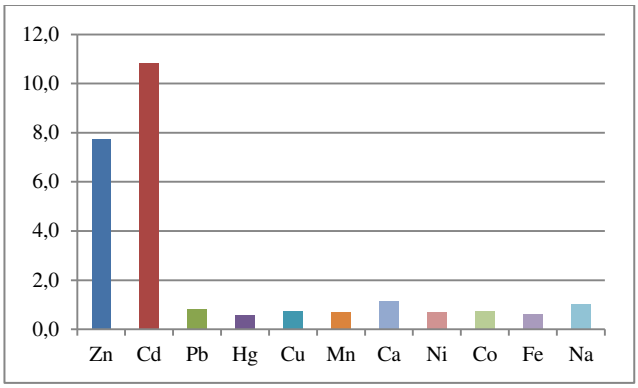

Figure 3.32 I/I_0 values for H**L2** in the presence of one equivalent of different metal ions. I is the emission intensity in the presence of one equivalent of metal ion and I_0 the intensity of the free ligand.

H**L2** behaves in a manner different from **L1**. The emission spectra of H**L2** in the presence of 1 eq. of several metal cations (Zn(II), Cd(II), Pb(II), Hg(II), Cu(II), Mn(II), Ca(II), Ni(II), Co(II), Fe(II), Na(I)) at neutral pH value, figure 3.32. In fact, the emission intensity increases both in the presence of Zn(II) and Cd(II). The other metals does not change or reduce the emission intensity in this conditions. The emission increases about eleven-fold in the presence of one Cd(II) equivalent and approximately eight-fold in the presence of one Zn(II) equivalent. We have also recorded H**L2** spectra in the presence of increasing Cd(II) amounts at pH 8 (figure 3.33a). The metal ion coordination leads to a linear intensity increase of emission up to the approximately addition of one Cd(II) equivalent. This is clearly shown also in figure 3.33b, where we reported the ligand emission intensity at 484 nm as a function of the Cd(II) equivalents added. A similar behavior is also found in the case of Zn(II).

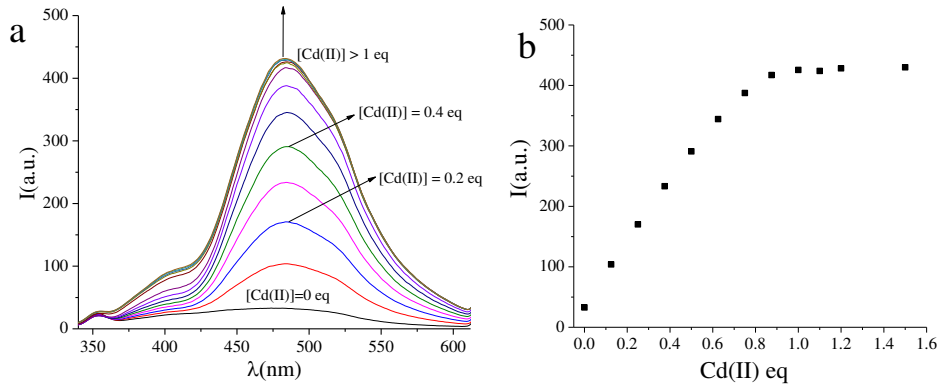

Figure 3.33 a) Emission spectra of H**L2** in water at pH 7 in the presence on increasing amounts of Cd(II). **b)** Fluorescence emission intensity of H**L2** at 484 nm in water at pH 7 in the presence on increasing amounts of Cd(II). ([H**L2**]= $4.8 \cdot 10^{-4}$M).

In conclusion, these data accounts for the formation of stable complexes with 1:1 stoichiometry at least in the case of Zn(II) and Cd(II). Both metals enhance the ligand emission with scarce selectivity. However, this ligand can be still promising for the detection of metal cations in real matrices. In fact, biological samples, such as cells or tissues, normally do not contain Cd(II) and, therefore, the present chemosensor may be of interest for Zn(II) sensing in biological media.

3.1.6.3 Fluorescence emission properties of the complexes with HL3 e H_2L4

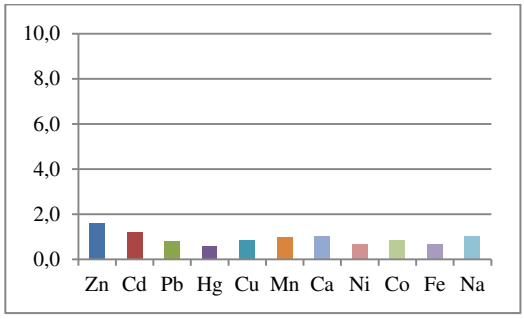

Figure 3.34 I/I_0 values for H**L3** in the presence of one equivalent of different metal ions. I is the emission intensity in the presence of one equivalent of metal ion and I_0 the intensity of the free ligand.

As shown by the preliminary experiment carried out recording emission spectra on solutions containing the ligand H**L3** and one eq. of different metals, all complexes result not emissive, figure 3.34.

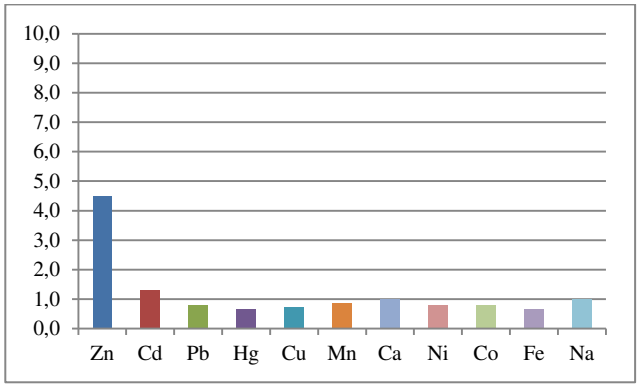

Figure 3.35 I/I_0 values for H_2**L4** in the presence of one equivalent of different metal ions. I is the emission intensity in the presence of one equivalent of metal ion and I_0 the intensity of the free ligand.

As shown by the preliminary experiment carried out recording emission spectra on solutions containing the ligand H_2**L4** and one eq. of different metals, the fluorescence intensity increases more than four-fold in the presence of Zn(II), too small to consider it a good chemosensor, while with the other metal ions there are only minor intensity changes, figure 3.35. The Cd(II) coordination causes a

fluorescence increase emission, which is two-fold increase in the presence of this metal ion.

3.1.6.4 Fluorescence emission properties of the complexes with L5

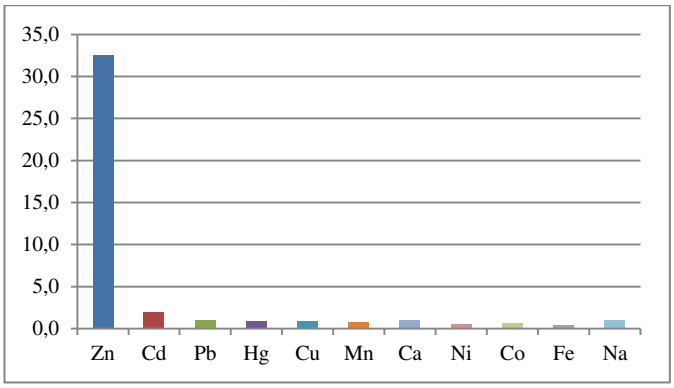

Figure 3.36 I/I_0 values for **L5** in the presence of one equivalent of different metal ions. I is the emission intensity in the presence of one equivalent of metal ion and I_0 the intensity of the free ligand.

As shown by the preliminary experiment carried out recording emission spectra on solutions containing the ligand **L5** and one eq. of different metals, the fluorescence intensity increases more than thirty-fold in the presence of Zn(II), while with the other metal ions there are only minor intensity changes, figure 3.36. The Cd(II) coordination causes a fluorescence increase emission, which is two-fold increase in the presence of this metal ion.

We recorded **L5** spectra in the presence of increasing Zn(II) amounts at pH 7 (figure 3.37a) and we have analyzed the intensity variation of emission at 390 nm as a function of the Zn(II) equivalents added (figure 3.37b).

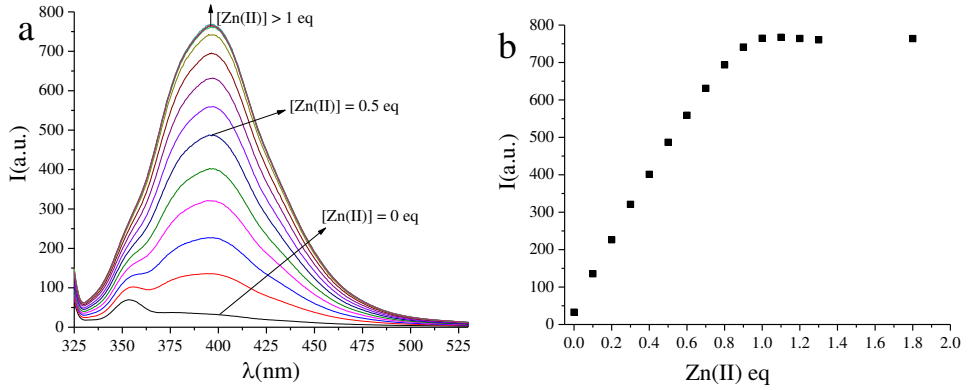

Figure 3.37 a) Emission spectra of **L5** in water at pH 7 in the presence on increasing amounts of Zn(II). **b)** Fluorescence emission intensity of **L5** at 400 nm in water at pH 7 in the presence on increasing amounts of Zn(II). ([**L5**]= $4.2 \cdot 10^{-4}$M).

The metal ion coordination leads to a linear intensity increase of emission up to the addition of approximately one Zn(II) equivalent (figure 3.37). The most interesting

finding, however, is the great selectivity for Zn(II), that makes **L5** the most promising chemosensor for Zn(II).

In conclusion, all five ligands form stable complexes with stoichiometry 1:1. In these complexes the metal ion is coordinated by the macrocyclic system and from the quinoline nitrogen.

Considering the fluorescence emission, paramagnetic cations, heavy metals and alkali or alkaline-earth ions give non-emissive complexes with all five ligands, while the Zn(II) and Cd(II) ones can be emissive. In the case of **L1** and **L5**, respectively, which contain one or two fluorogenic quinoline unit(s), result selective fluorescence chemosensors for the Zn(II) ion, which is the only metal ion capable to lead to a marked emission increase, in particular in the case of **L5**. This is due to inhibition of the PET from the amine groups of the cyclen units to fluorophore in its excited state upon metal coordination. In the case of **L2** both Zn(II) and Cd(II) binding increases the ligands fluorescence emission. In the case of H**L3** all complexes result not emissive. For H_2**L4** we have only a small fluorescence increase in the presence of Zn(II), too small to consider it a good chemosensor.

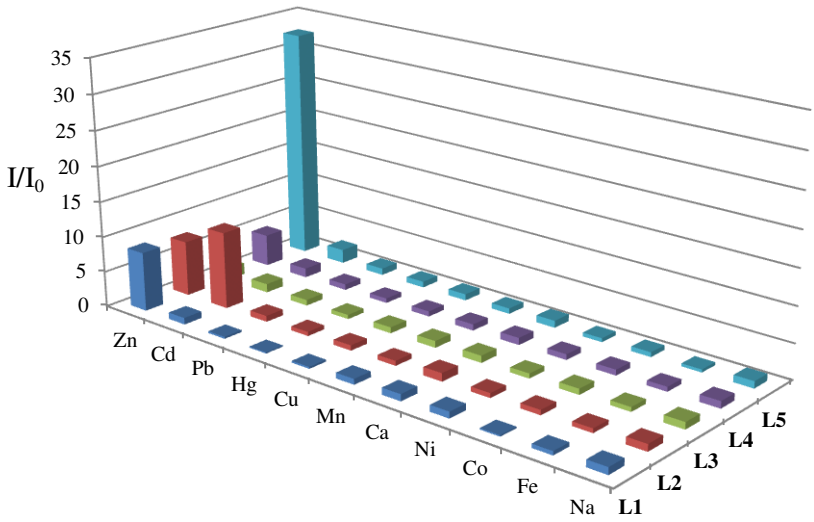

Figure 3.38 I/I_0 values for the four ligands in the presence of one equivalent of different metal ions. I is the emission intensity in the presence of one equivalent of metal ion and I_0 the intensity of the free ligand.

3.2 Zn(II)-based complex for anion sensing.

Synthetic Zn(II)-complexes are amongst the most commonly used as receptors and optical dyes for phosphate anions taking inspiration from the presence of this metal ion in the binding sites of various metallo-enzymes for which phosphate anions are substrates or inhibitors by reversible binding to one or more Zn(II) centers in their prostetic group. To analyze the effects of the coordination of inorganic phosphate anions on the optical properties of Zn(II) complexes, it can be of interest to compare the binding features of the different anions toward zinc(II). In fact, binding of the anions to the metal center strongly affects the structural and electronic characteristics of the complex, leading to changes in coordination sphere of zinc(II), in the charge distribution within the complex and, in many cases, also in the ligand conformation. This may result in marked changes in the optical properties of the Zn(II) complex. Pi, PPi and TPi normally form stable complexes with Zn(II) in solution. However, the three anions display a different affinity for this metal cation and, actually, the stability of the complexes increases in the order Pi < PPi < TPi... This trend is mainly due to the increasing negative charge gathered on the anions passing from Pi to TPi. Other effects, however, can influence the observed complex stability, in particular the number of oxygen atoms available for metal binding. In fact, its increase from Pi to TPi may also contribute to stabilize the complex with the larger triphosphate anion.

A large number of Zn(II)-based fluorescent chemosensors for phosphate derivatives that follow the basic structural design of a fluorophore-spacer-receptor architecture. The signaling process of the sensors often depends on the ability of the host-guest molecular recognition event to inhibit or initiate a Photoinduced Electron Transfer (PET) process from the covalently linked receptor to the chromophore leading to a generation (OFF-ON) or quenching (ON-OFF) of fluorescence, which are referred as Chelation Enhancement (CHEF) and Chelation Quenching of fluorescence (CHEQ) effects, respectively. In the specific case of Zn(II)-based luminescent dyes for phosphate derivatives, the metal center(s), by coordination, generally inhibits the quenching by an electron transfer process from the donor group(s) of the ligand to the excited state of the fluorophore moiety; therefore, the chemosensor system overall results emissive. Upon binding of the anion to the metal center(s) the PET process is fully or partially restored and a quenching of the fluorescence emission is observed.

3.2.1 Acridine based ligands

3.2.1.1 Ligand acid-base properties

In aqueous solution the amino groups of the synthesized ligands give acid-base equilibria that compete with metal ions coordination. Furthermore, ligand protonation can affect the fluorescence emission intensity. The ligand shows low solubility in aqueous solution especially at alkaline pH and for this reason the study was conducted in water-ethanol solution (50:50, vol:vol). The use of this medium ensures a good solubility from highly acidic pH, even lower than 2, up to pH 12, necessary condition to perform pH-metric titrations.

Protonation equilibria of the ligand Acry-bis[9]aneN_3 were studied with potentiometric and spectroscopic measurements (UV-visible absorption and fluorescence emission). By potentiometric measurement inspection, it can be observed as the ligand **L6** is able to bind up to five acidic protons. In the table 3.16 are reported the protonation constants determined in water-ethanol solution (50:50, vol: vol) for the free ligand.

Equilibrium	log K
$H^+ + L = [LH]^+$	10.56 (2)
$[LH]^+ + H^+ = [LH_2]^{2+}$	10.31 (1)
$[LH_2]^{2+} + H^+ = [LH_3]^{3+}$	6.79 (2)
$[LH_3]^{3+} + H^+ = [LH_4]^{4+}$	4.96 (3)
$[LH_4]^{4+} + H^+ = [LH_5]^{5+}$	2.75 (1)

Table 3.16 Protonation constants of **L6**, standard deviation in parentheses (298.1K).

From the data in tables 3.16 we can calculate the species distribution diagrams that are shown below in figures 3.39.

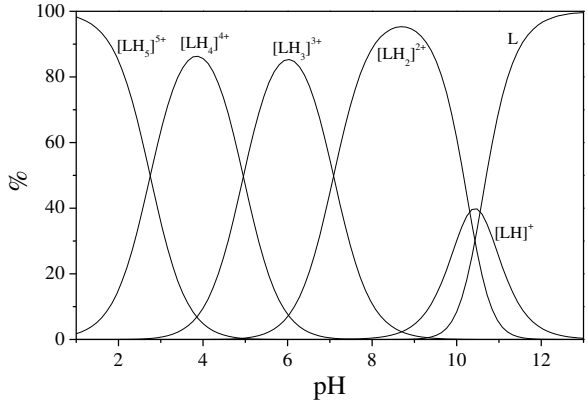

Figure 3.39 Distribution diagrams calculated by using the protonation constants for the ligands **L6** ([L]=10^{-3} M T=298.1K, NaCl = 0.1 M).

Looking at the figure 3.39 we see that the ligand is in its completely deprotonated form only for very alkaline pH. The species present in acidic pH are $[LH_4]^{4+}$ and $[LH_5]^{5+}$, while around the neutrality we have the simultaneous presence of species $[LH_3]^{3+}$ and $[LH_2]^{2+}$.

It is known as the nitrogen atom of the acridine unit has scarce basic characteristics (logK < 3). It is therefore very likely that the first four protonation equilibria involve aliphatic atoms present in the two subunits [9]aneN_3, which have more basic characteristics. Moreover, the first two constants are similar (10.56 and 10.31), suggesting that the first two protonation steps involve two amine nitrogen atoms of two distinct subunits. Same consideration can be done for the next two protonation steps (log K = 6.79 and 4.96), which, even if characterized by constants that differ from the previous, may be attributed to protonation steps taking place on two different subunits.

The last pronation constant (log K = 2.75) appears to be relatively low and may be assigned to the protonation of the acridinic nitrogen atom or of aliphatic amino group. This point was clarified by performing UV-visible spectrophotometric measurements at different pH values (figure 3.40).

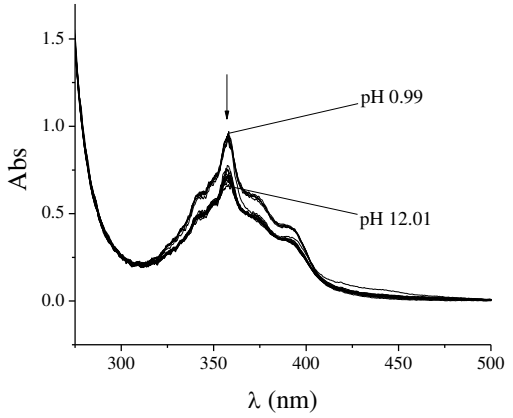

Figure 3.40 UV-visible spectrophotometric spectra of **L6** at different pH values

By recording spectra at different pH it has been possible to highlight how the shape of the acridinic band is not very influenced by pH. In fact, the absorption maximum of the band remains substantially unaltered at varying pH (λ_{max}= 358 nm). The differences reported between the different spectra consist of an absorbance increase at acid pH. To clarify this effect is shown in figure 3.41 the molar absorption coefficients at 358 nm as a function of pH, superimposed with the distribution diagram of protonated species.

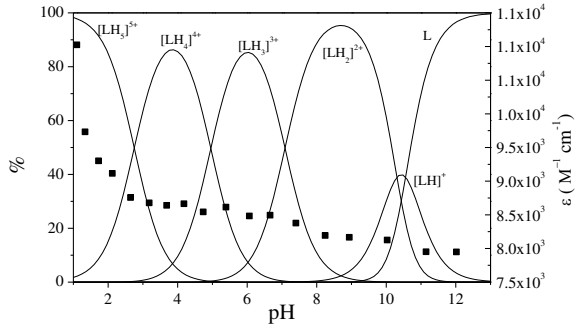

Figure 3.41 Molar absorption coefficients of **L6** at 358 nm as a function of pH, overlaid with the distribution diagram of protonated species.

From figure 3.41 is clear as the absorbance at 358 nm does not undergo significant variations at alkaline pH and at neutral pH, whereas at acid pH is observed a rapid increase of absorption, in particular at a pH below 2.5 where the predominant species becomes $[LH_5]^{5+}$. Knowing that the UV-vis absorption of this molecule is given by the acridinic unit, this variation can be attributed to the protonation of the heteroaromatic nitrogen atom. The fifth step of protonation has therefore attributed to the acridinic unit.

To study the chemosensor behavior fluorescence emission spectra were recorded with an excitation λ at 360 nm at different pH values (Figure 3.42a).

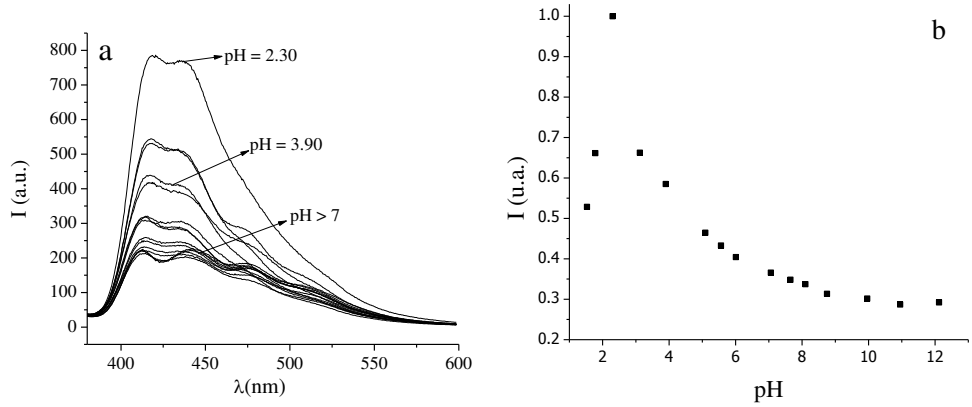

Figure 3.42 a) Emission spectra of **L6** at different pH values. **b)** Emission intensity at 434 nm of **L6** at different pH values. ([**L6**]= $5 \cdot 10^{-6}$M ; H_2O/EtOH 50:50 vol/vol).

Figure 3.42b shows the values of emission intensity measured at 434 nm as a function of pH. The fluorescence appears to be compatible with the protonation equilibrium. Observing the distribution diagram 3.64 it can be noted that for pH greater than 6, the ligand is in its form characterized by low protonation degree, corresponding to lower fluorescence emission, as it might be expected for the PET effect. We see, in fact, that the fluorescence decreases with the formation of the

species having low protonation degree. In particular from pH 5 ,increasing pH, we assist to the formation of the species $[LH_3]^{3+}$ and subsequently $[LH_2]^{2+}$, leading to the fluorescence decrease until values that remain almost constant when the $[LH]^{+}$ and L species are formed. Conversely for acidic pH there is an increase of fluorescence emission due to formation of the $[LH_4]^{4+}$ species, followed by a rapid decrease due to the formation of the species $[LH_5]^{5+}$.
Afterward we moved to investigate fluorescence emission due to the interaction of the ligand with some metal ions.

3.2.1.2 Metal ions coordination in water/ethanol solution.

To study the coordinative characteristics of the ligand Acry-bis[9]aneN_3 for metal cations, we have carried out potentiometric measurements as well as spectrophotometric measurements of fluorescence emission in solution of water-ethanol (50:50, vol:vol). This to ensure, as mentioned above, a greater solubility of the ligand and its complexes in a wide pH range.
In figure 3.43 there is a schematic representation of the ligand in which it is highlighted the presence of two coordinative sites consisting of the two subunits [9]aneN_3 which in principle are able to chelate metal ions to form mono- and dinuclear complexes.

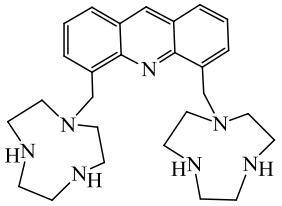

Figure 3.43 L6

The metal cations that have been studied are Zn(II), Cd(II) and Cu(II). As in previous cases we have studied these metals because Zn(II) and Cd(II) are able to inhibit the PET effect, giving fluorescent complexes, and Cu(II) since is an example of paramagnetic metal. To study the coordinative properties of the ligand first, potentiometric measurements were carried out in order to determine the stoichiometry of the formed complexes and their stability constants. Afterward we have analyzed the UV-vis absorption spectra as pH function assess changes that occur in the absorption of species which are formed; subsequently, by measurements of fluorescence emission characteristics of the ligand as fluorescence chemosensor for these cations and anions were investigated.
The formation constants determined by potentiometric studies for the various species formed by the ligand **L6** with the metal cations examined, are reported in table 3.17.

Equilibrium	***log K***		
	Zn^{2+}	Cu^{2+}	Cd^{2+}
$L + M^{2+} = [LM]^{2+}$	14.04 (2)	16.29 (5)	12.70 (2)
$[LM]^{2+} + H^{+} = [LMH]^{3+}$	8.96 (3)	9.13 (7)	9.25 (1)
$[LMH]^{3+} + H^{+} = [LMH_2]^{4+}$	-	6.15 (2)	-
$[LM]^{2+} + 2OH^{-} = [LM(OH)_2]$	6.67 (4)	6.64 (1)	6.75 (5)
$[LM]^{2+} + M^{2+} = [LM_2]^{4+}$	6.3 (1)	6.60 (4)	-
$[LM_2]^{4+} + OH^{-} = [LM_2OH]^{3+}$	-	8.28 (3)	-
$[LM_2OH]^{3+} + OH^{-} = [LM_2(OH)_2]^{2+}$	-	-	4.25 (3)
$L + 2M^{2+} + OH^{-} = [LM_2OH]^{3+}$	-	-	21.63 (1)

Table 3.17 Stability constants of the **L6** complexes with Zn(II), Cu(II) and Cd(II) standard deviation in parentheses. (T=298.1 K; H_2O/EtOH 50:50 vol/vol).

L6 forms stable mononuclear and binuclear complexes with the three metals. If we consider the constants for the addition of a second metal ion to the mononuclear complex it appearsclear as these are lower in the case of Zn(II) and Cu(II) if compared with the constants for the coordination of the first metal ions; as expected coordination of the second metal ion is affected by the presence of a positively charged ion already coordinated. In fact, while the first cation is added to a neutral ligand, the second will bind instead to a mononuclear complex bearing a bipositive charge implying thus a certain degree of repulsion. In the case of the ion Cd(II) the formation of the species $[Cd_2L]^{4+}$ is not observed in potentiometric titrations, while it is highlighted the formation of mono- and di-hydroxylated species. A characteristic of dinuclear complexes of Cd(II) and Cu(II) is to form stable hydroxylated species (arising from deprotonation of H_2O molecules coordinates); this is due to the incomplete coordinative sphere around the metal cations, in which in addition to the donor atoms of the ligand, are coordinated also the water molecules present. The formation of these species reduces the electrostatic repulsion between the metal centers and stabilizes the dinuclear complexes. In the case of Zn(II), these hydroxylated species are poorly soluble and their precipitation prevents the determination of their formation constants.

Referring to the individual subunits formed by the macrocycle [9]aneN$_3$, we can observe different constants in the coordination of the metal ions towards the ligand Acry-bis[9]aneN for the three metals.[34,35,36]

Equilibrium	Zn(II)	Cu(II)	Cd(II)
[9]aneN$_3$ + M^{2+} = $[LM]^{2+}$	11.6	15.6	9.5

Table 3.18 Stability constants of the [9]aneN3 complexes with Zn(II), Cu(II) and Cd(II)

Observing the constants in table 3.18 and comparing them with those of table 3.17, it can be noted that for the single macrocycle, the constants are lower than those of the studied ligand.

The greater stability with Acry-bis[9]aneN$_3$ can be sought in the increased interactions that stabilize the complexation. In fact, considering the large size of the studied cations we can assume that they cannot enter in the cavity of the ring but rather they remain above the plane formed by the nitrogen atoms. This allows the interaction of the acridine nitrogen atom, making the complex more stable. This effect is strong for Zn(II) and Cd(II), while just a slight increase in stability for Cu(II) can be highlighted. Concerning the first protonation constant of mononuclear complexes, should be noted, for all three metal ions, that there are values similar to those obtained for the first protonation of the free ligand. This may indicate that only one [9]aneN$_3$ unit is involved in the metal ion coordination.

From the data in tables 3.17 we can calculate the species distribution diagrams that are shown below in figures 3.44-3.46.

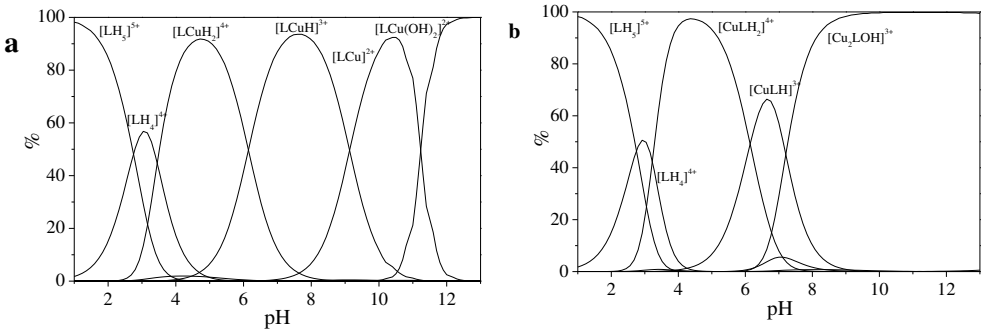

Figure 3.44 Species distribution diagrams of the **L6** complexes with one equivalent (**a**) and two equivalent (**b**) of Cu(II).

The most important species in the presence of one equivalent of Cu(II) , figure 3.44a, remains the mononuclear, protonated and not protonated. The free ligand falls in a range of pH clearly acid (protonated form). In figure 3.44b it is instead reported the distribution diagram referred to a **L6** solution containing two

[34] M DeRonde, D. Driscoll et al; *Inorg. Nucl. Chem. Lett*., **1975**, 11, 521
[35] T. Itoh, H. Hisada, Y. Fujii; *Inorg. Chim. Acta*, **1998**, 283, 51
[36] T. Arishima, K. Hamada, S. Takamoto; *Nippon Kagaku Kaishi*, **1973**, 1119

equivalents of Cu(II); here should be highlighted that in contrast to figure 3.44a around pH 7 there is a decrement of the species $[LCuH]^{3+}$ in favor of the dinuclear species $[LCu_2]^{4+}$ and $[LCu_2OH]^{2+}$, between which the second is the species most relevant for pH greater than 8. Instead, at acid pH the differences between the distribution diagrams calculated for one and two equivalents added are minimal.

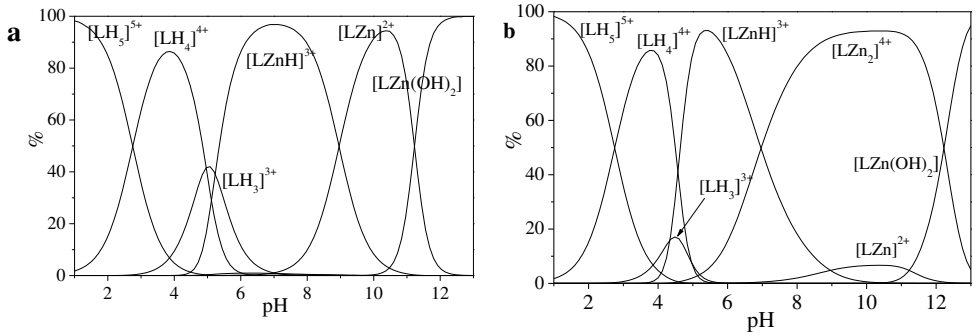

Figure 3.45 Species distribution diagrams of the **L6** complexes with one equivalent (**a**) and two (**b**) equivalent of Zn(II).

Concerning the ion Zn^{2+} (see Figure 3.45a whichrefers to the presence of 1 equivalent and figure 3.45b which refers to the presence of 2 equivalents) it is clear that for pH > 6, in the presence of 1 equivalent there is the formation of the species $[LZn]^{2+}$, however, with regard to the case with two equivalents there is the formation of a small amount of the species $[LZn]^{2+}$ and of a greater quantity of the species $[LZn_2]^{4+}$, which was not present in the previous case. At high alkaline pH there is the formation of neutral species $[LZn(OH)_2]$. At acidic pH, instead, there is no difference.

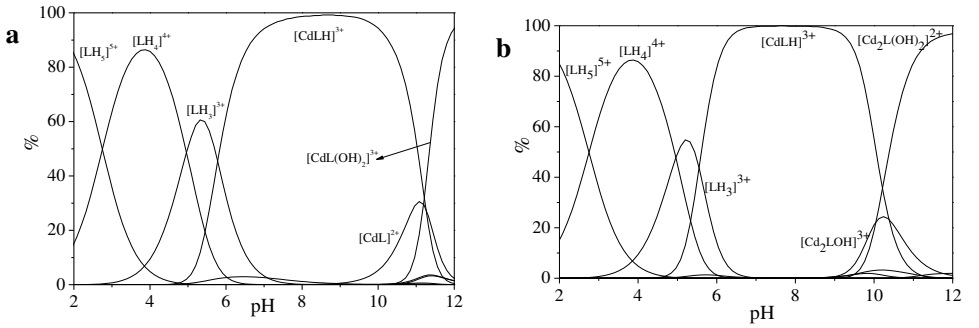

Figure 3.46 Species distribution diagrams of the **L6** complexes with one equivalent (**a**) and two (**b**) equivalent of Cd(II).

Considering the ion Cd(II) we have small variations between the species distribution diagrams (see figure 3.46a and 3.46b) referring to the presence of one equivalent and the presence of two equivalents. The major differences appearing

only at alkaline pH (between pH 10 and 12) where, with the presence of two equivalents of metal ion, the amount of the dinuclear species $[LCd_2OH]^{3+}$ and $[LCd_2(OH)_2]^{2+}$ increases at the expense of mononuclear species $[LCd]^{2+}$ and $[LCd(OH)_2]$.

3.2.1.3 UV-vis absorption spectra in the presence of Zn(II)

To investigate the changes in the UV-visible absorption of the ligands, occurring when a complex with metal ions is formed we have recorded UV-visible absorption spectra of the ligand in the presence of two equivalents of Zn(II) at different pH values (figure 3.47). As reference ion we have investigated cation Zn(II) the only able to inhibit the PET effect.

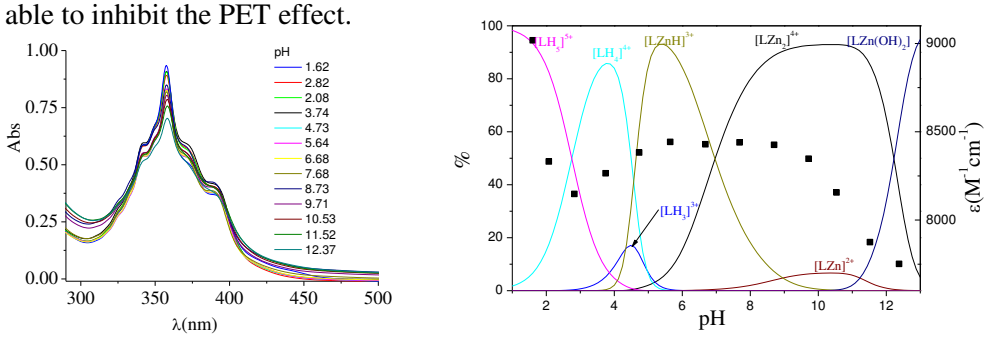

Figure 3.47 a) UV-vis spectra of **L6** in water at different pH value in the presence of two equivalents of Zn(II). **b)** Absorbance at 358 nm superimposed on the species distribution diagram.

Substantially the shape of the spectrum is not altered by the coordination, and the band of the acridine unit remains always characterized by a maximum at 358 nm (figure 3.47a), while, as highlighted in figure 3.47b the formation of the Zn(II) complexes produces an increased absorbance of the acridine unit; this is probably due to the interaction of the heteroaromatic nitrogen atom with the metal center.

3.2.1.4 Fluorescence emission characteristics of the complexes

After studying acid-base and coordination properties of the ligand by potentiometric and spectrophotometric measurements, we analyzed the emission properties of the ligand in order to verify their ability as fluorescence chemosensor for metal ions. This was done by recording fluorescence emission spectra of ligand solutions in the presence of each metal ion in order to check the possible variation in the emission intensity. The experiments were carried out at fixed pH values in the presence of increasing amount of the metal cations as well as at different pH values on solutions containing a single metal. As a first step ligand emission spectra with two equivalents of M(II) in ethanol/water (50:50 vol/vol) solution at pH 7 (figure 3.48) were recorded. In this way we were able to define the emission characteristics of the various complex species formed by each metal ion.

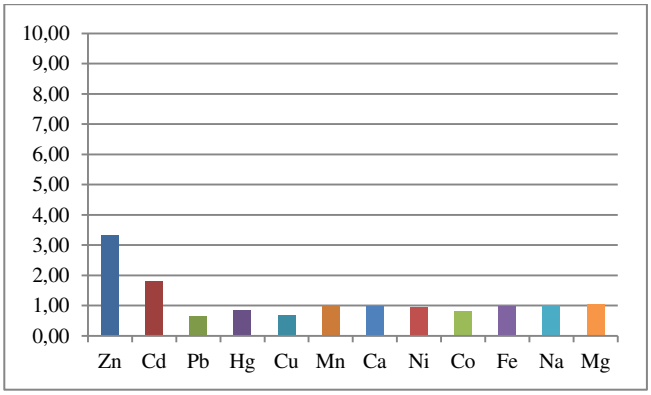

Figure 3.48 I/I_0 values for **L6** in the presence of one equivalent of different metal ions. I is the emission intensity in the presence of one equivalent of metal ion and I_0 the intensity of the free ligand.

As shown by the preliminary experiment carried out recording emission spectra on solutions containing the ligand **L6** and two equivalent of different metals, the fluorescence intensity increases more than five-fold in the presence of Zn(II), while with the other metal ions there are only minor intensity changes, figure 3.48. Based on these results, we investigated the coordination effects of Zn(II) on the **L6** emission properties, in particular by recording the **L6** emission spectra at different pH values in the presence of one or two equivalent(s) of Zn(II) (figure 3.49-3.50).

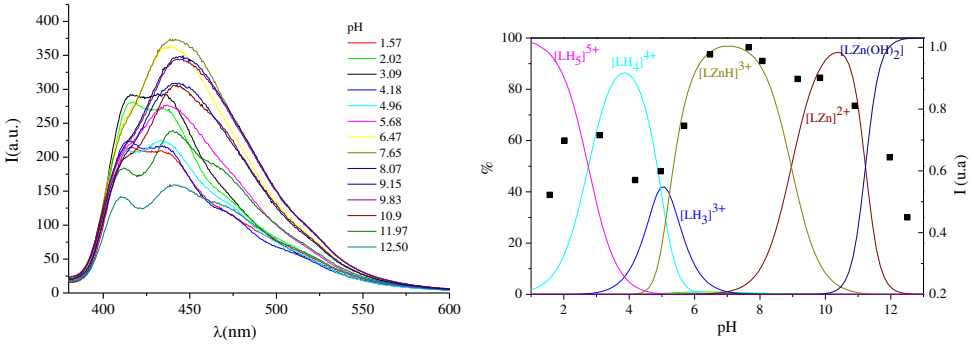

Figure 3.49 a) Fluorescence emission spectra of **L6** complex with one equivalent of Zn(II) at different pH values. **b)** Emission intensity at 435 superimposed on the species distribution diagram. ([**L6**]=$5\cdot10^{-6}$)

The emission spectra and the emission intensity at 435 nm as a function of pH in the presence of 1 equivalent (figures 3.49a-b) and 2 equivalents (figures 3.50a-b), highlight how the intensity of fluorescence emission increases with the formation of the Zn(II) complex. In fact, the formation of species $[LZnH]^{3+}$ generates an increase of the fluorescence emission at acidic pH, reaching a maximum around pH 7. In the region of pH 8-10 can be observed a slight decrease in the emission due to the formation of species $[LZn]^{2+}$, in the presence of one equivalent of Zn(II), and species of $[LZn_2]^{4+}$ and $[LZn]^{2+}$, in the presence of two equivalents of the metal ion.

This suggests that these species are less emissive of protonated species $[LZnH]^{3+}$. Finally, in the presence of one as well as two equivalents of metal ion, at alkaline pH, in correspondence of the formation of species $[LZn(OH)_2]$, we have a fluorescence emission decrease.

The fact that the protonated species $[LZnH]^{3+}$ is the most emissive can be explained considering that in this complex a unit [9]aneN_3 is involved in the coordination of the metal ion, while the other is protonated, inhibiting the PET effect.

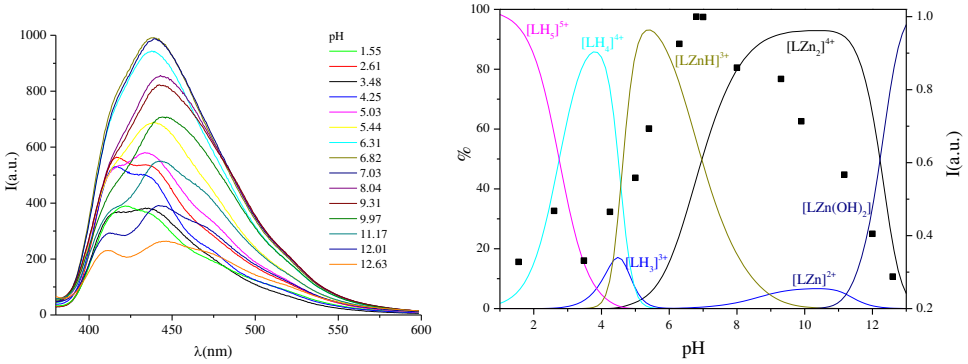

Figure 3.50 a) Fluorescence emission spectra of **L6** complex with two equivalents of Zn(II) at different pH values. **b)** Emission intensity at 435 superimposed on the distribution diagram of the species. ([L6]=$5\cdot10^{-6}$)

They were also recorded **L6** spectra in the presence of increasing amounts of Zn(II) at pH 7, figure 3.51.

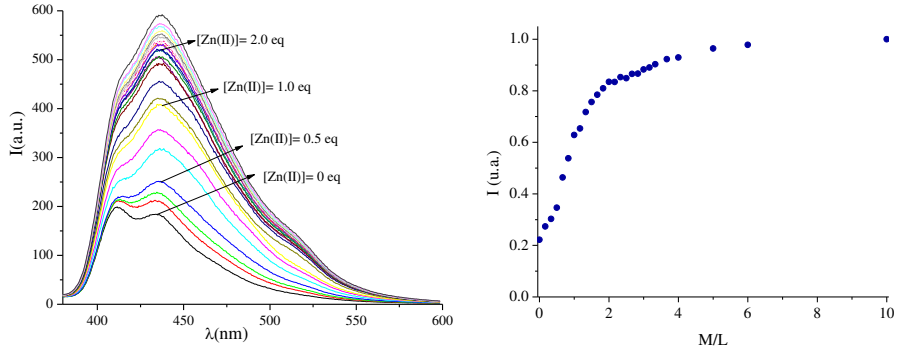

Figure 3.51 a) Emission spectra of **L6** in ethanol/water (50/50 vol/vol) at pH 7 in the presence on increasing amounts of Zn(II). **b)** Fluorescence emission intensity of L1 at 435 nm in ethanol/water at pH 7 in the presence on increasing amounts of Zn(II). ([**L6**] = $5\cdot10^{-6}$M).

For Zn(II) the addition of one equivalent of the metal ion causes an intense emission increase due to the progressive formation of mononuclear complexes in solution and in particular, at pH 7, of the species $[LZnH]^{3+}$. Further additions of Zn(II) cause the formation of dinuclear complexes, in particular of the species $[LZn_2]^{4+}$ and generate a further slight increase of emission. The observed increase in the presence of larger amounts of Zn(II), more than one equivalent is due to the

formation of the complex $[LZn_2]^{4+}$, where at variance of the mononuclear species $[LZn]^{2+}$, each unit [9]aneN$_3$ is involved in coordination of a metal ion, producing a further inhibition of PET effect through aliphatic amine nitrogen atoms .

3.2.1.5 Phosphate recognition by a dinuclear Zn(II) complex.

After studying the coordination properties of the ligand by potentiometric and spectrophotometric measurements, we analyzed the emission properties of the dinuclear Zn(II) complex in presence of different anions. We studied the spectrophotometric properties in the presence of inorganic phosphate (PO_4^{3-}, $P_2O_7^{4-}$, $P_3O_{10}^{5-}$), sulfates, nitrates and halides.

The formation constants determined by potentiometric studies of the various species formed by the ligand dinuclear Zn(II) complex with the inorganic phosphate, are reported in table 3.19

Reaction	Log K		
	$A^{n-} = PO_4^{3-}$	$A^{n-} = P_2O_7^{4-}$	$A^{n-} = P_3O_{10}^{5-}$
$Zn_2L^{4+} + A^{n-} = [Zn_2LA]^{(4-n)+}$	3.4(1)	4.7(2)	6.4(1)
$Zn_2L^{4+} + AH^{(n-1)-} = [Zn_2LA]^{(3-n)+}$		4.7(1)	6.2(2)
$Zn_2L(OH)^{3+} + A^{n-} = [Zn_2L(OH)A]^{(3-n)+}$	3.2(1)	4.2(1)	5.4(2)

Table 3.19 Stability constants of the $[Zn_2\mathbf{L6}]^{4+}$ complexes with inorganic phosphate. Standard deviation in parentheses. (298.1 K, 0.1 M $NaNO_3$).

By inspection of table 3.19, it can be observed as the dinuclear complex of Zn(II) forms stable adducts with the three inorganic phosphates. Afterward we have investigated the spectrophotometric properties of the adducts. As a first step complex emission spectra was recorded in presence of five equivalents of anions in aqueous solution at pH 7, figure 3.52.

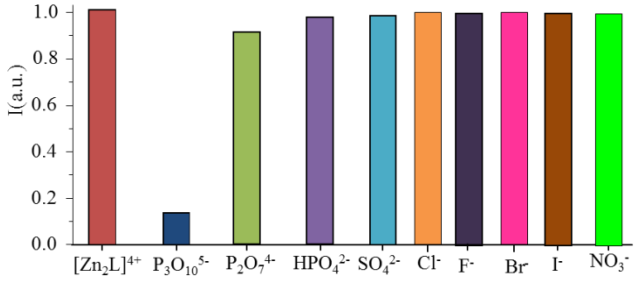

Figure 3.52 Fluorescence emission at 440 nm of dinuclear Zn(II) complex of **L6** in the absence and in the presence of 5 eq. of different anions at pH 7.2 ([**L6**] = $3 \cdot 10^{-6}$ M).

As we can clearly see in figure 3.52 only the triphosphate anion is able to decrease the fluorescence emission intensity at 440 nm, while the other anions do not alter the emission intensity. Studying in more detail the fluorescence spectra in the presence of triphosphate, figure 3.53, we can see how the addition of anion causes a

marked fluorescence intensity decrease until obtainment of system almost completely swichted-off with the addition of 1 eq of $P_3O_{10}^{5-}$.

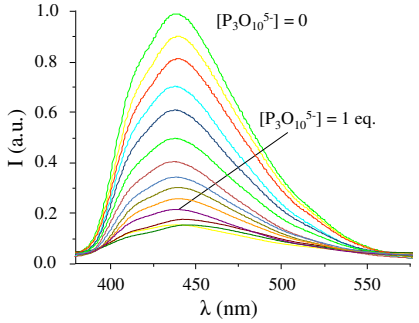

Figure 3.53 Emission spectra of dinuclear Zn(II) complex of **L6** in water at pH 7 in the presence on increasing amounts of $P_3O_{10}^{5-}$([**L6**] = $3 \cdot 10^{-6}$ M).

To understand this behavior in the presence of triphosphate we performed molecular dynamics calculations, computing structures expected in the presence of the three inorganic phosphates, figure 3.54 and 3.55.

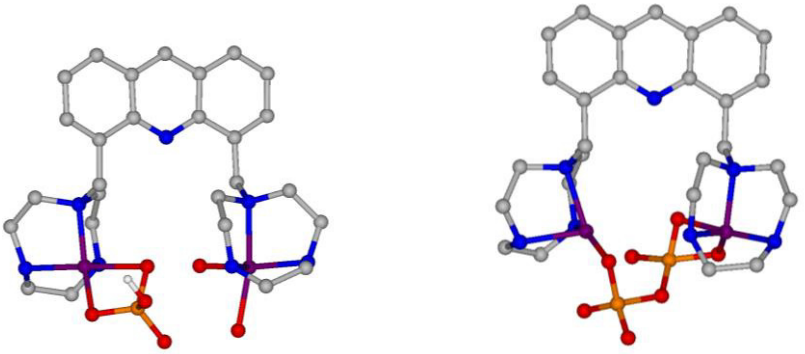

Figure 3.54 Calculated structure (DFT level of theory) for the adducts between the dizinc complex of **L6** with monophosphate and diphosphate.

As we can see in figure 3.54 the coordination of phosphate and diphosphate to the dinuclear complex of Zn(II) it is accompanied by a low number of interactions and by a deformation of the cavity formed between the two macrocycles. Instead, as we can see in figure 3.55, the coordination of the triphosphate is accompanied by the formation of a high number of interactions and any deformation of the complex. So we can state that the cause of optical selectivity is due to the high interaction between the dinuclear system and the triphosphate.

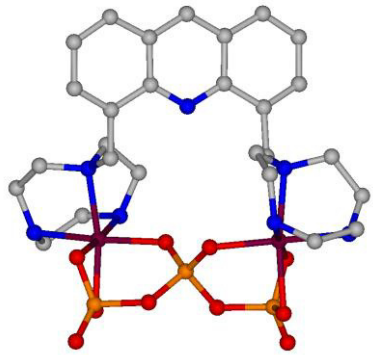

Figure 3.55 Calculated structure (DFT level of theory) for the adducts between the dizinc complex of **L6** with triphosphate.

3.2.2 Terpyridine based ligands.

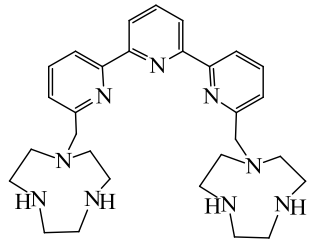

L7

L7 is characterized by two [9]aneN3 moieties bridged by a terpyridine (tpy) and it can assume in solution different possible conformations, among which the trans-trans and cis-cis (scheme 3.3).

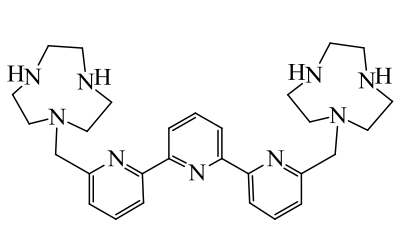

L7 (*trans-trans*)

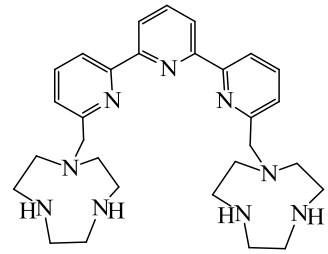

L7 (*cis-cis*)

Scheme 3.3

3.2.2.1 Ligand acid-base properties

Protonation equilibria of the ligand tpy-bis[9]aneN$_3$ were studied with potentiometric and spectroscopic measurements (UV-visible absorption and fluorescence emission). By potentiometric measurement it can be seen as the ligand **L7** is able to bind up to five acidic protons. In the table that follows it is reported

the protonation constants determined in water solution for the free ligand obtained through potentiometric measurements.

Equilibrium	log K
$H^+ + L = [LH]^+$	11.07 (9)
$[LH]^+ + H^+ = [LH_2]^{2+}$	10.67 (7)
$[LH_2]^{2+} + H^+ = [LH_3]^{3+}$	7.03 (9)
$[LH_3]^{3+} + H^+ = [LH_4]^{4+}$	5.57 (9)
$[LH_4]^{4+} + H^+ = [LH_5]^{5+}$	3.0 (1)

Table 3.20 Protonation constants of **L7**, standard deviation in parentheses (298.1°K).

From the data in tables 3.20 we can calculate the species distribution diagrams that are shown below in figures 3.56.

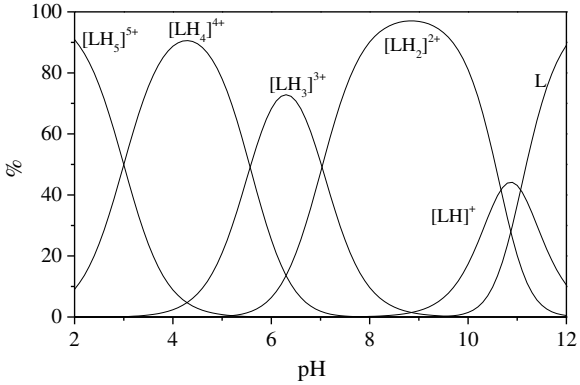

Figure 3.56 Distribution diagrams calculated by using the protonation constants for the ligands **L7** ([**L7**]=10^{-3} M T=298.1°K, $N(CH_3)_4Cl$ = 0.1 M).

Looking at the figure 3.56 we see that the ligand is in its completely deprotonated form only for very alkaline pH (pH > 11). The species present at acidic pH are $[LH_4]^{4+}$ and $[LH_5]^{5+}$, while around the neutrality we have the simultaneous presence of the species $[LH_3]^{3+}$ and $[LH_2]^{2+}$. It is known as the nitrogen atom of the terpyridine unit has basic characteristics ($\log K_1$ = 4.7; $\log K_2$ = 3.5). It is therefore very likely that the first three protonation equilibria involve aliphatic atoms present in the two subunits [9]aneN_3, which have more basic characteristics. Moreover, it can be noted that the first two constants are similar (11.07 and 10.67); this suggests that the first two protonation steps involve two amine nitrogen atoms belonging to two distinct subunits. The next protonation step (log K = 7.03), may be attributed to protonation step taking place on one [9]aneN_3 subunits.

The last two pronation constants (log K = 5.57 and log K = 3.0) appear to be relatively low and can correspond to the protonation of the terpyridinic nitrogen atom or aliphatic amino group. This point was further investigate by performing

UV-visible spectrophotometric and spectrofluorimetric measurements at different pH values (figure 3.57 – 3.58).

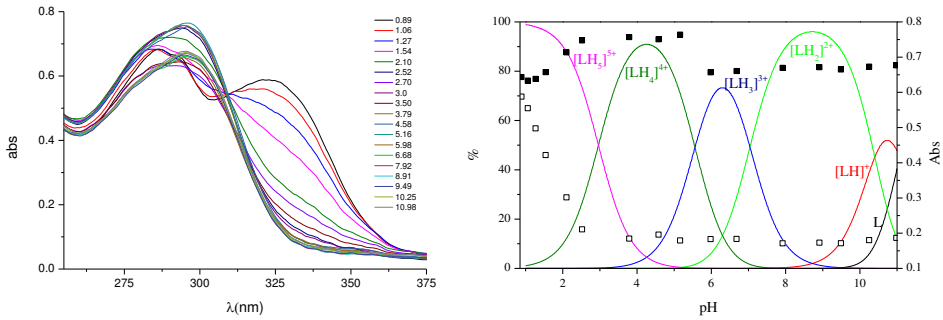

Figure 3.57 a) UV-vis spectra of **L7** in water at different pH value. **b)** Absorbance at 330 (□) and at 295 (■) nm superimposed on the species distribution diagram ([**L7**]=1.4·10^{-4} M).

As can be observed from the absorption spectra shown in figure 3.57a, the protonation of the ligand affects its UV-visible absorption spectrum : this variation is due to the protonation of the terpyridine unit. In fact, as reported in figure 3.57b the decrease of the band at 330 nm is attributed to the deprotonation of the species $[LH_5]^{5+}$ so that we can attribute to the deprotonation of the terpyridine unit, above pH 3 the absorption spectrum does not show significant variations.

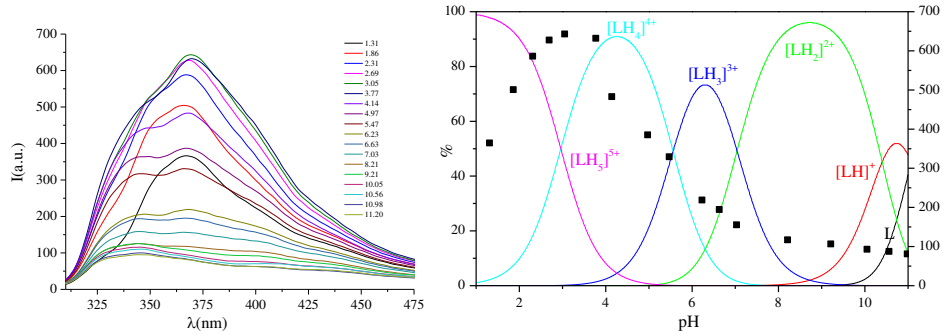

Figure 3.58 a) Fluorescence spectra of **L7** in water at different pH value. **b)** Fluorescence emission intensity at 375 (■) nm superimposed on the species distribution diagram ([**L7**]=1.4·10^{-4} M).

The fluorescence emission spectra of the ligand terpy-bis[9]aneN$_3$ is shown in figure 3.58. Also in this spectrum there is a marked influence of pH on emission intensity. Note how for pH values above neutrality system present a weak fluorescence emission. For pH values below 7 there is a marked increase in the emission intensity and a progressive formation of a band at about 375 nm which reaches the emission maximum at pH approximately equal to 3, then decreased to pH less than 3 with the fluorofora unit protonation. The fluorescence emission intensity at 375 nm is consistent with the observations regarding the succession of

the protonation balance. When most of the nitrogen atoms of the two aliphatic subunits [9]aneN_3 are not protonated, i.e. for values of pH higher than 7 (as can be seen from the distribution diagram in figure 3.58b) their non-bonding doublets non-engaged in the bond with a H^+. This gives rise to a fluorescence quenching by photoinduced electron transfer process (PET effect - in this regard see paragraph 1.4.1.1.2). This change in fluorescence emission with the variation of pH is the basis of the functioning of the ligand terpy-bis[9]aneN_3 as a sensor for metal cations, because the coordination of one or more of them can lead to important modifications of the fluorescence emission. Then comparing the distribution diagram of the ligand with the intensities of fluorescence emission at the variation of pH, it is known with greater clarity that the emission quenching occurs already for pH values higher than 4 which then leads the system to "turn off" for pH values greater than 7. In particular, it is observed as the fluorescence intensity decrease happens in parallel to the formation and then the increase of concentration of the species $[LH_2]^{2+}$ and $[LH_3]^{3+}$. This continues until the complete ”turn off” of the emission that occurs with the formation of species $[LH]^+$ and L. The data obtained from this last observation, coincide with the assumptions made previously, confirming them (PET effect).
Then we moved to investigate the emissions changes resulting from the interaction of the ligand with some metal cations, analyzing their suitability as a sensor.

3.2.2.2 Metal ions coordination in water solution.

To study the coordinative characteristics of the ligand tpy-bis[9]aneN_3 toward metal cations, we have performed potentiometric and spectrophotometric measurements of fluorescence emission in water solution. In figure 3.59 is reported a schematic representation of the ligand for which we can highlight the presence of two coordinative sites consisting of the two subunits [9]aneN_3 which in principle provide the ability to form mono- and dinuclear complexes with metal cations.

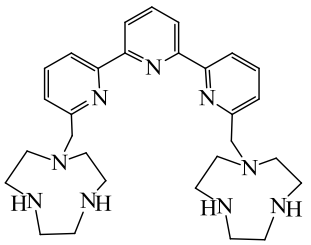

L7

Figure 3.59

The metal cations that have been studied are Zn(II), Cd(II) and Cu(II). As in previous cases we have been studied these metals because Zn(II) and Cd(II) are able to inhibit the PET effect, giving fluorescent complexes and Cu(II) as an example of paramagnetic metal. To study the coordinative properties of the ligand first,

potentiometric measurements were carried in order to determine the stoichiometry of the formed complexes and their stability constants. Obtained this information we have analyzed the UV-vis absorption spectra as pH function to investigate changes in the absorption of species which are eventually formed. Afterward, through fluorescence emission experiments the characteristics of the ligand as fluorescence chemosensor for these cations were verified.

The formation constants determined by potentiometric studies for the various species formed by the ligand **L7** with the metal cations examined, are reported in table 3.21.

Equilibrium	Zn(II)	Cd(II)	Cu(II)	Pb(II)
$M^{2+} + L \rightleftarrows [LM]^{2+}$	16.31 (2)	17.41 (3)	21.33 (2)	15.33 (1)
$[LM]^{2+} + H^{+} \rightleftarrows [LHM]^{3+}$	10.12 (4)	9.85 (5)	9.65 (4)	10.21 (5)
$[LHM]^{3+} + H^{+} \rightleftarrows [LH_2M]^{4+}$	7.91 (6)	7.5 (1)	7.48 (3)	8.01 (9)
$[LH_2M]^{4+} + H^{+} \rightleftarrows [LH_3M]^{5+}$	2.98 (1)	3.2 (1)	2.83 (4)	3.03 (3)
$[LM]^{2+} + M^{2+} \rightleftarrows [LM_2]^{4+}$	11.89 (6)	12.62 (5)	14.24 (2)	10.11 (4)
$[LM_2]^{4+} + 2OH^{-} \rightleftarrows [LM_2(OH)_2]^{2+}$	8.13 (3)	7.48 (2)	7.74 (1)	8.34 (5)
$[LM_2]^{4+} + M^{2+} \rightleftarrows [LM_3]^{6+}$	8.78 (2)	9.06 (2)	11.52 (3)	7.52 (7)
$[LM_3]^{6+} + OH^{-} \rightleftarrows [LM_3(OH)]^{5+}$	5.86 (3)	6.21 (1)	5.43 (6)	6.83 (3)
$[LM_3(OH)]^{5+} + OH^{-} \rightleftarrows [LM_3(OH)_2]^{4+}$	3.71 (8)	4.01 (4)	3.26 (8)	4.22 (2)

Table 3.21 Stability constants of the **L7** complexes with Zn(II), Cd(II), Cu(II) and Pb(II) standard deviation in parentheses. (T=298.1 K ;).

L7 forms stable mononuclear and binuclear complexes with the four metals. If we consider the constants for the addition of a second and third metal ion to the mono- and di- nuclear complex, these,are lower than those for the coordination of the first and second metal ion; as expected coordination of the second or third metal ion is affected by the presence of a positively charged ion(s) already coordinated. In fact, while the first cation is added to a neutral ligand, the second will bind to a mononuclear complex with bipositive charge. The third ion will bind instead to a dinuclear complex tetrapositive undergo in this way a certain degree of repulsion. A characteristic of di- and tri- nuclear complexes of M(II) is to form stable mono- and di- hydroxylated species (arising from deprotonation of H_2O molecules coordinates); this is due to the incomplete coordinative sphere around the metal cations, in which in addition to the donor atoms of the ligand, there is coordination of water molecules present. From the data in tables 3.21 we can calculate the species distribution diagrams that are shown below in figures 3.60-3.61. We report as representative example the diagrams of the existing species in the presence of different concentrations of Zn(II).

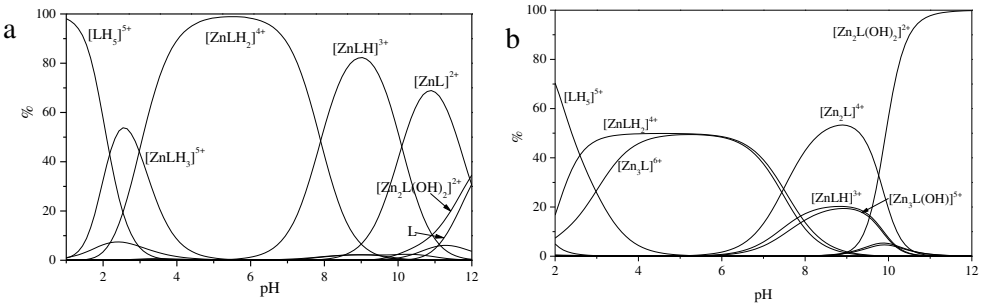

Figure 3.60 Distribution diagrams of the Zn(II) complexes formed by receptor **L7** with one (a) and two (b) equivalent of Zn(II) (**L7**, NMe4Cl, 0.1 M, 298.1 K).

Figure 3.53a shows the distribution diagram of a **L7** solution in the presence of one equivalent of Zn(II) ion. As expected there is a predominance of mononuclear complex species that forms protonated species at acidic pH or weakly alkaline. In particular, pH values about 5-6 there is an almost total predominance of the species $[LH_2Zn]^{4+}$. At alkaline pH we assist to a limited formation of dinuclear complex, with emergence of the dinuclear hydroxylated species at pH higher than 10. The free ligand is present in very small amount at pH significantly alkaline or, in its protonated form at acidic pH.

Figure 3.60bshows the distribution diagram of a **L7** solution containing two equivalents of Zn(II). To be noted how the presence of the dinuclear complex is limited to pH values higher than 8, with formation of the dinuclear hydroxylated species at pH significantly alkaline. For pH values below 8 instead, there is the formation of mononuclear complexes in their protonated forms and not protonated trinuclear complexes. The free ligand is present in minimum percentage in the protonated form for acidic pH values.

Finally, figure 3.61 shows the distribution diagram of a **L7** solution containing three equivalents of Zn(II). In this case it is observed almost exclusively the formation of the trinuclear complex, with the hydroxylated species at alkaline pH values and the species $[LZn_3]^{6+}$ for pH values ranging from 7 and 4. Below this pH value it is possible to observe the presence of the mononuclear complex in its protonated form and a small percentage of protonated free ligand.

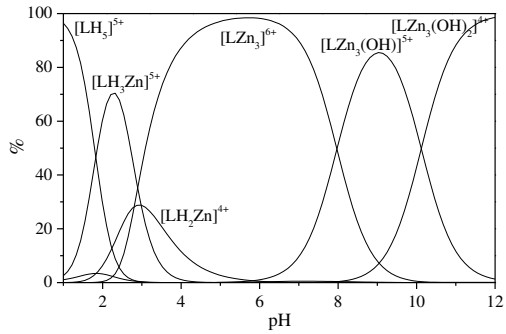

Figure 3.61 Distribution diagrams of the Zn(II) complexes formed by receptor **L7** with three equivalent of Zn(II) (**L7**, NMe4Cl, 0.1 M, 298.1 K).

3.2.2.3 UV-vis absorption spectra in the presence of M(II)

The first recorded spectra have been obtained from measurements carried out on aqueous solutions of ligand with concentration of $4 \cdot 10^{-5}$ M, buffered to pH = 7.3, in the presence of increasing amounts of metal ion.

Figure 3.62a shows the UV-visible absorption spectra in the presence of increasing amounts of Zn(II). It is clear as the ligand terpy-bis[9]aneN_3 present initially, i.e. in the absence of metal ion, possess absorption band at 290 nm. After the first addition of the metal ion the band starts to shift toward a longer wavelength, then leveling off at 315 nm. The formation of this band is diagnostic of the interaction between the subunits tpy and the metal center, and its complete development takes place following the addition of one equivalent of Zn(II). This is well illustrated by figure 3.62b, where we reported the values of absorbance at 315 and 295 nm as a function of the equivalents of Zn(II) added. Thanks to these observations we can state that, among the three receptor sites of the ligand agent, the first metal cation binds to the subunit tpy. The interaction with the second and third metal cation, therefore, involves the subunits [9]aneN_3 and implies no change in the absorption bands. Spectra recorded under similar conditions by addition of equivalents of Pb(II) and Cu(II) exhibit the same behavior, confirming that the formation of the 1:1 complex involving the tpy also in these two cases

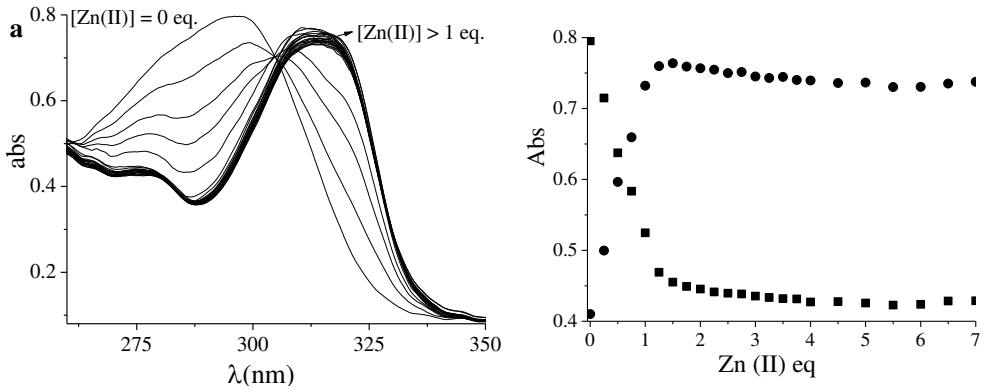

Figure 3.62 a) UV-vis spectra and **b)** absorbance at 295 (■) and 315 (●) nm of **L7** in water solution at pH 7 in the presence of increasing amounts of Zn(II) ([**L7**]=$1.4 \cdot 10^{-4}$ M)

Ion Cd(II) shows rather different behavior. Observing the absorbance change at 315 nm as a function of the number of equivalents of Cd(II) added (figure 3.63), it is clear as the complete formation of the absorption band at longer wavelength is obtained with the addition of 0.5 equivalents of ion Cd(II).

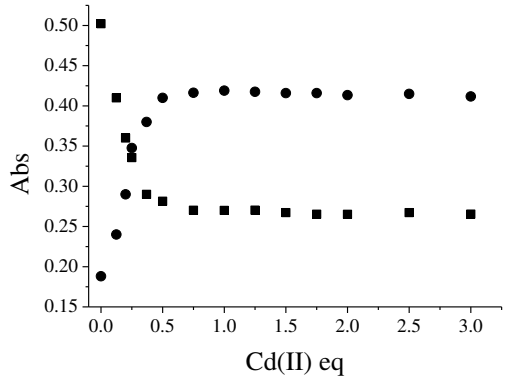

Figure 3.63 absorbance at 295 (■) and 315 (●) nm of **L7** in water solution at pH 7 in the presence of increasing amounts of Cd(II) ([**L7**]=$1.4 \cdot 10^{-4}$ M)

This may suggest that the ligand form with the ion Cd(II) complex with a stoichiometry of 2:1, which was not observed with potentiometric measurements. Further potentiometric measures are currently ongoing to determine the exact stoichiometry of this species and its stability constant. The formation of species with molar ratio Cd(II): L = 1:2 can be related to the tendency of the ion Cd(II) to form hexacoordinated complexes, much greater tendency than the other three metal cations tested. Most likely this species contains two units tpy coordinates with one Cd(II), as shown in figure 3.64.

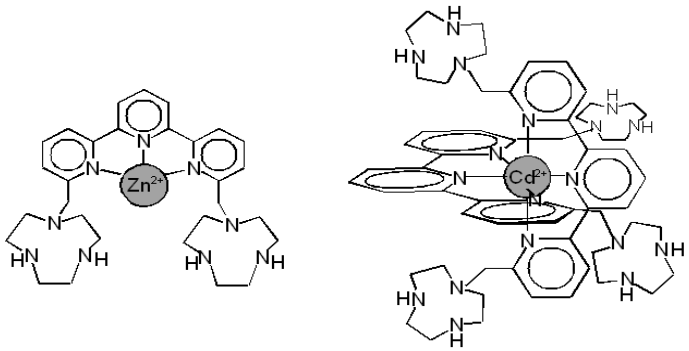

Figure 3.64 Proposed structure of the **L7** complex 1:1 with Zn(II) and 2:1 with Cd(II).

3.2.2.4 Fluorescence emission characteristics of the complexes

After studying acid-base and coordination properties of the ligand by potentiometric and spectrophotometric measurements, we analyzed the emission properties of the ligand in order to verify their ability as fluorescence chemosensors for metal ions. This was done by recording fluorescence emission spectra of ligand solutions in the presence of each metal ion in order to check the possible variation in the emission intensity. The experiments were carried out at fixed pH values in the presence of increasing amount of the metal cations as well as at different pH values on solutions containing a single metal and each. As a first step were recorded ligand emission spectra with one equivalent of M(II) in aqueous solution at pH 7. In this way we were able to define the emission characteristics of the various complex species formed by each metal ion.

In a preliminary experiments, we recorded the emission spectra of **L7** in the presence of 3 eq. of several metal cations (Zn(II), Cd(II), Pb(II), Hg(II), Cu(II), Mn(II), Ca(II), Ni(II), Co(II), Fe(II), Na(I)) at neutral pH, figure 3.65. This experiments showed that the fluorescence intensity increases more than three-fold in the presence of Zn(II) and about two-fold in presence of Cd(II), while with the other metal ions there are only minor intensity variations. In particular, in the presence of Pb(II), Hg(II), Cu(II), Fe(II), Mn(II) and Co(II) is an intensity decrease, due to the heavy atom effect in the case of Pb(II) and Hg(II) and paramagnetic effect in the case of Cu(II), Mn(II), Fe(II) and Co(II).

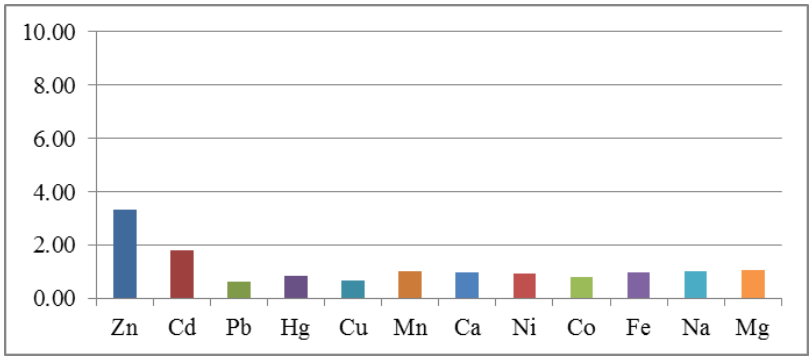

Figure 3.65 I/I_0 values for **L7** in the presence of one equivalent of different metal ions. I is the emission intensity in the presence of one equivalent of metal ion and I_0 the intensity of the free ligand.

Based on these results, we investigated the coordination effects of Zn(II) on the **L7** emission properties, in particular by recording the **L7** emission spectra at different pH values in the presence of one and three equivalent(s) of Zn(II) (figure 3.65-3.67) and at fixed pH values in presence on increasing amounts of Zn(II) (figure 3.68).

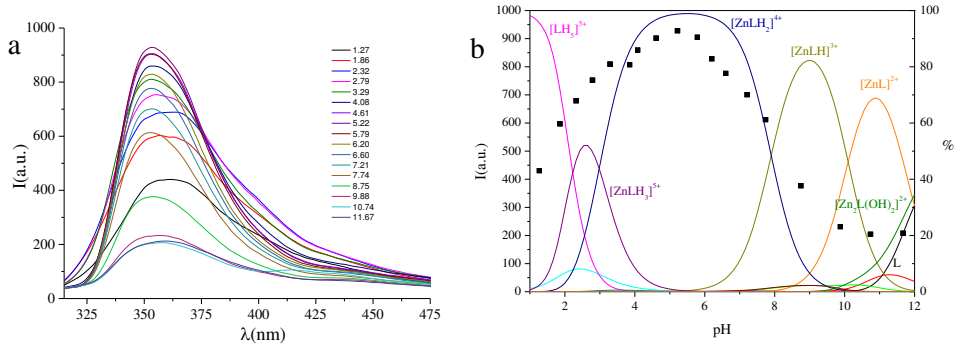

Figure 3.66 a) Fluorescence spectra of **L7** in water solution with one equivalent of Zn(II) at different pH value. **b)** Fluorescence emission intensity at 375 (■) nm superimposed on the species distribution diagram.

Figure 3.66a shows the fluorescence emission spectra of a ligand solution ($4 \cdot 10^{-5}$M) in the presence of one equivalent of Zn(II) to vary the pH and in figure 3.66b shows the relative fluorescence emission superimposed on the species distribution diagram. It is clear as the system emits more in an acid environment, while for pH values greater than 7 there is a progressive fluorescence decrease. Observing figure 3.59b is also clear as the emission intensity increase coincides with the formation of the species $[LH_3Zn]^{5+}$, reaching the maximum with the formation of the species $[LH_2Zn]^{4+}$ while the fluorescence decrease coincides with the formation of the species $[LHZn]^{3+}$. These observations are consistent with the previous results, as we have seen for the mononuclear complex (formed from a synergistic interaction between the tpy subunit and a [9]aneN_3) and showing emissivity until the deprotonation of the aliphatic nitrogen of the subunit [9]aneN_3 not involved in the

coordination, which can thus determine the fluorescence quenching due to PET effect. The emission intensity is significantly higher than that of the free ligand at the same pH value, the system is therefore emissive, but the enhancing is modulated by pH.

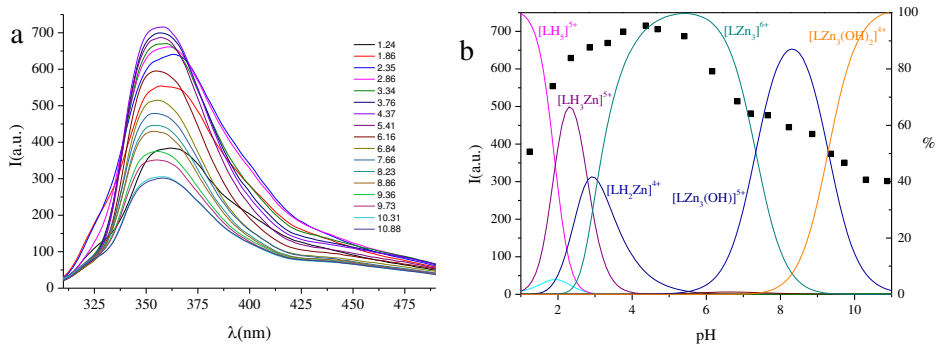

Figure 3.67 a) Fluorescence spectra of **L7** in water solution with three equivalent of Zn(II) at different pH value. **b)** Fluorescence emission intensity at 355 (■) nm superimposed on the species distribution diagram.

Figure 3.67a shows the fluorescence emission spectra and figure 3.67b shows the emission intensity at 355 nm of a ligand solution ([L]=$2\cdot10^{-5}$) in the presence of three equivalents of Zn(II). The systems behave in a similar way to the previous case and are pH dependent. To be noted as the emission intensity increases with the formation of species $[LH_2Zn]^{4+}$ and the formation of the trinuclear complex, but then decreases drastically for alkaline pH values, with formation of the hydroxylated trinuclear species. The emission intensity is significantly higher than in the case of the presence of only one equivalent of Zn(II), so we worked on a more diluted solution.

The same tests carried out in the presence of the ion Cd(II) reveal a behavior almost identical to that due to the coordination of the ion Zn(II). Both in the presence of one or three equivalents of the cation Cd(II) the increase of the fluorescence intensity of the system is modulated by pH, and proportional to the amount of ion in solution. The emission intensity is, however, less than that due to the interaction of the ligand with the ion Zn(II) and is not significantly greater than that of the free ligand; while in the presence of Cu(II) and Pb(II) the behavior is substantially different since the addition of these ions causes a fluorescence emission decrease.

Then we moved to study the behavior of the fluorescence fixed pH with additions of metal ion. Figure 3.68a shows the fluorescence emission spectra of a ligand solution ([L]=$4\cdot10^{-5}$), with progressive addition of Zn(II). We can see a marked emission intensity increase from the first addition of metal, with the attainment of a plateau of emission to the exceedance of 3 equivalents of Zn(II), being this a concentration ratio in which the three coordinative sites of the ligand are all

occupied. The emission intensity at 353 is more evident in figure 3.68b examining the emission intensity compared to the addition of progressive metal ion in solution. The fluorescence increase depends on the progressive occupation of the binding sites, which prevent their non-bonding doublets to give effect PET with consequent "turning on" of the fluorescence. We noted some changes of the slope in the emission intensity: such changes occur to the achievement of one, two and three equivalents of metal cation in solution and depend on the formation of complex species mono-, di-, and tri-nuclear, resulting in stable occupation of the binding sites.

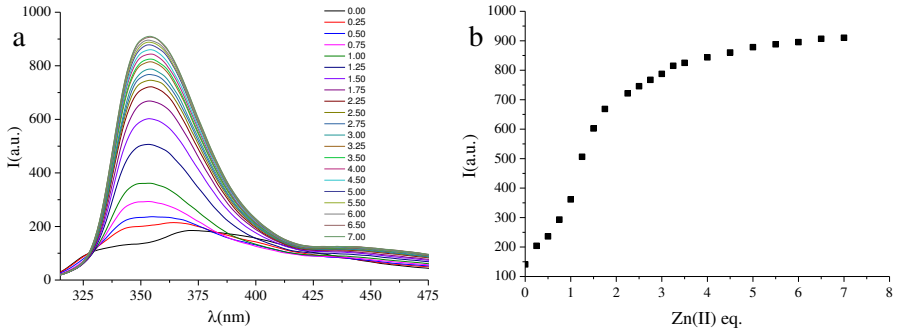

Figure 3.68 a) Emission spectra of **L7** in water at pH 7 in the presence on increasing amounts of Zn(II). **b)** Fluorescence emission intensity of **L7** at 355 nm in water at pH 7 in the presence on increasing amounts of Zn(II). ([**L7**] = $5 \cdot 10^{-4}$M).

In figures 3.69a and 3.69b are shown respectively the fluorescence emission spectra and the emission intensity for the progressive addition of Cd(II) in the same operating conditions. As can be seen, the system has a behavior similar to the case of the Zn(II), showing a significant fluorescence increase with the addition of metal ion. In figure 3.69b are obvious the slope variations in correspondence with the formation of the various stoichiometries of the complexes. Instead,for the ion Zn(II), there is a marked change of slope once reached a molar ratio between metal and ligand of 0.5:1, confirming the formation of a complex with this stoichiometry, already observed spectrophotometrically. Successive additions of Cd(II) lead to a further fluorescence emission increase gradually that other coordinative sites of the ligand (subunits [9]aneN_3) are occupied.

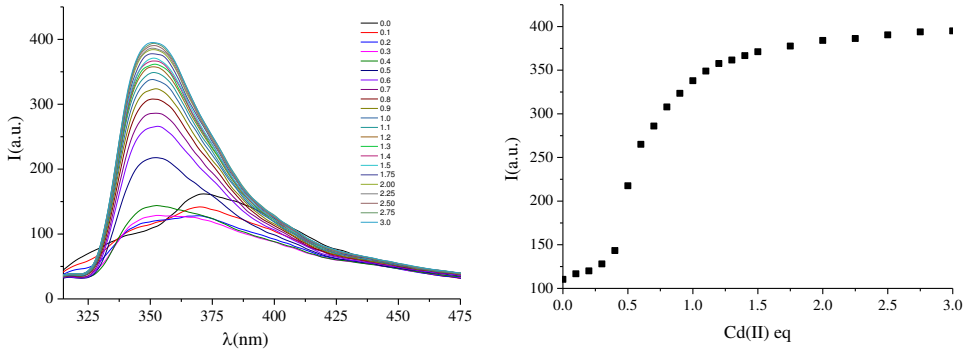

Figure 3.69 a) Emission spectra of **L7** in water at pH 7 in the presence on increasing amounts of Cd(II). **b)** Fluorescence emission intensity of **L7** at 355 nm in water at pH 7 in the presence on increasing amounts of Zn(II). ([**L7**] = $5 \cdot 10^{-4}$M).

3.2.2.5 Phosphate recognition by a mononuclear Zn(II) complex.

Potentiometric, ^{1}H NMR and UV-Vis studies showed that **L7** as free ligand possesses a very low binding ability for inorganic phosphates in aqueous solution. The stability constants of the complexes determined through potentiometric measurements are reported in tables 3.22.

Reaction	Log K	
	$P_2O_7^{4-}$	$P_3O_{10}^{5-}$
$[H_2L]^{2+} + [A]^{n-} = [H_2LA]^{(2-n)+}$	2.9(1)	2.7(1)
$[H_2L]^{2+} + [HA]^{n-1} = [H_3LA]^{(3-n)+}$	3.2(4)	2.9 (1)
$[H_3L]^{3+} + [HA]^{n-1} = [H_4LA]^{(4-n)+}$	3.2(1)	3.1(1)
$[H_4L]^{4+} + [HA]^{n-1} = [H_5LA]^{(5-n)+}$	3.4(1)	3.2(1)

Table 3.22 Stability constants of the **L7** complexes with di- and tri-phosphate, standard deviation in parentheses. (T = 298.1 K, I = 0.1 M).

From the data in tables 3.22, we can calculate the competition diagram distribution of the species that are shown below in figures 3.70. As we can see in figure 3.70, the overall percentages of the adducts formed by **L7** with $P_2O_7^{4-}$ and $P_3O_{10}^{5-}$ as a function of pH in a competitive system containing **L7**, $P_2O_7^{4-}$ and $P_3O_{10}^{5-}$ in equimolecular ratio, in the absence of Zn(II), the ligand **L7** do not possess any type of selectivity towards diphosphate and triphosphate, as you might be expected even seeing stability constants

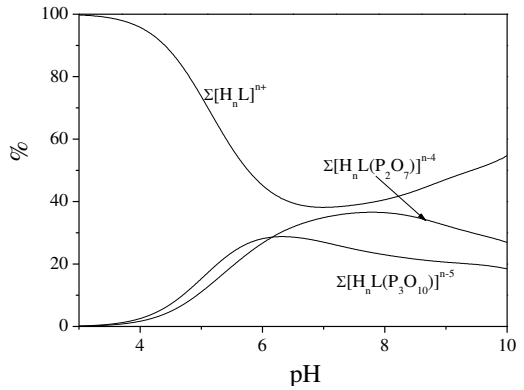

Figure 3.70 Overall percentages of the adducts formed by **L7** with $P_2O_7^{4-}$ and $P_3O_{10}^{5-}$ as a function of pH in a competitive system containing **L7**, $P_2O_7^{4-}$ and $P_3O_{10}^{5-}$ in equimolecular ratio

This scarce binding ability of **L7** for phosphate anions has been attributed to the trans-trans conformation assumed by the ligand in solution (this is the most stable conformation also for tpy in solution, which brings the two macrocyclic units to set far from each other, thus preventing the formation of clefts/pockets of suitable dimension for an efficient substrate encapsulation). However, Zn(II) binding by the tpy unit of **L7** to give at pH = 7.0 the complex $[ZnH_2\mathbf{L7}]^{4+}$ (the only species present in solution at neutral pH from potentiometric measurements) causes the conversion of the ligand from the trans-trans to the cis-cis conformation, as we can see in figure 3.71.

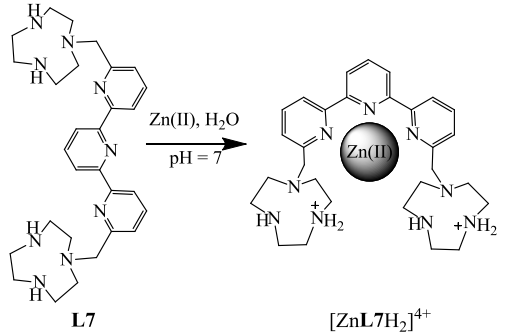

Figure 3.71 Schematic representation of the conformational changes of **L7** upon interaction with Zn(II) and formation of the complex $[Zn\mathbf{L7}H_2]^{4+}$ at pH = 7.0 in water.

More interestingly, Zn(II) binding strongly affects the fluorescence emission of **L7** as a marked enhancement of the fluorescence emission is observed up to the addition of 1 equiv. of Zn(II) at pH = 7.0. As a consequence of the cis-cis conformation assumed by **L7** upon Zn(II) binding to the tpy unit, the species $[ZnH_2\mathbf{L7}]^{4+}$ shows a marked tendency to bind PPi over a wide pH range according to potentiometric measurements (table 3.23). On the contrary, the binding ability of the same complex towards Pi and TPi is remarkably lower.

Reaction	Log K		
	PO_4^{3-}	$P_2O_7^{4-}$	$P_3O_{10}^{5-}$
$[ZnL]^{2+} + [A]^{n-} = [LZnA]^{(2-n)+}$	3.0(1)	4.8(1)	3.8(1)
$[ZnLH]^{3+} + [A]^{n-} = [ZnLHA]^{(3-n)+}$	3.2(1)	5.2(1)	4.0(1)
$[ZnLH_2]^{4+} + [A]^{n} = [ZnLH_2A]^{(4-n)+}$	3.6(1)	6.4(1)	4.1(1)
$[ZnLH_2]^{4+} + [HA]^{n-1} = [ZnLH_3LA]^{(5-n)+}$	3.2(1)	6.2(1)	3.8(1)

Table 3.23 Addition constants of phosphate anions to the Zn(II) complex with **L7** (T=298.1K, I = 0.1 M).

From the data in table 3.23, we can calculate the competition diagram distribution of the species that are shown below in figures 3.72. As we can see in figure 3.72, the overall percentages of the adducts formed by the Zn(II) complex with PO_4^{3-}, $P_2O_7^{4-}$ and $P_3O_{10}^{5-}$ as a function of pH in a competitive system containing Zn(II), **L7**, PO_4^{3-}, $P_2O_7^{4-}$ and $P_3O_{10}^{5-}$ in equimolecular ratio, the system presents a good selectivity towards $P_2O_7^{4-}$. In fact, the adduct between the mononuclear complex of Zn(II) and this anion is the most present for pH values above 4

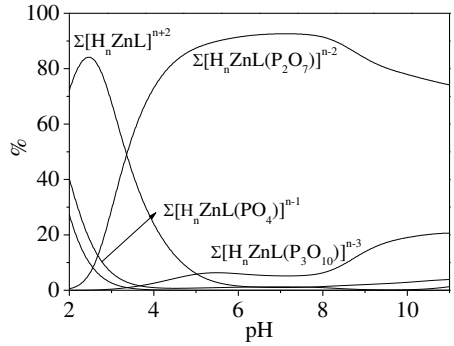

Figure 3.72 Overall percentages of the adducts formed by the Zn(II) complex with PO_4^{3-}, $P_2O_7^{4-}$ and $P_3O_{10}^{5-}$ as a function of pH in a competitive system containing Zn(II), **L7**, PO_4^{3-}, $P_2O_7^{4-}$ and $P_3O_{10}^{5-}$ in equimolecular ratio

DFT calculations performed on the adduct formed between $[ZnH_2\mathbf{L7}(H_2O)_2]^{4+}$ (Zn(II) is considered pentacoordinated, thanks to two additional water molecules as normally found in 1:1 complexes with tpy) and $P_2O_7^{4-}$ with an implicit simulation of the aqueous environment, suggest that PPi is not directly bound to the metal center. The PPi anion is encapsulated within the cleft delimited by the two protonated [9]aneN3 units and does not replace the water molecules in the coordination sphere of the metal; it prefers to establish a hydrogen bonding network involving both the coordinated water molecules and the ammonium groups of the receptor (figure 3.73).

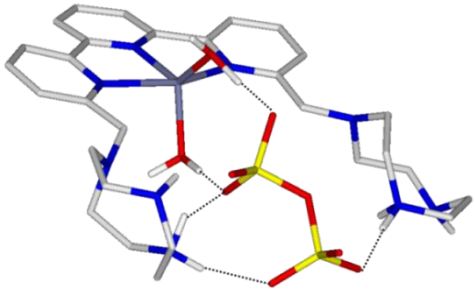

Figure 3.73 Calculated structure for the $[ZnH_2\mathbf{L7}]^{4+}$/ $P_2O_7^{4-}$ complex (DFT level of theory).

This kind of interaction is responsible of the quenching of the fluorescence at pH = 7 of the 1:1 Zn(II) complex up to the addition of 1 equiv. of PPi (figure 3.74). In fact, the decreased charge on the [9]aneN_3 units may allow the polyamine groups to restore a PET process to the excited fluorophore. Of note, the emission of the complex $[ZnH_2\mathbf{L7}]^{4+}$ is not affected by the presence of Pi and only 8% reduced by a three-fold excess of TPi, confirming the weaker interactions of these anions with the metal based receptor. **L7** represents, therefore, a unique case of receptor which couples anion recognition and sensing, mainly thanks to an "allosteric effect" exerted by a metal cation. The Zn(II), in fact, does not acts as a direct anchoring site for PPi through coordinative bonds, but induces a conformation change in the receptor structure, which allows substrate binding via weak, non-coordinative forces.

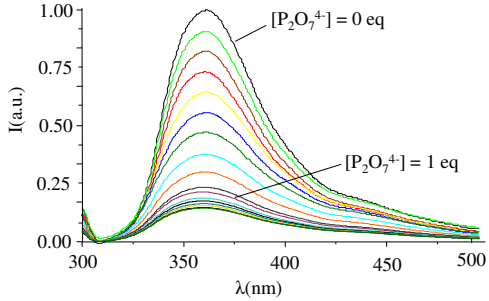

Figure 3.74 Fluorescence emission spectra of the Zn/**L7** system (1:1 molar ratio) in the presence of increasing amounts of $P_2O_7^{4-}$ in aqueous solution at pH 7.

The consequent new organization of the binding sites imparts to the receptor selectivity in both anion binding and fluorescence sensing, figure 3.75.

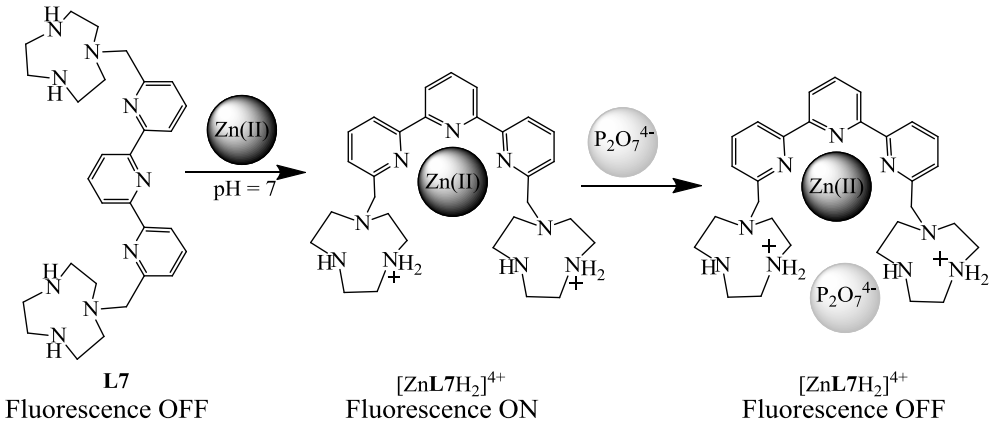

Figure 3.75 Conformational change and selective coordinating of diphosphate anion.

3.2.3 Selective recognition of uracil-containing molecules with a fluorescent dizinc(II) complex.

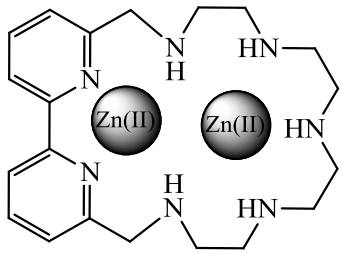

Figure 3.76 Dizinc(II) complex of **L8** in water solution, called hereafter **1**.

Selective binding of nucleobases and nucleosides is involved in a number of biological processes including protein synthesis, genome duplication, and signal transduction. Nucleobases/nucleosides derivatives can also be potent pharmacological agents. They actually play a crucial role in the current treatment of cancer and viral infections as the primary components of highly active anti-retroviral therapy. Examples can be the anticancer drug 5-fluorouracyl (5-FU) and the anti-HIV agent azidothymidine (AZT). As a consequence, there is a current interest in the design and synthesis of new receptors able to recognize specific, isolated, nucleobases.

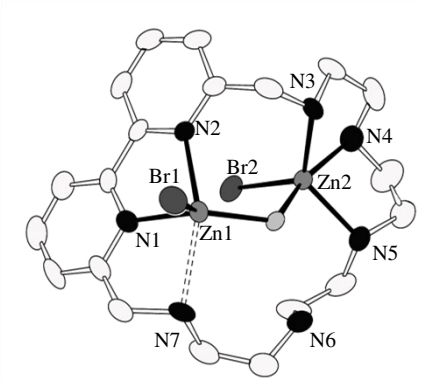

Figure 3.77 ORTEP-3 view of complex $[Zn_2(\mathbf{L8}H)(OH)Br_2]^{2+}$. Hydrogen atoms have been omitted for clarity

Bond	(Å)
Zn1-N1	2.032
Zn1-N2	2.218
Zn1-N7	2.478
Br1-O1	2.382
Zn1-O1	1.928
Zn2-O1	2.104
Zn2-N3	2.143
Zn2-N5	2.142
Zn2- N4	2.155
Zn1-Zn2	2.499

Table 3.24 Bond distances in $Zn_2\mathbf{L8}$

3.2.3.1 Speciation and complex stability in aqueous solution

Binding of U, 3',5'-UpU, 3',5'-UpA, AZT and 5-FU was firstly analyzed by means of potentiometric titrations, in order to establish the stoichiometry of the ternary complexes, to analyze the protonation/deprotonation equilibria that can potentially be involved in the complexation process and, finally, to verify the presence of possible selectivity pattern among the substrates under investigation. The adducts formed in aqueous solution and the corresponding formation constants are shown in table 3.19, while distribution diagrams of the complexes formed in solution in the presence of U, 5-FU, AZT and 3',5'-UpU are given in figure 3.78.

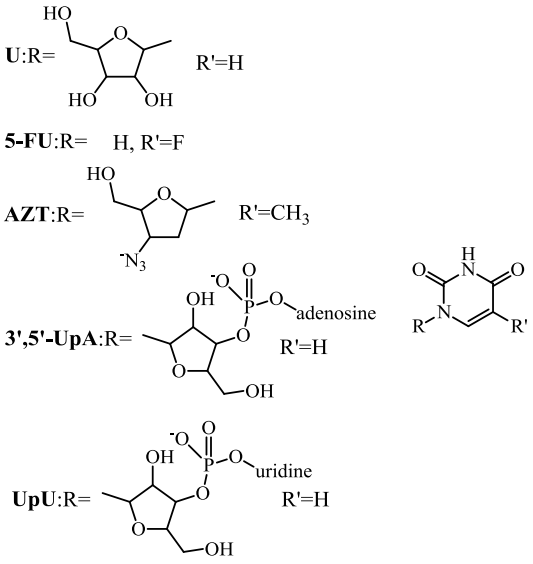

Figure 3.78 Studied substrate

The diagrams for the complexes with 3',5'-UpA are similar to that shown for U. Considering U, 5-FU, AZT and 3',5'-UpA binding, the data in table 3.25 and figure 3.79 clearly show that the dizinc complex can bind one or two substrate molecules affording stable $[\mathbf{1}[S(H_{-1})]]^{3+}$ and $[\mathbf{1}[S(H_{-1})]_2]^{3+}$ complexes, respectively (S = U, 5-FU, AZT or 3',5'-UpA). In all cases substrate binding occurs at slightly acidic pH values with simultaneous release of an acidic proton and formation of a $[\mathbf{1}[S(H_{-1})]]$ adduct (S = U, AZT, 5-FU and 3',5'-UpA) (figure 3.78). Considering that these substrates contain a deprotonable -CO-NH-CO- imide function and behave as weak acids in aqueous solution ($pK_a > 9$ for U, AZT, 3',5'-UpU, 3',5'-UpA, $pK_a = 8.01$ for 5-FU), the process of proton release observed upon binding to the dizinc complex may be attributed to a metal-assisted deprotonation process of their imide unit and simultaneous coordination of the negatively charged nitrogen donor to the metal. Potentiometric titration carried out in the presence of nucleosides/dinucleotides not containing a similar functional group (G, C, A, 3',5'-ApA, 3',5'-CpC and 3',5'-GpG) pointed out that no interaction occur in solution with the $[Zn_2L]^{4+}$ complex, indicating that the presence of a -CO-NH-CO- moiety is a necessary requisite for substrate anchoring to the dizinc complex. A similar binding mode was firstly proposed by Kimura and co-workers to explain selective binding of thymidine, uridine (U) and their derivatives over guanosine, cytidine or adenosine (A) by receptors based on the $[Zn(cyclen)]^{2+}$ complex[37].

[37] S. Aoki, E. Kimura, *Chem. Rev.*, **2004**, 104 769-788

	U[a]	3',5'-UpA[a]	AZT	5-FU
Equilibrium	Log K			
$[\mathbf{L8}Zn_2] + [S(H_{-1})] = [\mathbf{L8}Zn_2[S(H_{-1})]]$	8.1(1)	6.1(1)	7.5(1)	5.8(1)
$[\mathbf{L8}Zn_2{\cdot}[S(H_{-1})]] + [S(H_{-1})] = [\mathbf{L8}Zn_2[S(H_{-1})]_2]$	7.2(1)	4.9(1)	6.4(1)	4.8(1)

Equilibrium	Log K
$[\mathbf{L8}Zn_2] + [UpU(H_{-1})] = [\mathbf{L8}Zn_2[UpU(H_{-1})]]$	8.0(1)
$[\mathbf{L8}Zn_2{\cdot}[UpU(H_{-1})]] = [\mathbf{L8}Zn_2[UpU(H_{-2})]] + H^+$	8.1(1)

Table 3.25 Addition constants of deprotonated substrates to complex $[\mathbf{L8}Zn_2]$ determined at 298.1 K in NMe_4NO_3 0.1 M.

Interestingly, table 3.25 shows that the constant for the addition of the first and the second deprotonated substrate ($S(H_{-1})$) to the $[Zn_2L]^{4+}$ and $[Zn_2L[S(H_{-1})]]^{3+}$ complexes, respectively, are rather similar, differing of *ca* 1 log units. This observation suggests that that the two anionic species are likely to be bound, almost independently, by a single Zn(II) ion, as sketched in figure 3.79.

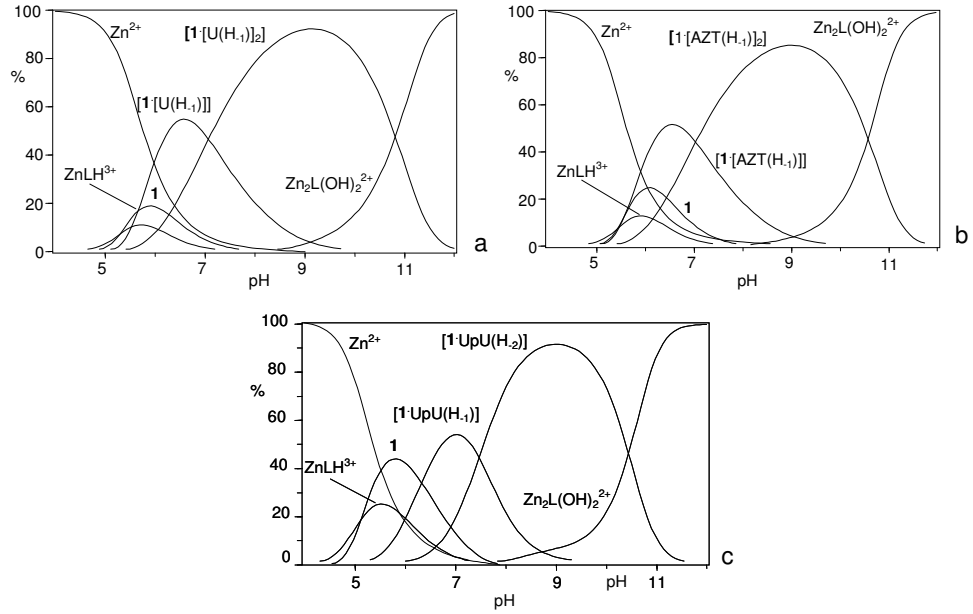

Figure 3.79 Distribution diagrams for of the complexes formed by $[Zn_2L]^{4+}$ with U (**a**), AZT (**b**) and 3',5'-UpU (**c**)($[Zn_2L]^{4+} = 5{\cdot}10^{-5}$ M, [U] = [AZT] = [UpU] = $1{\cdot}10^{-4}$ M, NMe_4NO_3 0.1 M, 298.1 K).

Finally, binding of hydroxide anions at alkaline pH values to Zn(II) leads to detachment of substrates from the metal centers and formation of hydroxy complexes, as expected considering the high affinity of the OH^- anion for Zn(II).
Despite the same species formed in solution, U, AZT, 5-FU and 3',5'-UpA show a different binding affinity for the dizinc complex. The data in table 3.25 point out that the addition constants of the substrates to **1** decrease in the order U < AZT <

3',5'-UpA ≈ 5-FU. Several factors may influence the binding ability of these substrates to **1**, in particular the different σ-donor properties of the deprotonated imide function and the presence of large and hindering substituents linked to the uracil moiety. Hydrophobic and π-stacking interactions between the heteroaromatic ring of the substrates and the dipyridine unit can also contribute to determine the stability of the adducts. Of note, the less stable complexes are formed by 5-FU and 3',5'-UpA. While the former contains an electron withdrawing group, which reduce the σ-donor ability of the deprotonated imide nitrogen, the latter bears a bulky adenosine moiety, affording a sterically hindered adduct with complex **1**.

As previously reported, 3',5'-UpU displays a somewhat different behaviour. As in the case of U, binding of 3',5'-UpU occurs at slight acidic pH values *via* deprotonation of an uracil moiety upon metal binding and leads to the formation of a $[\mathbf{1}[UpU(H_{-1})]^{3+}$ species, containing a single-deprotonated dinucleotide. This process is followed at neutral pH value by release of a second acidic proton, which can be reasonably attributed to deprotonation of the second uracil unit of UpU to form a $[\mathbf{1}[UpU(H_{-1})_2]^{2+}$ complex. In the latter species each uracil moieties of 3',5'-UpU is likely to be bound to a single metal ion, as sketched in figure 3.80b

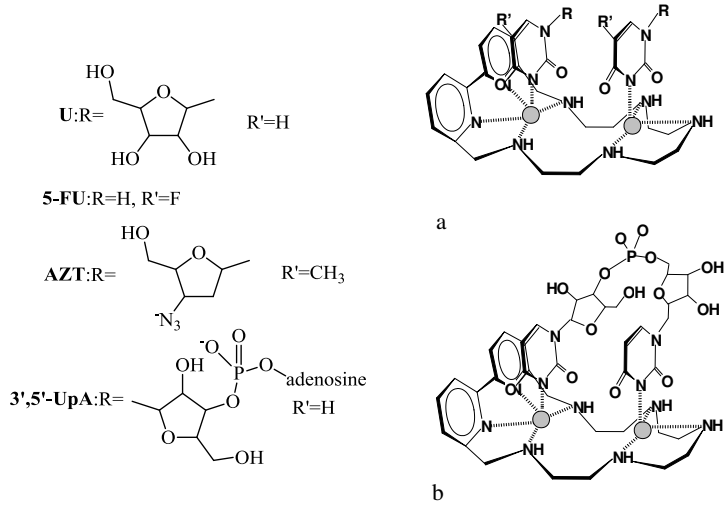

Figure 3.80 (**a**) Proposed binding mode of U, AZT, 5-FU and 3',5'-UpA in the $[\mathbf{1}[S(H_{-1})]_2]$ complex and (**b**) of UpU in $[\mathbf{1}[UpU(H_{-1})_2]$

Substrate binding was also confirmed by ^{1}H NMR experiments recorded at different pH values on solutions containing the substrates and complex $[Zn_2L]^{4+}$. The binding process is accompanied by line broadening of the ^{1}H NMR signals at room temperature and therefore the measurements were carried out at 45°C. In the case of 3',5'-UpA and 3',5'-UpU, the line broadening is more marked preventing any reliable attribution of the signals even heating a 70 °C. The spectra recorded in the

presence of AZT, 5-FU show a progressive downfield shift of the signals of the nucleobase from pH ca 5 to pH 8.5-9, where increasing amounts of the complexes $[\mathbf{1}[S(H_{-1})]]^{3+}$ and $[\mathbf{1}[S(H\text{-}1)]_2]^{2+}$ are formed in solution, as shown in figure 3.73 for AZT.

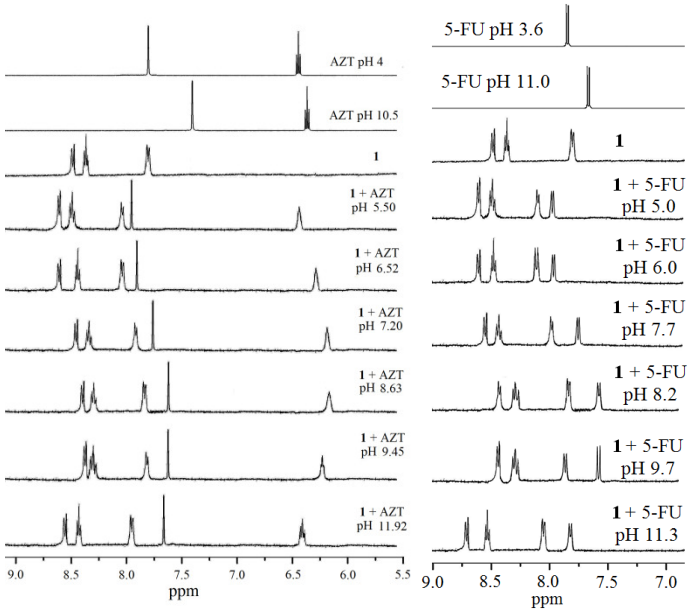

Figure 3.81 ^{1}H NMR spectra of **1** with AZT and 5-FU at different pH values.

Interestingly enough, the downfield shifts observed upon binding by **1** are by far higher than those found for deprotonation of free substrates. This result is quite unusual considering that deprotonation is accomplished via simultaneous binding to the positively charged metal center, which should reduce the negative charge gathered within the aromatic moieties. In principle, this would generate smaller downfield shifts than that found for deprotonation of the free nucleobases. However, downfield shift of aromatic protons can be also due to interactions between aromatic or heteroaromatic systems, in particular the formation of π-stacking contacts. This possible interaction mode is strongly confirmed by the downfield shift of the aromatic protons observed for the dipyridine unit of 1 complexes upon substrate binding, which increase in the order 5-FU < AZT < U, paralleling the addition constant value of these substrates to the 1 complex. Steric factors due to the presence of different substituents on the aromatic rings of U, AZT and 5-FU may contribute to the strength of the stacking interaction. However, the weaker π-stacking interaction between 5-FU and dipyridine reasonably also reflects the electron-withdrawing effect of the fluoride substituent, which reduces the electron density on the aromatic ring and consequently decreases the interaction with electron-poor dipyridine system.

Finally, the signals of both substrates and dipyridine protons bear a marked upfield shift at pH values greater than 9.5 and at pH 11.5 their chemical shift is almost equal to that observed for the free complex **1** and the deprotonated nucleobases, in keeping with their release from the dizinc complex upon hydroxide binding to Zn(II) observed in the potentiometric titrations at alkaline pH values. Of note, no effect was observed by addition of nucleosides C, G or A confirming the absence of any detectable interactions between these substrates and complex **1.**

Results of the conformational searches carried out on the 1:2 adducts formed by macrocycle-dizinc complex (**1**) with U, UpA, 5FU and AZT are shown in figure 3.82-3.83. In all adduct, the bipyridyl unit is coordinated to a zinc ion, while the other metal is coordinated by the nitrogen atoms of the aliphatic chain. The coordination spheres of the metal ions are defined also by a bridged hydroxo group and by two substrate molecules. Each substrate group is coordinated to a zinc ion through the deprotonated imidic nitrogen, the coordination being reinforced by additional H-bonds involving carbonyl oxygen and secondary nitrogens of the macrocycle. This kind of reinforced coordination bond has been already reported by several authors, about the interaction of metal complexes of aza-macrocycles with substrates containing imidic functions.

In all cases, two different conformers were found, respectively featured by the substrate molecules located on the same side (*cis*-conformation in the following – figure 3.82) or on the opposite side (*trans*-conformation – figure 3.83) respect to the binuclear complex. In all the *cis* conformers the two metal ions are bridged by a substrate molecule trough the deprotonated imide nitrogen and a carbonyl oxygen. The chelating binding mode of the bipyridine unit determines a significant degree of coplanarity of the aromatic rings in all the *cis* (dihedral angles ranging from 21.6° to 22.15°) and *trans* adducts (maximum value for the dihedral angle 8.6°).

As the *trans* conformers are concerned, it is worth noting that the overall conformation assumed by the binuclear complex in all the 1:2 adducts is very similar to the crystal structure obtained for the $[Zn_2(H\mathbf{L8})(OH)Br_2]^{2+}$ cation, figure 3.77, so confirming the reliability of the modelling procedure.

On the other hand, the *cis* conformers feature the two substrates units located on the same side of the dizinc complex (figure 3.82). The centroid-centroid distances between the two guest units fall in the range 3.7 (AZT) - 4.6 Å (UpA) and the aromatic rings form dihedral angles ranging from 17.8° (AZT) to 40.8° (U). As shown by figure 3.82, in all the 1:2 compounds, the substrate molecule linked to the zinc coordinated by the heteroaromatic nitrogens, is able to interact also with a pyridine ring of the bipyridine unit. Centroid-centroid distances featuring these interactions are slightly longer than in the case of substrate-substrate interaction

(from 4.5 Å (AZT) to 4.8 Å (5FU and UpA) – dihedral angle values in the range 55.4 (AZT) -67.9° (UpA)).

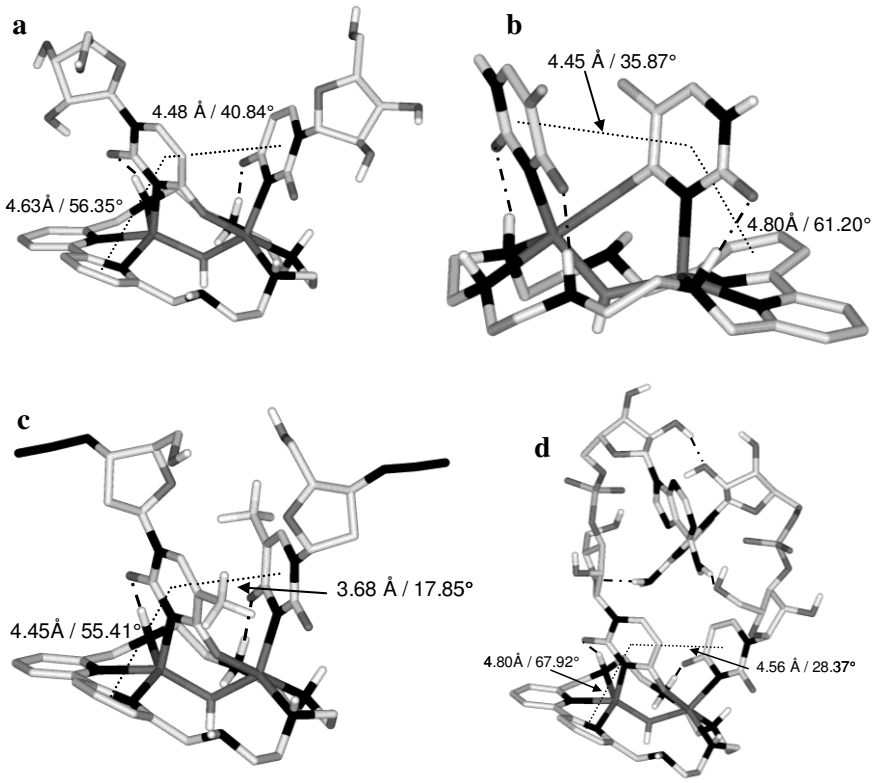

Figure 3.82 *cis*-Conformers for the 1:2 adducts formed by macrocycle-dizinc complex (**1**) with U (a), 5FU (b), AZT (c) and UpA (d).

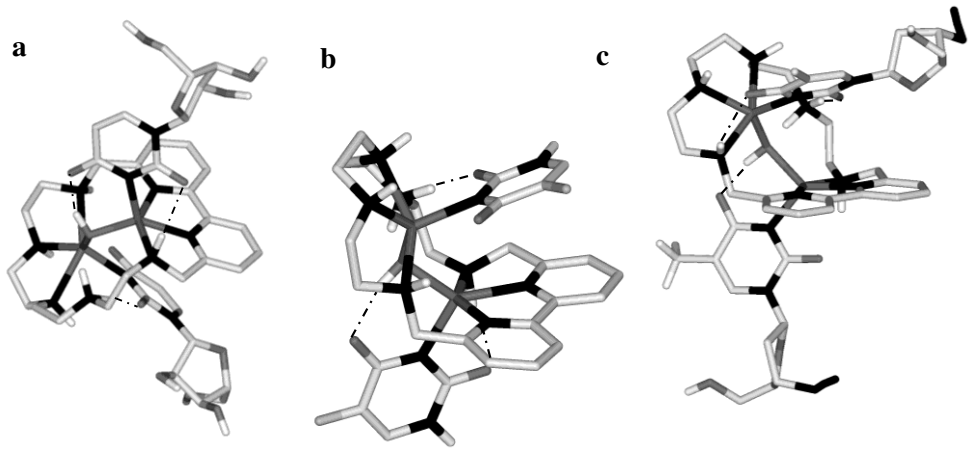

Figure 3.83 ***trans*-**Conformers for the 1:2 adducts formed by macrocycle-dizinc complex (**1**) with U(a), 5FU(b), AZT(c).

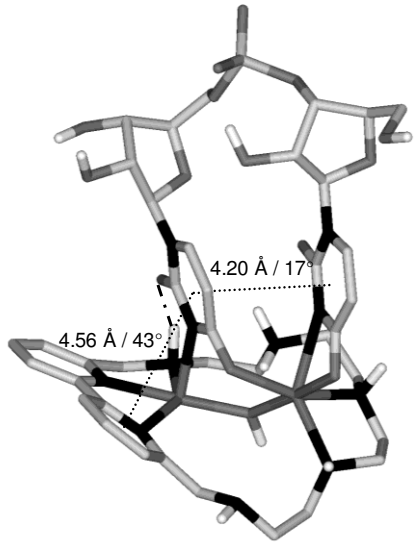

Figure 3.84 Conformer for the 1:1 adduct formed by macrocycle-dizinc complex **(1)** with UpU.

While the *trans* conformers are the lowest in energy for the U, 5FU and AZT substrates (ΔE = 1.44, 2.63 and 4.17 kJ/mol for the *cis* conformers, respectively), it is the highest energy structure for $Zn_2L(UpA)_2$ (ΔE = 5.94 kJ/mol).

As the UpU is concerned, only the 1:1 stoichiometry was considered and the minimized structure (figure 3.84) shows the deprotonated imidic nitrogen of each uracil unit coordinated to a zinc ion, similarly to what found in the 1:2 complexes. The two uridine residues are located on the same side of the complex, whose overall structure is very similar to what seen in the *cis* conformers of the other studied substrates. The centroid-centroid distances and dihedral angle values featuring the uridine-uridine and uridine-pyridine ring interactions are 4.20 Å/17° and 4.56 Å/43°, respectively, and they are located in the lowest values side of the range reported for the 1:2 complexes, suggesting the presence of stronger π-π stacking interaction in the UpU adduct.

Concluding, the three rather parallel aromatic groups at close distance from each other found in the ground states of UpU and UpA complexes are most likely responsible for the exciplex emissions measured in aqueous solutions at 1:1 (UpU) or 1:2 (UpA) molar ratios. Moreover, conformations similar to those most likely featuring the excited states, but already present in the ground states could be invocated to explain the quick formation of the exciplexes, confirmed by the short τ_2 values measured for this two systems.

On the other hand, the Uridine adduct, whose lowest energy structure is characterized by trans conformation, shows an exciplex emission, similarly to UpU and UpA, which apparently does not agree with the above reported deductions.

However it is interesting to note that the *cis/trans* ΔE found for the uridine adduct is 1.44 kJ/mol, while 2.63 and 4.17 kJ/mol ΔE values were found for 5FU and AZT, respectively. It could be suppose that a certain percentage of *cis* conformer, low but enough to give a measurable exciplex emission, is present in aqueous solution only in the case of uridine.

3.2.3.2 Fluorescence emission properties of the adducts with $[Zn_2L8]^{4+}$.

The dizinc complex **1** shows the typical absorption spectrum of dipyridine (a band at ca 279 nm) and an emission spectrum featuring a single band at 330 nm. While the absorption spectrum is not affected by the presence of all substrate under investigation, addition of U, UpA, UpU and AZT to a solution of **1** in the pH range 5-9, where the $[\mathbf{1}[S(H_{-1})]_2]^{2+}$ (S = U, UpA or AZT) or $[\mathbf{1}[UpU(H_{-1})_2]^{2+}$ species are formed in solution, remarkably affect the fluorescence emission spectrum, giving rise to a decrease of the emission intensity at 330 nm and to the formation of a broad band with a maximum at 440 nm, as shown in figure 3.85 for U. As shown in figure 3.85a and 3.85b for U, addition of increasing amount of the nucleoside to a solution of **1** at pH 9 leads to a decrease of the fluorescence emission at 330 nm and to a new intense, non-structured and red-shifted emission band with a maximum at 440 nm. The emission intensity at 440 nm increases linearly up to 1.5:1 and 1.8:1 UpA and U to **1** molar ratio, respectively, to achieve a constant value for molar ratios greater than 3 (UpA) and 2.4 U, in keeping with the formation of stable 1:2 adducts between the substrates and the dimetal complex. These spectral changes account for an exciplex-type emission in ternary adducts, probably due to a π-stacking complex in the excited state, involving dipyridine and Zn(II)-bound U or UpA. Of note, the exciplex emission is strongly pH-dependent. In fact, the emission intensity emission at 440nm increases from pH 6 to 9 and then decreases at more alkaline pH values (Figure 3.85c and 3.85d). Of note, superimposition of the distribution curves of the complexes and the fluorescence emission intensity at 440nm at different pH values suggests that the exciplex emission is given only by the $[\mathbf{1}[S(H_{-1})]_2]^{2+}$ adducts, as shown in figure 3.85d for U, while the formation of the 1:1 adducts $[\mathbf{1}[S(H_{-1})]]^{3+}$ does not alter the original spectra of the dipyridine moiety.

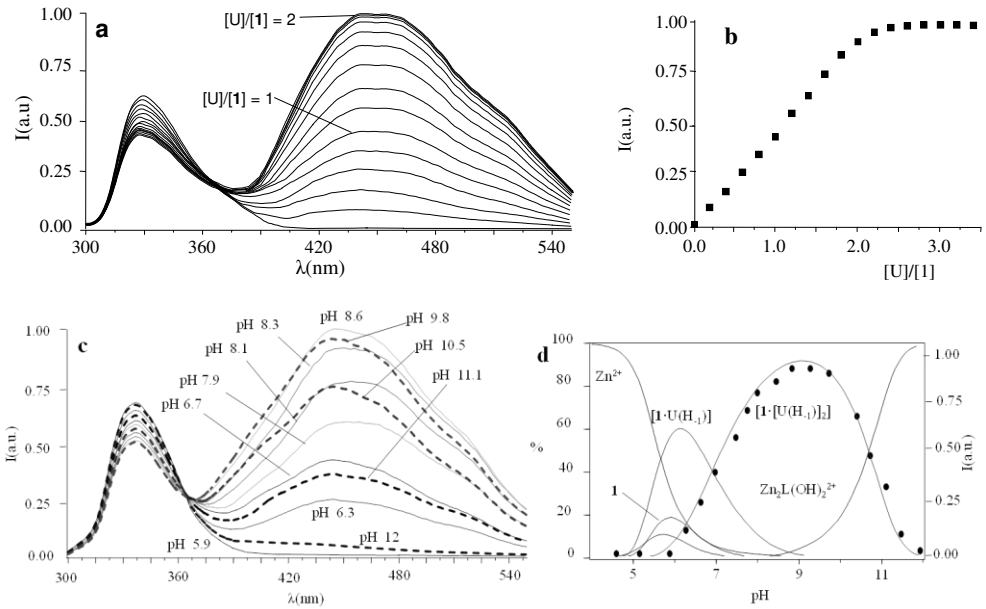

Figure 3.85 (**a**) Fluorescence spectra and (**b**) emission intensity of **1** at 440 nm in presence of increasing amounts of U at pH 9; (**c**) fluorescence emission spectra at different pH values and (**d**) emission intensity at 440 nm (•, right y axis) as a function of pH superimposed to the distribution curves of the complexes (solid curves, left y axis) for a system containing **1** and U in 1:2 molar ratio (**1**= $2.5 \cdot 10^{-5}$ M, λ_{exc}= 290 nm, 298.1 K).

The emission is therefore due to metal-assisted assembly of three heteroaromatic units fixed at short distances. In the $[\mathbf{1}[S(H_{-1})]]^{3+}$ complexes the nucleobase can be either anchored to the metal cations far from the dipyridine unit or bound to the Zn^{2+} close to the fluorogenic unit, but with a spatial disposition which prevents the formation stacking interaction. A similar behaviour is found in the case of 3',5'-UpU, where the exciplex emission is due to the formation of the $[\mathbf{1}[UpU(H_{-1})_2]]^{2+}$ adduct, containing two uracil moieties bound to complex **1**. Conversely, the $[\mathbf{1}[UpU(H_{-1})]]^{3+}$ adduct, containing a single uracil unit bound to the complex does not display any exciplex emission.

Nucleosides A, G and C and dinucleotides 3',5'-ApA, 3',5'-GpG, and 3',5'-CpC do not show any exciplex, confirming that these substrates do not interact, or interact very weakly, with complex **1**. More interestingly, 5-FU does not produce exciplex emission and AZT gives an emission at 440 nm weaker than that observed for U and UpU, figure 3.86. This behaviour can be related to the weaker interactions of the heteroaromatic ring of AZT and 5-FU with dipyridine in excited state, as already observed in the ground state from the ^{1}H NMR spectra of the complexes.

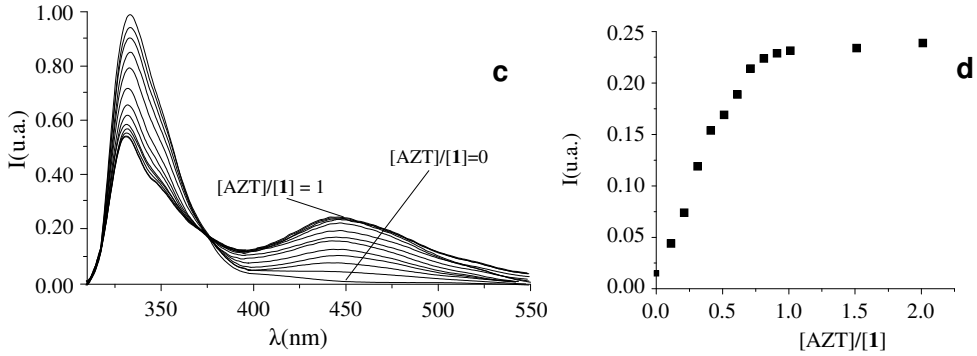

Figure 3.86 Fluorescence spectra (**a**) and (**b**) emission intensity of **1** at 440 nm in presence of increasing amounts of AZT at pH 9; ([**1**] = $2.5 \cdot 10^{-5}$ M, λ_{exc} = 290 nm, 298.1 K).

3.2.4 Phosphate binding by a novel Zn(II) complex featuring a trans-1,2-diaminocyclohexane ligand. Effective anion recognition in water.

This receptor design is inspired by metallo-enzymes, for which phosphates act as substrates or inhibitors by reversibly coordinating to one or more Zn(II) ions in the enzymatic pocket. Although these strategies have been widely exploited in recent literature, a synergetic combination of the two approaches is still largely unexplored. In this context, we have synthesized receptor $\mathbf{L9}^{2-}$ featuring an iminodiacetate (IDA) moiety appended to a polyamine macrocycle containing two trans-1,2-diaminocyclohaexane (DAC) units and a pyrrole ring. Apart from a H-bonding pyrrole unit, this receptor features two potential binding sites for metal cations, the IDA subunit and the DAC-based macrocyclic moiety. Both IDA and DAC are indeed well known chelating agents for metal cations. Because DAC is also strongly basic, due to its ability to "chelate" the proton between the two amine groups, it is expected that the macrocyclic unit will be protonated in a wide pH range, in which coordination of amine to Zn(II) would be inhibited.

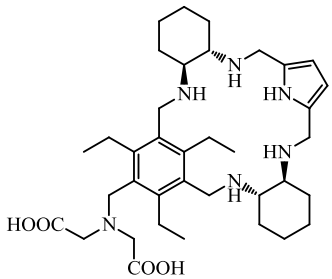

Figure 3.87 H_2L9

These characteristics could make receptor H_2**L9** capable of binding Zn(II) ions to one or both binding sites depending on the pH of the solution. Even in the presence

of the protonated macrocycle, however, Zn(II) mediated bridging of the two binding sites of the receptor by phosphate anions may occur through electrostatic and H-bonding interactions with ammonium ions and cooperatively enhance recognition in a wide range of pH. With this in mind, we have investigated the protonation and Zn(II) binding properties of H_2**L9**, as well as the binding ability of the resulting Zn(II) complexes toward both inorganic phosphate anions (monophosphate, pyrophosphate and triphosphate) and the ATP and ADP nucleotides.

3.2.4.1 Receptor protonation and Zn(II) binding.

To analyze the binding properties of the receptor and of its Zn(II) complex toward phosphate anions, we carried out a preliminary study on protonation and Zn(II) binding of $\mathbf{L9}^{2-}$ by means of potentiometric measurements in aqueous solution. The species formed and the corresponding protonation and Zn(II) binding constants are reported in table 3.26;

Equilibrium	LogK
$H^+ + L^{2-} = HL^-$	10.67 (5)
$H^+ + HL^- = H_2L$	9.60 (6)
$H^+ + H_2L = H_3L^+$	8.15 (1)
$H^+ + H_3L+ = H_4L^{2+}$	3.37 (1)
Equilibrium with Zn(II)	Log K
$Zn^{2+} + L^{2-} = [ZnL]$	11.53 (3)
$[ZnL] + H^+ = [ZnLH]^+$	8.5 (3)
$[ZnLH]^+ + H^+ = [ZnLH_2]^{2+}$	8.24 (3)
$[ZnLH_2]^{2+} + H^+ = [ZnLH_3]^{3+}$	6.52 (3)
$[ZnLH_3]^{3+} + H^+ = [ZnLH_4]^{4+}$	3.51 (8)
$[ZnL] + OH^- = [ZnL(OH)]^-$	5.45 (2)
$[ZnL(OH)]^- + OH^- = [ZnL(OH)_2]^{2-}$	3.61 (3)

Table 3.26 Protonation and Zn(II) binding constants of receptor $\mathbf{L9}^{2-}$

Figure 3.88 shows the species distribution diagrams in the presence (3.88b) and in the absence of Zn(II) (3.88a). Due to the scarce solubility of the Zn(II) complex at acidic pH values, all measurements were carried out at 308.1 K. Under these conditions, no precipitation is observed in the pH range used in the potentiometric titrations.

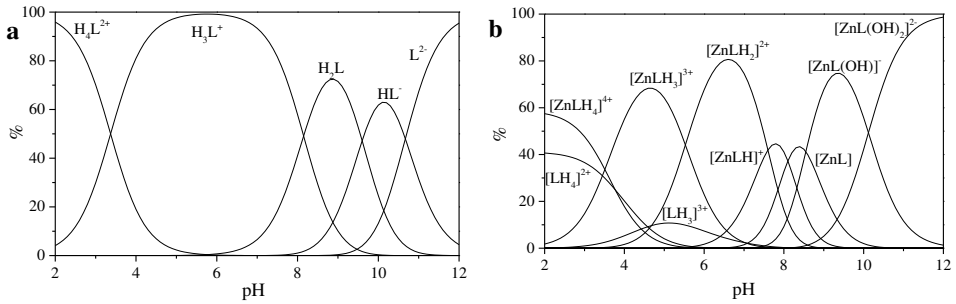

Figure 3.88 Distribution diagrams of (a) the protonated species, and (b) the Zn(II) complexes formed by receptor $\mathbf{L9}^{2-}$ (NMe4Cl, 0.1 M, 308.1 K).

For comparison purposes, we also determined the protonation and the Zn(II) binding constants of N-methyliminodiacetate (MIDA) as a model for the IDA moiety of the receptor, whereas measurements on the model for the DAC moiety could not be carried out because of a much too limited range of solubility of the corresponding macrocyclic model structure (table 3.27).

Equilibrium	LogK
$H^+ + L^{2-} = HL^-$	8.59 (5)
$H^+ + HL^- = H_2L$	2.40 (5)
Equilibrium with Zn(II)	Log K
$Zn^{2+} + L^{2-} = [ZnL]$	8.64 (3)
$[ZnL] + OH^- = [ZnL(OH)]^-$	5.43 (2)

Table 3.27 Protonation and Zn(II) binding constants of ligand MIDA (NMe_4Cl = 0.1 M, 308.1 K; L^{2-} indicates the dianionic form of MIDA)

Concerning protonation of $H_2\mathbf{L9}$, $\mathbf{L9}^{2-}$ and $H\mathbf{L9}^-$ anionic species are present in the alkaline pH region, as expected for polyamine carboxylate ligands (figure 3.88a). The corresponding protonation constants are unusually high, suggesting that the two DAC moieties of the macrocyclic subunit of the receptor are involved in the first two steps. Indeed, the basicity of DAC (log K = 9.96) is higher than that of MIDA (log K = 8.59). The third protonation step most likely occurs on the tertiary amine of the IDA subunit because the second protonation constant of DAC is significantly smaller (log K = 6.47). Finally, the last protonation step at acidic pH values can occur either on the DAC unit or on a carboxylate moiety.

Focusing on Zn(II) coordination, despite the presence of two potential binding sites for metal cations, the formation of dinuclear metal complexes was never observed, even in the presence of an excess of Zn(II). Rather, several mononuclear Zn(II) complexes are formed through a number of protonation–deprotonation steps occurring on the ligand or on the metal, respectively (table 3.27 and figure 3.88b). Because DAC and the fully deprotonated MIDA form strong complexes with Zn(II), ($[Zn(DAC)]^{2+}$, log K = 7.74; [Zn(MIDA)], log K = 8.64), one would expect that receptor $\mathbf{L9}^{2-}$, featuring both binding groups in the structure, would form an

exceptionally strong complex. Counterintuitively this is not observed, as the log K value of 11.53 for the formation of the [Zn**L9**] complex is smaller than that could be intuitively anticipated, and even smaller than the values reported for linear or cyclic tetraamines. On a closer inspection, however, this result may not be anomalous, when considering that conformational restrictions may hinder coordination of the metal ion to the macrocycle and that competition between the two binding sites for the same ligand may weaken the individual group interactions. As a consequence, the metal ion likely features a low coordination number in the complex and, therefore, its coordination sphere is not fulfilled by receptor donors, leaving 'free' binding sites available for exogenous substrate anchoring. This conclusion is confirmed by the formation of hydroxo-complexes ($[Zn\mathbf{L9}(OH)]^{-}$ and $[Zn\mathbf{L9}(OH)_2]^{2-}$) at high pH values, showing that the [Zn**L9**] complex can accept additional ligands in its coordination sphere. The most interesting finding that can be inferred from table 3.19 is the marked protonation tendency of the [Zn**L9**] complex, giving $[ZnLH_x]^{x+}$ species, where the first two protonation constants are notably high (log K = 8.50 and 8.24, respectively). The consequence of this tendency, which can be appreciated from the distribution plot of figure 3.88b, is that the species largely prevalent at physiological pH, where binding of phosphate is relevant, is the diprotonated complex $[Zn\mathbf{L9}H_2]^{2+}$, suggesting that under these conditions the DAC moieties would give little or no contribution to metal ion binding. In other words, at physiological pH, Zn(II) would essentially bind to the MIDA moiety and would therefore be available for binding to phosphate. To test this hypothesis, 1H NMR spectra of the receptor were recorded, in the presence and in the absence of Zn(II), at pH value such that the $\mathbf{L9}^{2-}$ and [Zn**L9**] species, or the $H_2\mathbf{L9}$ and $[Zn\mathbf{L9}H_2]^{2+}$ species, were the prevalent species in solution, i.e. at pH 12, 8.9, 9, and 6.6, respectively. Because the fast-exchange regime on the NMR spectroscopy timescale was consistently observed in NMR experiments, the chemical shift variations of the single set of signals were monitored. In figure 3.89 are reported the chemical shift differences (CSD) observed in the above spectra for the protonated and the unprotonated species. It can be easily appreciated that negligible random CSDs are exhibited by the protonated species upon addition of Zn(II), whereas marked downfield CSDs are induced by the metal ion on the macrocycle signals for the unprotonated species. This evidence strongly supports binding of Zn(II) to the DAC moieties of the macrocycle in the unprotonated species, which is substantially inhibited when the DAC moieties are protonated, in agreement with the above hypothesis.

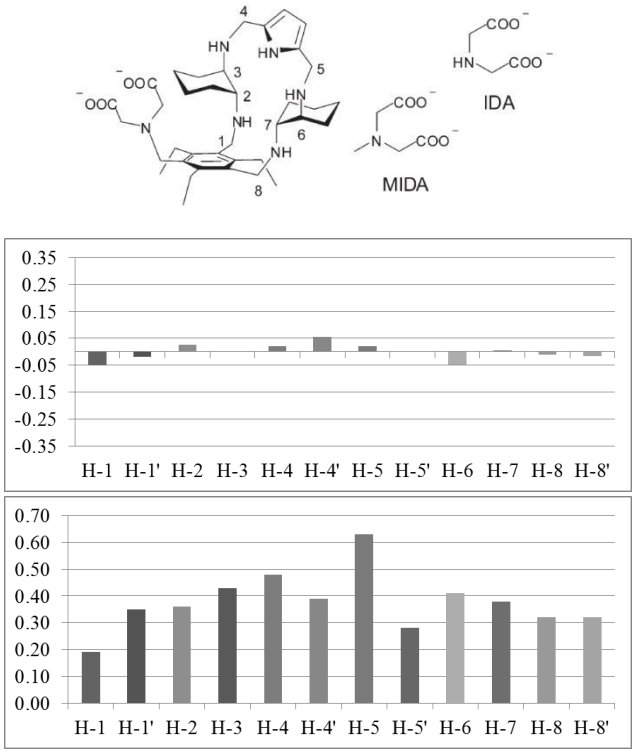

Figure 3.89 Plots of the chemical shift differences (CSDs) between receptor $\mathbf{L9}^{2-}$ in the presence and in the absence of Zn(II), at 500 MHz in D_2O at T = 298.1 K. The signals of the macrocyclic moiety are reported in plots: (a) diprotonated; (b) unprotonated. For the numbering scheme.

3.2.4.2 Phosphate anion binding.

Binding of monophosphate, diphosphate, triphosphate, ADP and ATP to $\mathbf{L9}^{2-}$ and its Zn(II) complexes was investigated through potentiometric, ^{1}H and ^{31}P NMR measurements in aqueous solutions at 308.1 K. In the potentiometric measurements, the anion-to-receptor molar ratios were varied from 0.5 to 4, in order to ascertain the stoichiometry of the adducts. In all cases, data elaboration evidenced only 1:1 adducts between the metal-free receptor or the Zn(II) complex and the phosphate anions, with no evidence of adducts of higher stoichiometry, in agreement with polyamine-based receptors. Potentiometric measurements showed that free receptor $\mathbf{L9}^{2-}$ can hardly bind to phosphate anions. Monophosphate is not bound at any pH value, whereas, with the other anions, only the H_3L^+ form of the receptor gave adducts of modest affinity. The corresponding association constants are reported in table 3.28.

Equilibrium	Log K
$H_3L^+ + P_2O_7^{4-} = [H_3LP_2O_7]^{3-}$	3.21 (3)
$H_3L^+ + HP_2O_7^{3-} = [H_4LP_2O_7]^{2-}$	3.05 (3)
$H_3L^+ + P_3O_{10}^{5-} = [H_3LP_3O_{10}]^{4-}$	3.48 (2)
$H_3L^+ + HP_3O_{10}^{4-} = [H_4LP_3O_{10}]^{3-}$	3.18 (3)
$H_3L^+ + ADP^{3-} = [H_3LADP]^{2-}$	3.04 (2)
$H_3L^+ + HADP^{2-} = [H_4LADP]^-$	3.12 (2)
$H_3L^+ + HATP^{3-} = [H_4LATP]^{2-}$	3.41 (1)
$H_3L^+ + HATP^{2-} = [H_5LATP]^-$	3.35 (1)

Table 3.28 Stability constants of complexes formed by the protonated form of receptor **L9**$^{2-}$ (H_3L^+) and diphosphate, triphosphate, ADP and ATP measured at 308.1K in 0.1 M NMe_4Cl.

The low affinities observed can be understood considering that only the monocharged (H_3L^+), weakly interacting, form is populated above pH 4, whereas below pH 4, where the discharged form (H_4L^{2+}) is present, anionic guests are protonated as well. The observed behavior is in sharp contrast to that of polyamine receptors, which give highly charged, strongly binding polyammonium cations at neutral or slightly acidic pH values. The presence of Zn(II) coordinated to the receptor dramatically enhanced the binding affinity for all the investigated anions, giving rise to several adducts with the Zn complex in different protonation states. The results of potentiometric measurements are reported in table 3.29, where the addition constants of triphosphate to the Zn(II) complex of MIDA are also reported for comparison. Because the exclusive formation of 1:1 adducts was revealed in all cases by data treatment, an independent confirmation was sought by recording ^{31}P NMR spectra of anionic substrates by addition of increasing amounts of the Zn(II) complex at pH 7. As in proton spectra, the fast-exchange regime on the NMR spectroscopy timescale was consistently observed in ^{31}P NMR spectra, so that the chemical shift variations of the averaged signals were monitored. As shown in figure 3.90 for TP, the addition induced an upfield shift of both ^{31}P resonances of the anion, which increased linearly up to 0.9:1 anion/complex mole ratio and reached a plateau above 1.1:1 ratio. Analogous behavior was found for the other anionic substrates.

Comparison of tables 3.28 and 3.29 clearly shows that the anionic substrates form much more stable adducts with the Zn(II) complexes than with the zinc-free polyammonium cations of the same charge. For example, the addition constant of $P_3O_{10}^{5-}$ to the $[ZnLH]^+$ complex is ca. 3 orders of magnitude larger than that for the addition to the H_3L^+ cation. Analogous enhancements have been observed for PP, ATP and ADP The higher binding affinity for phosphate anions displayed by the protonated Zn(II) complexes with respect to the unprotonated Zn(II) complexes can be ascribed to the presence of the metal center, which can behave as the anchoring

point for the phosphate unit(s), and to the protonated DAC units, which provide electrostatic interactions with the anion charge, possibly reinforced by H-bonding to the pyrrolic ring.

Equilibrium with phosphate	LogK
$ZnL + HPO_4^{2-} = [ZnLHPO_4]^{2-}$	3.55 (7)
$ZnLH^{+} + HPO_4^{2-} = [ZnLH_2PO_4]^{-}$	3.98 (7)
$ZnLH_2^{2+} + HPO_4^{2-} = [ZnLH_3PO_4]$	4.05 (8)
$ZnLH_3^{3+} + HPO_4^{2-} = [ZnLH_4PO_4]^{+}$	4.15 (8)
Equilibrium with diphosphate	
$ZnL + P_2O_7^{4-} = [ZnLP_2O_7]^{4-}$	4.75 (5)
$ZnL + HP_2O_7^{3-} = [ZnLHP_2O_7]^{3-}$	4.45 (5)
$ZnLH^{+} + HP_2O_7^{3-} = [ZnLH_2P_2O_7]^{2-}$	5.54 (5)
$ZnLH_2^{2+} + HP_2O_7^{3-} = [ZnLH_3P_2O_7]^{-}$	6.23 (8)
$ZnLH_2^{2+} + H_2P_2O_7^{2-} = [ZnLH_4P_2O_7]$	6.08 (8)
$ZnLH_3^{3+} + H_2P_2O_7^{2-} = [ZnLH_5P_2O_7]^{+}$	6.20 (8)
Equilibrium with triphosphate	
$ZnL + P_3O_{10}^{5-} = [ZnLP_3O_{10}]^{5-}$	5.53 (4)
$ZnLH^{+} + P_3O_{10}^{5-} = [ZnLHP_3O_{10}]^{4-}$	6.84 (4)
$ZnLH_2^{2+} + P_3O_{10}^{5-} = [ZnLH_2P_3O_{10}]^{3-}$	8.02 (5)
$ZnLH_2^{2+} + HP_3O_{10}^{4-} = [ZnLH_3P_3O_{10}]^{2-}$	7.77 (6)
$ZnLH_3^{3+} + HP_3O_{10}^{4-} = [ZnLH_4P_3O_{10}]^{-}$	7.92 (6)
Equilibrium with ADP	
$ZnL + ADP^{3-} = [ZnLADP]^{3-}$	4.09 (6)
$ZnL + HADP^{2-} = [ZnLHADP]^{2-}$	3.98 (6)
$ZnLH^{+} + HADP^{2-} = [ZnLH_2ADP]^{-}$	4.52 (6)
$ZnLH_2^{2+} + HADP^{2-} = [ZnLH_3ADP]$	5.15 (8)
$ZnLH_3^{3+} + HADP^{2-} = [ZnLH_4ADP]^{+}$	5.75 (8)
Equilibrium with ATP	
$ZnL + ATP^{4-} = [ZnLATP]^{4-}$	5.2 (1)
$ZnLH^{+} + ATP^{4-} = [ZnLHATP]^{3-}$	6.1 (1)
$ZnLH_2^{2+} + ATP^{4-} = [ZnLH_2ATP]^{2-}$	6.84 (8)
$ZnLH_2^{2+} + HATP^{3-} = [ZnLH_3ATP]^{-}$	6.93 (7)
$ZnLH_3^{3+} + HATP^{3-} = [ZnLH_4ATP]$	7.04 (7)
Equilibrium with MIDA and triphosphate	
$Zn(MIDA) + P_3O_{10}^{5-} = [Zn(MIDA)P_3O_{10}]^{5-}$	4.45 (2)
$Zn(MIDA) + HP_3O_{10}^{4-} = [Zn(MIDA)HP_3O_{10}]^{4-}$	4.35 (3)
$Zn(MIDA) + H_2P_3O_{10}^{3-} = [Zn(MIDA)H_2P_3O_{10}]^{3-}$	4.07 (4)

Table 3.29 Addition constants of the phosphate anions to the Zn(II) complexes of receptor $\mathbf{L9}^{2-}$ (Zn**L9**) and MIDA (Zn(MIDA)). Measured at 308.1 K in 0.1 M NMe4Cl.

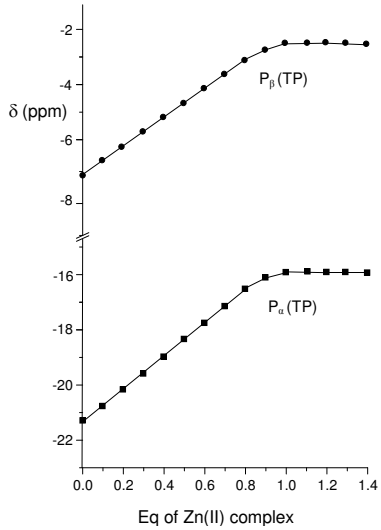

Figure 3.90 Plot of the chemical shifts of the terminal (P_β) and central (P_α) phosphorous nuclei of TP in the presence of an increasing amount of the Zn(II) complex of **L9** at 162 MHz, pH 7 and 308 K.

Bridging of the two binding sites by phosphate would therefore enhance the affinity for the anionic guest in a synergetic fashion. This effect is particularly evident in the case of triphosphate, for which the addition constants of triphosphate in its fully deprotonated form ($P_3O_{10}^{5-}$) to the ZnL, $[ZnLH]^+$ and $[ZnLH_2]^{2+}$ species are 5.53, 6.84 and 8.02 log units, respectively, with an increase larger than 2.5 log units from the [ZnL] to the $[ZnLH_2]^{2+}$ complex. Likewise, the addition constants of $HP_2O_7^{3-}$ and ATP^{4-} to the $[ZnLH_2]^{2+}$ complex are ca. 1.8 and 1.6 log units, respectively, larger than those found for the addition to [ZnL]. Clearly, the above differences are too large to be ascribed exclusively to the increased charge of the receptor. As a matter of fact, with the exception of monophosphate, the anions are so strongly bound that their adducts represent the major species in the pH range 4–9.5, as shown by the distribution diagrams of the complexes formed by diphosphate, triphosphate and ATP in figure 3.91.

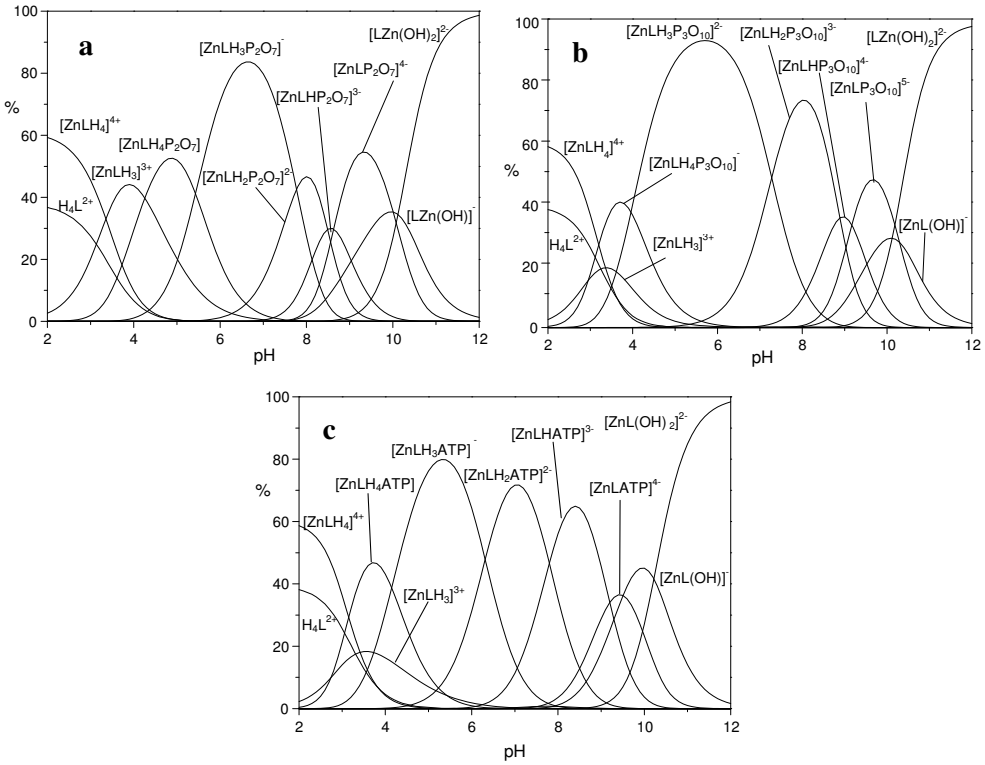

Figure 3.91 Distribution diagrams of the adducts formed by (a) PP, (b) TP and (c) ATP with the Zn(II) complexes of receptor **L9**. Conditions: [$\mathbf{L9}^{2-}$] =[Zn(II)] = [PP] = [TP] = [ATP] = $1 \cdot 10^{-3}$ M, NMe4Cl 0.1 M, 308.1 K.

At pH > 9.5, the formation of the hydroxo-complexes $[ZnL(OH)_x)]^{x-}$ (x = 1, 2) effectively competes with phosphate anion binding, while at pH < 4 the formation of ternary adducts is inhibited by the presence of protonated anions, and/or metal decomplexation. As a support to our hypothesis, in agreement with the view that the affinity enhancement is due to the concomitant bridging of binding sites, the monodentate MP, which is incapable of binding to both sites, shows weak binding scarcely dependent on protonation. Likewise, binding of TP to the Zn(II) complex of MIDA, which lacks the protonated macrocycle site, clearly shows modest affinities compared to those observed for receptor **L9**. At first glance, the data in table 3.29 seem to indicate that TP forms the most stable complexes. However, the interpretation of the stability constants is complicated by the different acid–base characteristics of the substrates as well as by the presence of multiple simultaneous equilibria, which make it difficult to compare the binding ability of the receptor at a given pH and to evaluate selectivity patterns. This issue can be addressed by considering a competitive system containing the receptor and equimolecular amounts of each anionic substrate, and calculating the percentages of the

complexed anions over a wide pH range. Figure 3.92 displays the plot obtained for a competitive system containing the Zn(II) complex of **L9** and five phosphate anions.

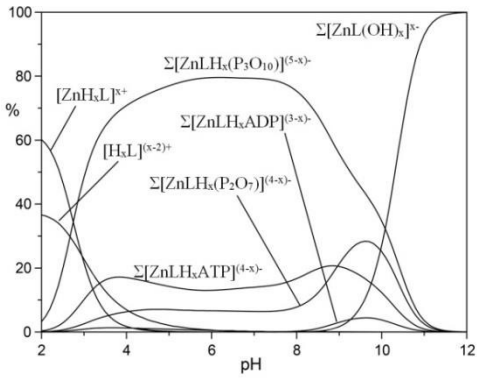

Figure 3.92 Overall percentages of the adducts between the Zn(II) complex of 1 and the phosphate anions in a competing system containing Zn(II), L9, monophosphate, diphosphate, triphosphate, ADP and ATP in equimolecular amounts. Conditions: $[Zn^{2+}]=[\mathbf{L9}]=[PO_4]=[P_2O_7]=[P_3O_{10}]=[ADP]=[ATP]=1\cdot10^{-3}$ M, NMe4Cl 0.1 M, 308 K.

Figure 3.92 clearly shows that the Zn(II) receptor preferentially binds to triphosphate over all other nucleotide and inorganic phosphate anions in the pH range of 3 to 10. At neutral pH, triphosphate, ATP and diphosphate are complexed in 80%, 13% and 7%, respectively. The ternary adduct with ADP is present in only minor amounts (<5%) at alkaline pH values, whereas the adduct with MP is not formed at any pH. The selectivity for triphosphate over both diphosphate and ATP is somewhat unexpected, because triphosphate and diphosphate show a similar binding ability for Zn(II) and its complexes with polyamine ligands. Furthermore, in most cases nucleotide anions, in particular ATP, form more stable complexes than inorganic phosphates, due to the interaction with positively charged hosts not only through the triphosphate chain, but also through the nucleobase, which shows H-bonding and/or π-stacking interactions with the receptor. To elucidate the binding mode of inorganic and nucleotide anions to the Zn(II) receptor, we recorded ^{1}H and ^{31}P NMR spectra as a function of pH on solutions containing the Zn(II) complex of **L9** and the nucleotides in 1:1 molar ratio. Figure 3.93 shows the chemical shifts of the ^{31}P signals of triphosphate, ATP, diphosphate and ADP, in the presence and in the absence of the metal complex. In all cases, a strong dependence of chemical shifts on pH and on binding to the Zn(II) receptor can be easily appreciated. The latter induced a marked and systematic downfield shift of the ^{31}P signals with respect to the uncomplexed phosphate. Notably, the CSD between the free and the complexed phosphates tends to peak in the pH range between 6 and 7, that is in the range where the receptor shows the largest binding ability and in which the protonated complex is predominant. It is also worth noting that the stronger the

binding the larger the shift, suggesting that the proximity of phosphate to the Zn ion, as detected by the ^{31}P NMR chemical shift, follows the same trend of the binding affinity for the five anions under scrutiny, because stronger binding provides larger amounts of phosphate complexes in the weighted average of species under the ^{31}P signal. Interestingly, the chemical shifts of the P_α of both ATP and ADP are essentially insensitive to metal coordination, indicating that the phosphorous adjacent to the adenosine moiety is not involved in binding, most likely because of the hindrance of the adenosine moiety against the macrocyclic portion of the receptor, as observed for polyammonium hosts.

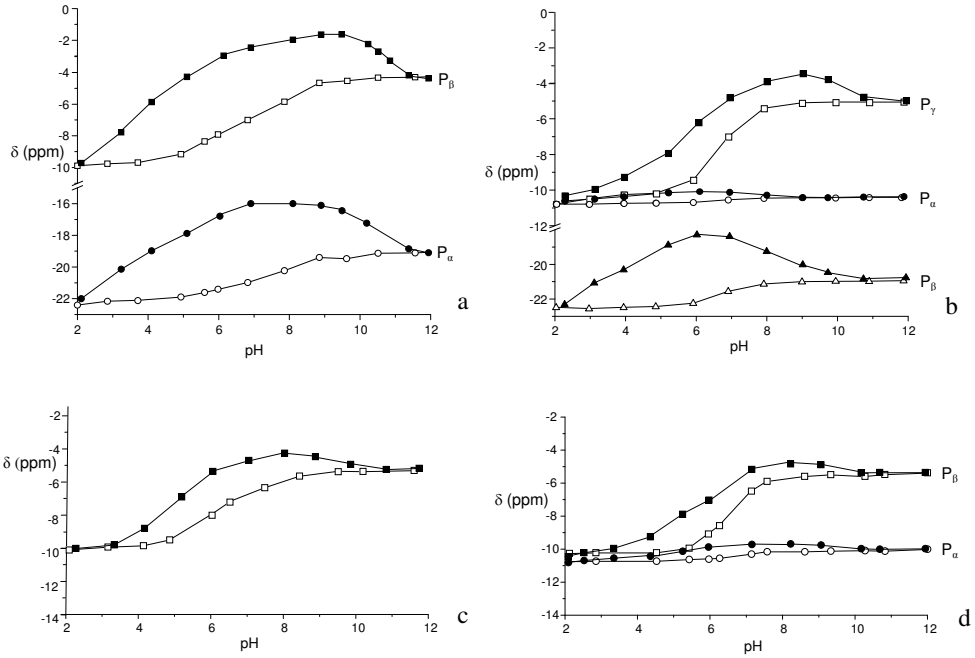

Figure 3.93 pH dependence of the ^{31}P NMR signals (162 MHz) of (a) P_3O_{10}, (b) ATP, (c) P_2O_7, and (d) ADP in the presence (filled symbols) and in the absence (empty symbols) of the Zn(II) complex of **L9**. Conditions: [**L9**]=[Zn^{2+}]=[P_3O_{10}]=[P_2O_7]=[ADP]=[ATP]=$5\cdot10^{-3}$ M, 308.1 K.

Furthermore, the P_β signal of ATP shows a maximum CSD of 3.8 ppm at pH 6, whereas the P_γ and the P_β of ADP exhibit a much shallower CS trend between pH 9 and 5. This evidence suggests that the terminal phosphates P_γ of ATP and P_β of ADP bind to the metal ion all through this pH range, whereas the P_β of ATP comes into play on interaction with the doubly protonated macrocycle. This explains not only the larger binding ability of ATP with respect to ADP, but also the larger stability of the triphosphate adduct, which does not suffer from the steric hindrance between the macrocycle and the adenosine moiety, thus showing the analogous trend of both ^{31}P signals. The contribution to binding of the nucleoside portion of ATP and ADP is revealed by the ^{1}H NMR spectra as a function of pH. In figure

3.94, the plot of the anomeric H1' and the adenine H2 and H8 protons is reported for ATP binding to the free and the Zn(II) complexed receptor.

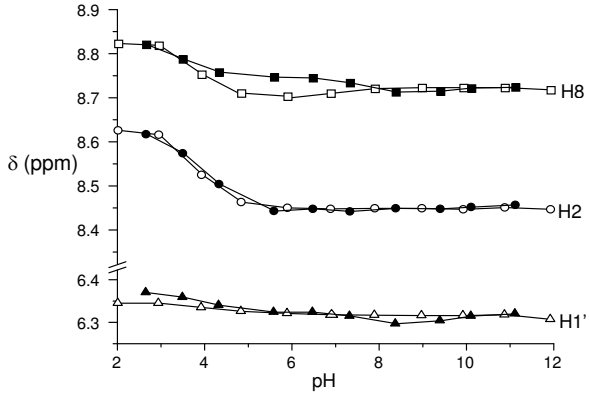

Figure 3.94 pH dependence of the 1H NMR signals (400 MHz) of the H8 (top) and H2 (middle) adenine protons and of the anomeric H1' (bottom) proton of the sugar moiety of ATP in the presence (filled symbols) and in the absence (empty symbols) of the Zn(II) complex of **L9**. Conditions: [**L9**] =[Zn(II)] = [ATP] = $5 \cdot 10^{-3}$ M, 308.1 K.

As can be seen, the corresponding CSDs are essentially null, indicating that little or no contribution to binding comes from the nucleoside residue, in contrast to the active role in stabilization often observed with positively charged hosts, in particular polyammonium cations, through H-bonding, π-stacking and hydrophobic interactions. Finally, although experimental data do not allow a direct assessment, the pyrrolic group of the macrocyclic portion of the receptor may likely contribute to reinforce the binding interaction through H-bonding to the oxygen atoms of the phosphate anions. All the experimental evidence seems to demonstrate that concerted phosphate binding to the Zn(II) ion and to the protonated DAC macrocycle significantly enhances the binding ability of receptor **L9** toward di- and triphosphates in the pH range of physiological interest.

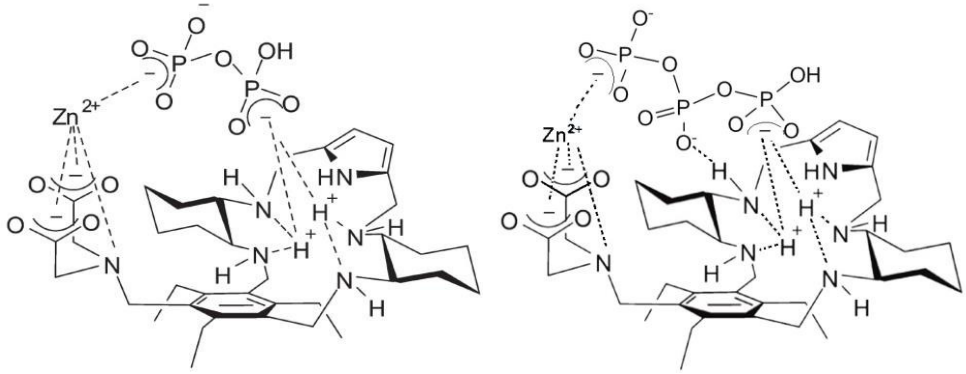

Figure 3.95 Sketch of adduct featuring the Zn(II)-mediated diphosphate (a) or triphosphate (b) bridging the two binding sites of diprotonated receptor H_2**L9**.

A sketch of the proposed receptor–Zn(II)–phosphate adduct of the ternary complex $[Zn\mathbf{L9}H_3P_2O_7]^-$ and $[Zn\mathbf{L9}H_3P_3O_{10}]^{-2}$, in agreement with experimental data, is depicted in figure 3.78.

3.3 Colorimetric chemosensor for anionic species

In principle, anions could be also recognized by changes in the colour of the receptors. However, the absorption spectra of chtomogenci units are normally scarcely affected by anion binding. To overcome this drawback, we can use the 'indicator displacement approach, which use an indicator, normally a pH indicator, whose color change upon binding by the receptor. If the anion is bound more strongly than the indicator, the indicator is displaced form the receptor and recovers its original color, as sketched in figure 3.96

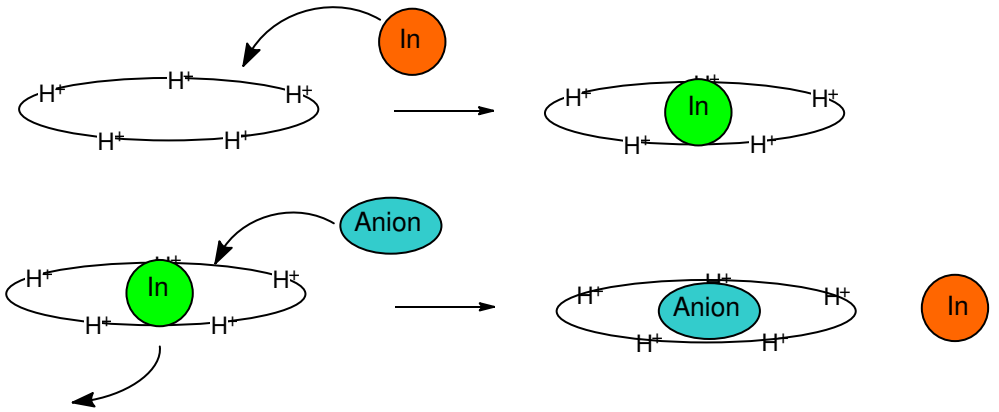

Figure 3.96 The indicator displacement assay

To this purpose, we selected four pH indicators (fluorescein, phenopthalein, bromo cresol purple, phenol red), whose color changes in different pH regions. As receptor we chose a ligand composed by four cyclam units bridged by four 1,3-dimethylenbenzene rings shown in figure 3.97, synthesized by the research group of Prof. Raphael Tripier (University of Brest, France), and conventionally named "xylyl-tetracyclam" (**L10**). This receptors contains a large number of protonable amine groups and a large cavity and, therefore, it possesses the necessary requisite to bind large guest anions, such as pH indicators.

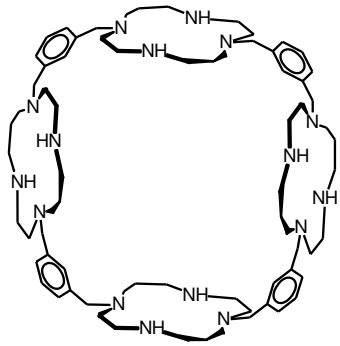

Figure 3.97 xylyl-tetracyclam (**L10)**

Necessary prerequisite in the studies of anions coordination by polyamine systems is the receptor analysis of acid-base properties. Therefore, the ligand protonation constants were determined by potentiometric measurements, which are reported in Table 3.30.

Equilibrium	**Log K**
$2\ H^+ + H_2L^{2+} \rightleftharpoons (H_4L)^{4+}$	9.92 (8)
$H^+ + (H_4L)^{4+} \rightleftharpoons (H_5L)^{5+}$	8.54 (9)
$H^+ + (H_5L)^{5+} \rightleftharpoons (H_6L)^{6+}$	9.0 (1)
$H^+ + (H_6L)^{6+} \rightleftharpoons (H_7L)^{7+}$	7.6 (1)
$H^+ + (H_7L)^{7+} \rightleftharpoons (H_8L)^{8+}$	7.7 (1)
$H^+ + (H_8L)^{8+} \rightleftharpoons (H_9L)^{9+}$	6.6 (1)
$H^+ + (H_9L)^{9+} \rightleftharpoons (H_{10}L)^{10+}$	2.2 (1)

Table 3.30 Protonation constants of **L10**, standard deviation in parentheses (298.1°K, NaCl = 0.1 M).

The potentiometric measurements showed that the ligand acts as a proton sponge. This is confirmed by the fact that the ligand has never been observed completely deprotonated in our experimental conditions and even at very alkaline pH (pH = 11) is found mainly in its form $H_2\mathbf{L}^{2+}$.

By using the protonation constants reported in table 3.30, we can determine the distribution diagram for the species present in the solution shown in figure 3.98.

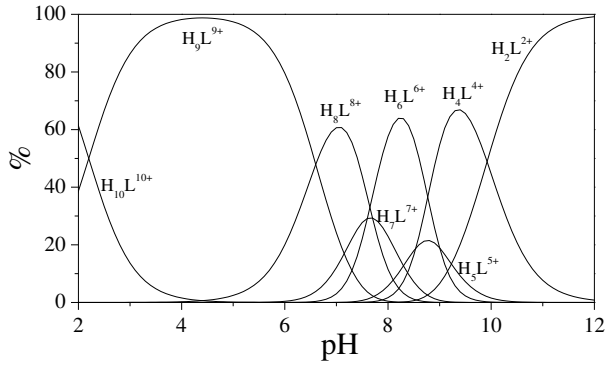

Figure 3.98 Distribution diagrams of the protonated species for ligands **L10** ([L]=10^{-3} M 298.1°K, NaCl = 0.1 M).

Preliminary studies of mechanics and molecular dynamics carried on the ligand in different protonation states, $(H_4L)^{4+}$, $(H_8L)^{8+}$ and $(H_9L)^{9+}$, showed that the receptor is flexible enough and preferably assumes an open conformation (figure 3.99). Furthermore it features a cavity large enough to allow the interaction with a pair of pH-indicator anions

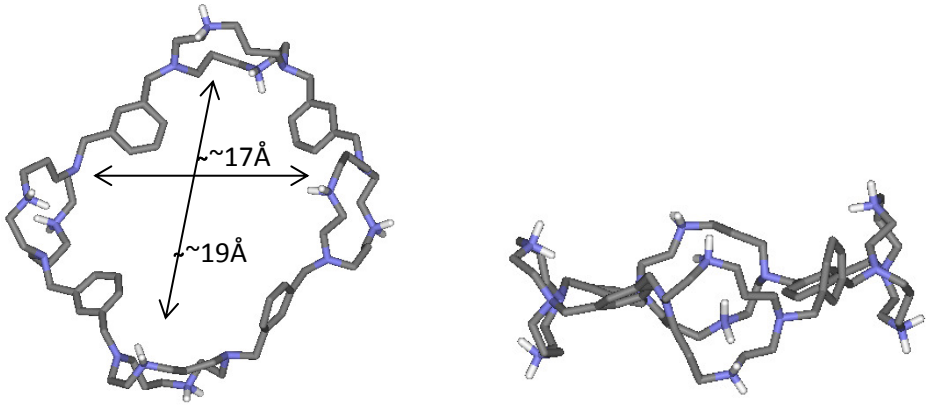

Figure 3.99 Lowest energy conformer of the octaprotonated form $(H_8L)^{8+}$ of the receptor. For simplicity, only the hydrogen atoms acids are shown.

3.3.1 Studied pH-indicators.

3.3.1.1 Phenolphthalein

Phenolphthalein is a known pH indicator featuring three protonation steps, figure 3.100.

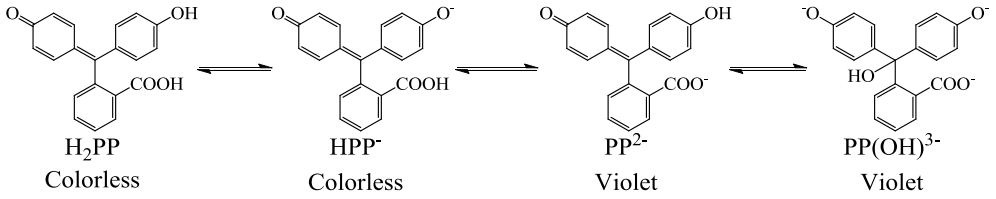

Figure 3.100 Phenolphthalein acid-base equilibria in aqueous solution.

The pK_a related to protonation equilibria, determined by potentiometric in our experimental conditions, table 3.31

Equilibrium	pK_a
$PP(OH)^{3-} = PP^{2-}$	12.00 (3)
$PP^{2-} + H^+ = HPP^-$	9.50 (4)
$HPP^- + H^+ = H_2PP$	9.05 (2)

Table 3.31 Protonation constants of **PP**, standard deviation in parentheses (298.1K, $N(CH_3)_4Cl$ = 0.1 M).

We recorded the indicator UV-visible absorption spectra at different pH values obtained in our experimental conditions, and the results are shown in figures 3.100. The phenolphthalein in its PP^{2-} form, prevailing at alkaline pH values, is characterized by a band at 552 nm, whose intensity increases from pH 8 to 11. Also in this case, if we superimpose distribution diagram of the protonated species with the molar absorption coefficient at 552 nm, it can be observed that the changes observed in the UV-visible spectra are related to the deprotonation of HPP^- to give PP^{2-}. This deprotonation step implies a naked eye a net color change of the solution from colorless (form HPP^-) to violet, the typical color of the form PP^{2-}. It was not observed any spectral change in the case of deprotonation of PP^{2-} to give $PP(OH)^{3-}$.

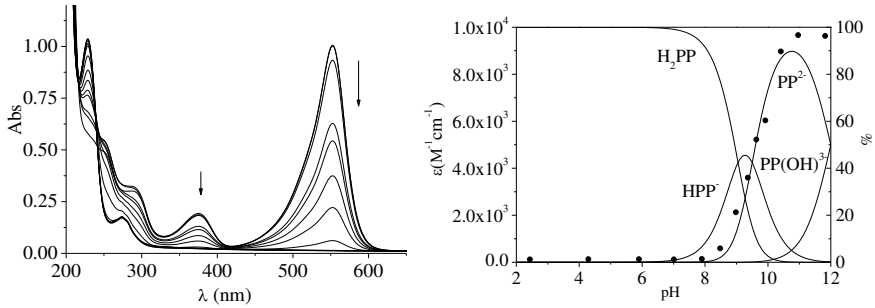

Figure 3.101 a) UV-visible absorption spectra of phenolphthalein in water at different pH values. **b)** fluorescence emission intensity of phenolphthalein at 552 nm compared to the distribution diagrams of the protonated species. $[H_2PP] = 1.04 \cdot 10^{-4}$ M

3.3.1.2 Bromocresol purple

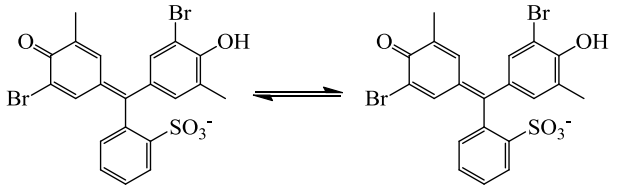

Figure 3.102 Bromocresol purple acid-base equilibria in aqueous solution

The pK_a relative to the protonation equilibrium of bromocresol purple determined under our experimental conditions, table 3.32.

Equilibrium	pK_a
$BCP^{2-} = HBCP^-$	6.2 (1)

Table 3.32 Protonation constants of **BCP**, standard deviation in parentheses (298.1K, $N(CH_3)_4Cl$ = 0.1 M).

We also recorded UV-visible absorption spectra at variable pH, and the results are shown in figure 3.103. Bromocresol purple in its HBCP form, prevailing at acid pH, is characterized by a band at 432 nm. Increasing pH from about 4 to 8, we can observe disappearance of the band at 432 nm and the simultaneous appearance of a new absorption band at 600 nm, attributable to deprotonation of HBCP to give BCP^-. This deprotonation step implies a naked eye net color change of the solution from from yellow to purple.

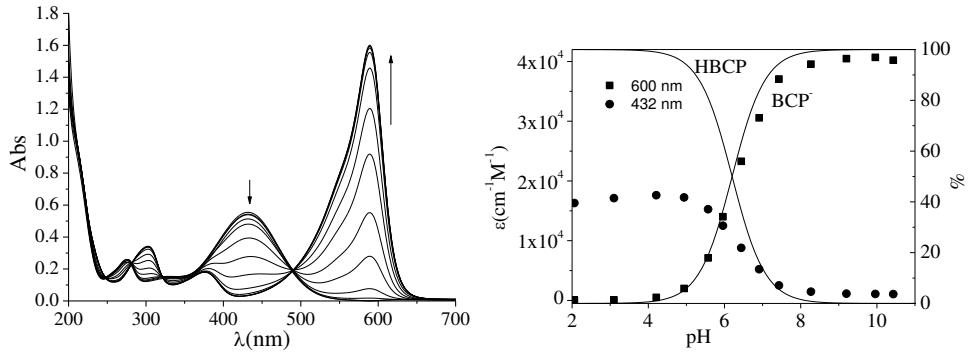

Figure 3.103 a) UV-visible absorption spectra of bromocresol purple in water at different pH values. **b)** fluorescence emission of bromocresol purple at 558 and 433 nm compared to the distribution diagrams of the protonated species of bromocresol purple. [BCP]= $3.15 \cdot 10^{-5}$ M

3.3.1.3 Phenol red

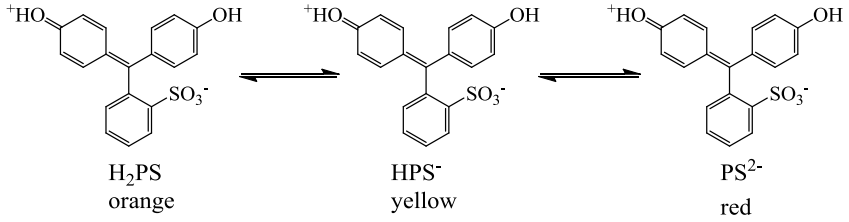

Figure 3.104 Phenol red acid-base equilibria in aqueous solution

The pK_a for the equilibria , determined by potentiometric under our experimental conditions table 3.33.

Equilibrium	pK_a
$PS^{2-} + H^+ = HPS^-$	7.7 (1)
$HPS^- + H^+ = H_2PS$	1.2 (1)

Table 3.33 Protonation constants of **PS**, standard deviation in parentheses (298.1K, $N(CH_3)_4Cl$ = 0.1 M).

We recorded UV-visible absorption spectra at variable pH, obtaining the results shown in figure 3.105. The phenol red in its form HPR^-, prevailing at acid pH, is characterized by a band at 433 nm. Increasing pH from 6 to 10, we can observe the disappearance of the band at 433 nm and the simultaneous appearance of a new band at 558 nm. These spectral changes can be attributed to the equilibrium between monoprotonated HPR^- and deprotonated PR^{2-}. The distribution diagram overlapped with the molar absorption coefficient at 558 and 443 nm shows the deprotonation of both phenol groups is responsible for the observed changes in the UV-visible spectra. This deprotonation step gives rise to a naked eye color change of the solution from from yellow to purple.

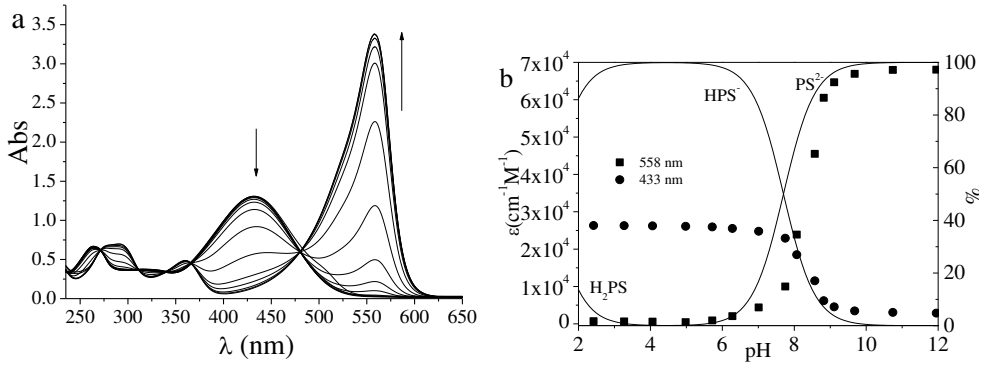

Figure 3.105 a) UV-visible absorption spectra of phenol red in water at different pH values. **b)** fluorescence emission of phenol red at 558 (■) and 433 (●) nm compared to the distribution diagrams of the protonated species of phenol red. [PR]= $4.97 \cdot 10^{-5}$ M

3.3.1.4 Fluorescein

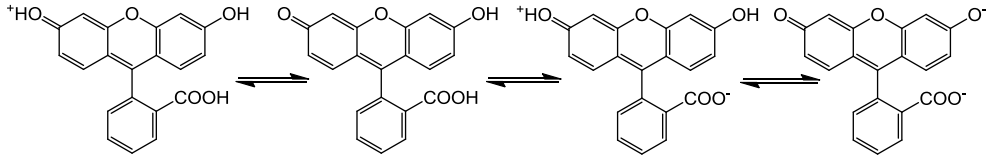

Figure 3.106 Fluorescein acid-base equilibria in aqueous solution.

Fluorescein undergoes three protonation equilibria in aqueous solution, whose protonation constants under our experimental conditions table 3.34.

Equilibrium	pK_a
$F^{2-} + H^+ = HF^-$	5.7 (1)
$HF^- + H^+ = H_2F$	4.1 (1)
$H_2F + H^+ = H_3F^+$	1.8 (1)

Table 3.34 Protonation constants of **PS**, standard deviation in parentheses (298.1K, $N(CH_3)_4Cl$ = 0.1 M).

We also recorded UV-visible absorption spectra of fluorescein at different pH values, obtaining the results shown in figures 3.106. With increasing pH, it is observed the formation of an absorption band at 490 nm, typical of the dianionic form of fluorescein, and the simultaneous disappearance of the band at 436 nm. The trend of the molar extinction coefficient at 490 nm is similar to that of the species F^{2-} in the distribution diagram, while that at 436 nm shows a slight increase corresponding to the formation of the species HF^- followed by a decrease when forming the species F^{2-}.

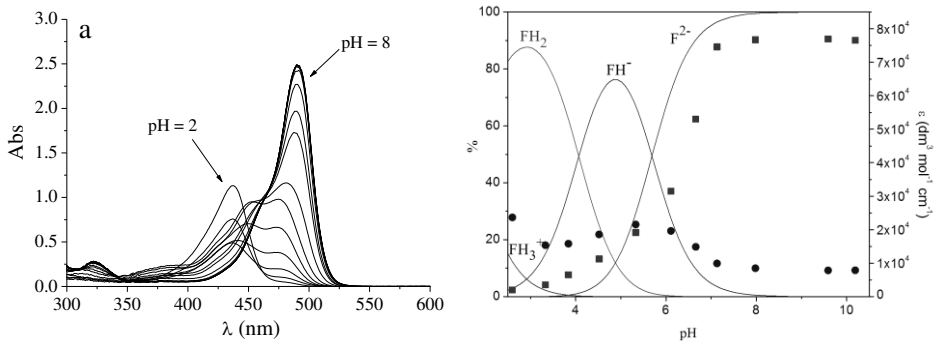

Figure 3.107 a) UV-visible absorption spectra of fluorescein in water at different pH values. **b)** fluorescence emission of fluorescein at 490 (■) and 436 (●) nm compared to the distribution diagrams of the protonated species of fluorescein. $[H_2F] = 4.97 \cdot 10^{-5}$ M

The recorded spectra (figure 3.107) shows the characteristic absorption bands of the fluorescein four protonated forms. For clarity, we have reported in figure 3.108 the spectra recorded at four pH values where the four protonated forms of fluorescein are largely prevalent in solution.

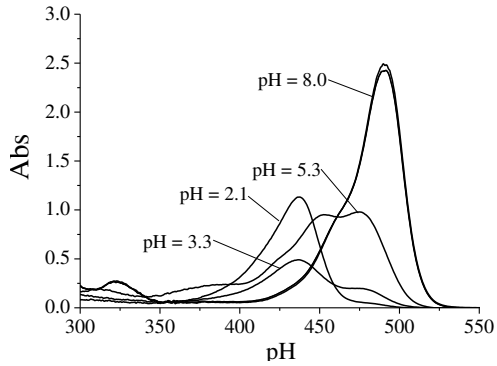

Figure 3.108 Characteristic absorption bands of the four forms of fluorescein with different protonation degree.

3.3.2 Indicators interaction with xylyl-tetracyclam.

The interaction of the four indicators with ligand xylyl-tetracyclam was studied in aqueous solution mainly through spectrophotometric measurements and potentiometric.

3.3.2.1 Interaction with Phenolphthalein

To analyze the interaction between the receptor and phenolphthalein, were first recorded the UV-visible absorption spectra at different pH values of the indicator in the presence of the receptor. We have reported in figure 3.109 the recorded spectra and the molar extinction coefficient measured at 552 nm. As in the case of the free phenolphthalein, it is to be noted a marked absorbance increase at alkaline pH.

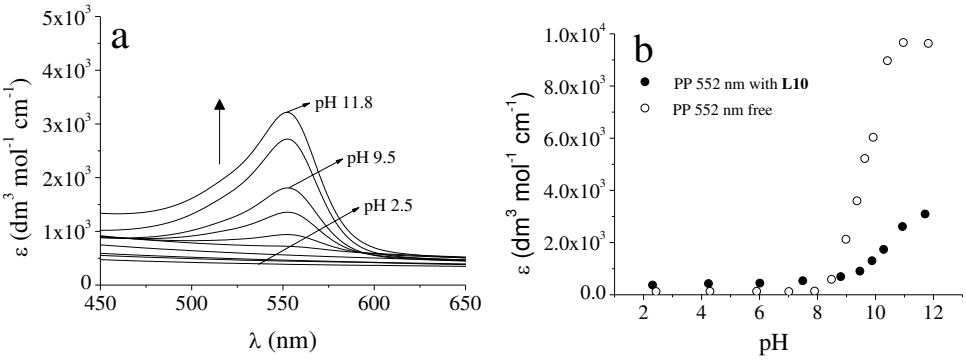

Figure 3.109 a) **UV-visible absorption spectra of phenolphthalein in water at different pH values in presence of one equivalent of** L10 **.** b) **pH dependence of molar extinction coefficient at 552 nm as a function of pH with and without** L10 **. [**L10**=PP]= 1.04·10^{-4} M**

In the presence of the receptor, the absorbance increase at 552 nm is observed at slightly more alkaline pH values. This behavior suggests that the interaction with the receptor it makes less favorable by the deprotonation process phenolphthalein,

which in fact occurs at more alkaline pH in presence of the macrocyclic system. It should be noted that at alkaline pH, the receptor contains several not protonated nitrogen atoms. The latter can stabilize protonated forms of the phenolic groups of phenolphthalein via hydrogen bonds of the type -OH···N(H)-, which can stabilize the phenolphthalein protonated forms (H_2PP and HPP^-). Conversely, the low number of ammonium groups and the low receptor charge ensure that the charge-charge interactions between phenolphthalein and macrocycle, which would stabilize the forms of the indicator more negative and $PP(OH)^{3-}$, are weak and inefficient. This makes that the deprotonation process $HPP^- \rightleftharpoons PP^{2-} + H^+$ appears essentially not favored by indicator coordination by the scarcely protonated forms of the receptor.

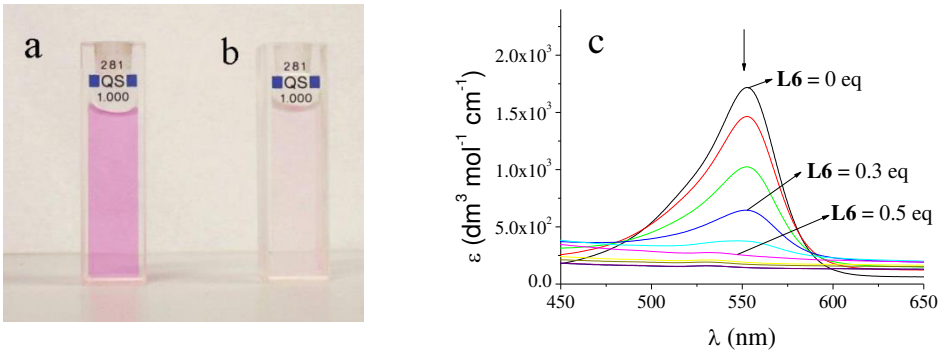

Figure 3.110 a) Free phenolphthalein at pH 10. **b)** phenolphthalein with 1 equivalent of **L10** at pH 10. **c)** phenolphthalein UV-visible absorption spectra in presence of increasing ligand amounts at pH = 10. ([PP]=$1.04 \cdot 10^{-4}$).

The maximum difference between the molar extinction coefficient in the absence and in presence of the ligand is observed at pH = 11. However, a substantial difference can be already observed starting from pH = 9. At the same concentration, the complexed phenolphthalein shows an absorbance significantly lower. In figure 3.109 we have reported the spectra recorded at pH = 10 by addition of increasing ligand amounts to a phenolphthalein solution. The addition produces a color change from deep purple to almost colorless. In fact, the phenolphthalein absorption band decreases progressively up to a 1:2 molar ratio between **L10** and phenolphthalein. In the presence of larger amounts of xylyl-tetracyclam, the molar extinction coefficient remains almost constant. This indicates the formation of a complex with a 1:2 stoichiometry between xylyl-tetracyclam and phenolphthalein.

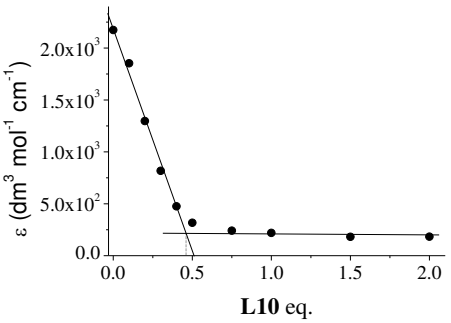

Figure 3.111 Phenolphthalein molar extinction coefficient at pH 10 in the presence of **L10** increasing amounts. [PP]= $1.04 \cdot 10^{-4}$ M

These results leads us to suppose that the two phenolphthalein units are coordinated simultaneously by the receptor.

3.3.2.2 Interaction with bromocresol purple

Also in this case, to analyze the interaction between the **L10** and BCP, we recorded UV-visible absorption spectra of BCP in the presence of the receptor at different pH values (figure 3.112). As in free bromocresol purple in the absence of the receptor, we can note significant spectral changes by changing pH. In this case, however, the absorbance decrease at 432 nm and the absorbance increase at 600 nm takes place in a different pH region, between pH 3.5 and 6 instead of between pH 5.5 and 7.5, as highlighted in figure 3.112.

This implies that the indicator deprotonation ($HBCP^-$ to BCP^{2-}) in the ligand presence takes place at more acidic pH values. In other words, the interaction with the receptor decreases the pK_a for the equilibrium $HBCP^- \rightleftharpoons BCP^{2-} + H^+$. The fact that $HBCP^-$ deprotonation is more favored in the ligand presence can be reasonably attributed to a stabilization of the dianionic species BCP^{2-} due to its interaction with the macrocycle, which is in forms with a high protonation degree in this pH region.

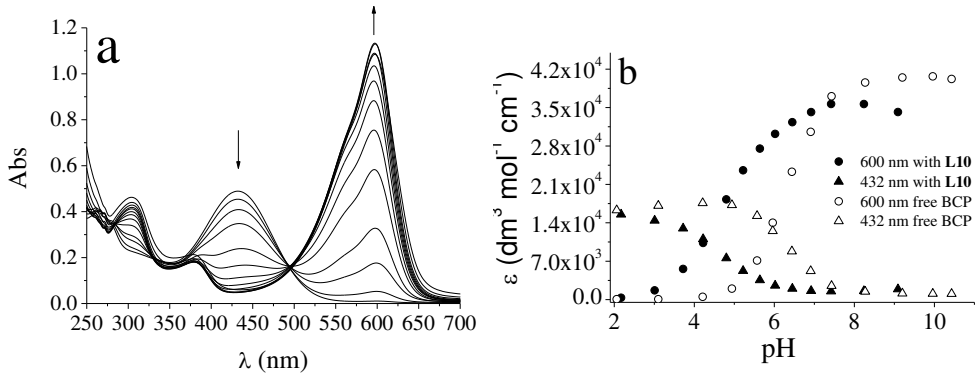

Figure 3.112 a) UV-visible absorption spectra of bromocresol purple in water at different pH values in presence of one equivalent of **L10**. **b)** Trend of molar extinction coefficient at 600 nm and 432 nm as pH function with and without **L10**. [**L10**=BCP]= $3.15 \cdot 10^{-5}$ M.

The maximum difference between the molar extinction coefficients of both the band at 432 nm and that at 600 nm measured in the absence and in the presence of **L10** is observed at pH = 5.5. Therefore, we recorded the UV-vis spectra of BCP at this pH value in the presence of increasing amounts of **L10** (figure 3.113).

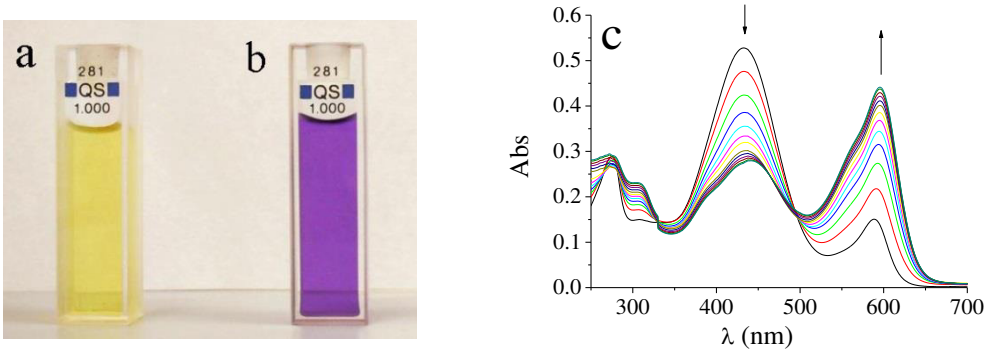

Figure 3.113 a) Free bromocresol purple at pH 5.5. **b)** Bromocresol purple with 1 equivalent of **L10** at pH 5.5. **c)** Bromocresol purple UV-visible absorption spectra in presence of increasing amounts of ligand at pH = 5.5. [BCP]=$3.15 \cdot 10^{-5}$.

During the addition it is observed a color change of the solution from yellow to purple perceptible at naked eye.

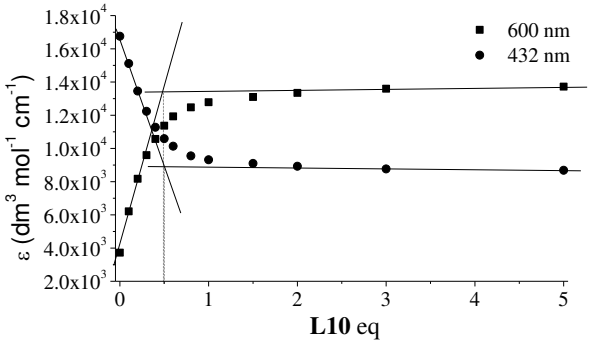

Figure 3.114 Bromocresol purple molar extinction coefficient at pH 5.5 in the presence of **L10** increasing amounts. [BCP]= $3.15 \cdot 10^{-5}$ M.

Figure 3.113 show the molar extinction coefficient variation at 432 nm and 600 nm in the presence of increasing **L10** amounts. As in the case of phenolphthalein, the results suggest the formation of complex with a 1:2 stoichiometry between **L10** and BCP.

3.3.2.3 Interaction with phenol red

We recorded UV-visible absorption spectra of phenol red in the presence of **L10** at different pH values, as shown in figure 3.115. As in the case of the free phenol red, the figure 3.105 shows significant spectral changes by changing pH. As already observed for bromocresol purple and phenolphthalein, the absorbance decrease at

433 nm and the absorbance increase at 558 nm takes place in a different field of pH, e.g., between pH 6 and 9, instead of between pH 7.5 and 10, as highlighted in figure 3.115. This implies that deprotonation of the indicator ($HPS^- \rightleftharpoons PS^{2-}$) in the presence of the ligand takes place at more acid pH values. In other words, as in the BCP case, the interaction with the receptor decreases the pK_a of the equilibrium $HPS^- \rightleftharpoons PS^{2-} + H^+$. The fact that the HPS^- deprotonation is more favored in the presence of the receptor,can be attributed to the stabilization of the highly negative charged form of the indicator, PS^{2-}, by binding with the receptor, which results already strongly protonated at slightly alkaline pH values and therefore highly positively charged. At these pH values interactions via hydrogen bond can be established between the phenolic group of the indicator and not protonated receptor amino groups, which may favor the -OH group deprotonation through a proton transfer process from the indicator to the ligand.

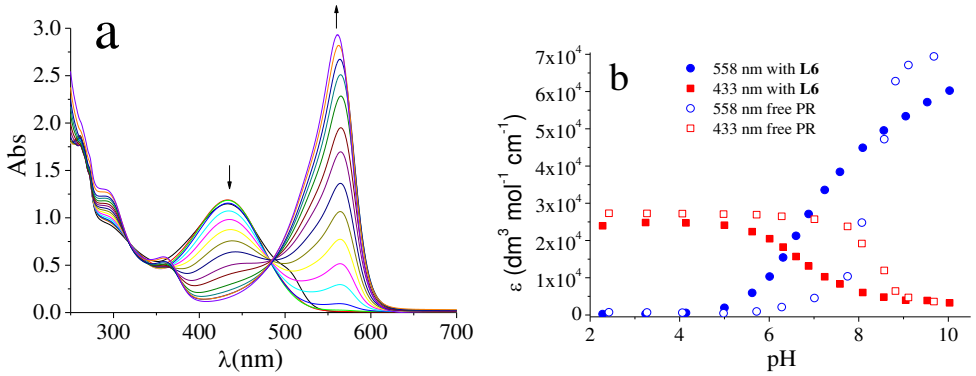

Figure 3.115 a) UV-visible absorption spectra of phenol red in water at different pH values in presence of one equivalent of **L10**. **b)** pH-dependence of molar extinction coefficient at 558 nm and 433 nm as pH function with and without **L10**. [**L10**=BCP]= $3.15 \cdot 10^{-5}$ M.

The largest difference between the molar extinction coefficients of both the band at 433 nm to 558 nm measured in the absence and in the presence of the ligand is observed at pH = 7.5. Therefore, we recorded the UV-vis spectra of the indicator at this pH value in the presence of increasing amounts of **L10.**

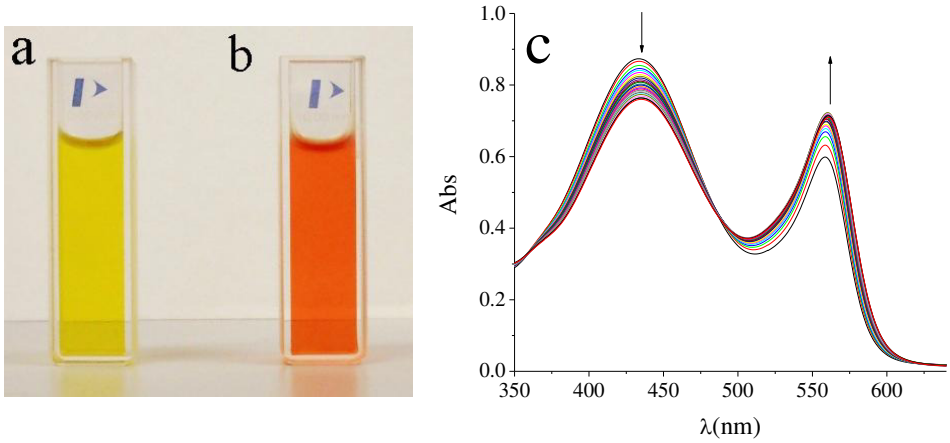

Figure 3.116 a) Free phenol red at pH 7.5. **b)** Phenol red with one equivalent of **L10** at pH 7.5. **c)**Phenol red UV-visible absorption spectra in presence of increasing ligand amounts at pH = 7.5. [PR]=$4.97 \cdot 10^{-5}$.

These spectral differences result in a color change of the solution from yellow to orange perceptible at naked eye (figure 3.116).

Figure 3.117 show the molar extinction coefficient changes at 433 nm and 558 nm in the presence of increasing amounts of **L10**. This suggests, as in the case of phenolphthalein and bromocresol violet, the formation of complexes with 1:2 receptor/substrate stoichiometry.

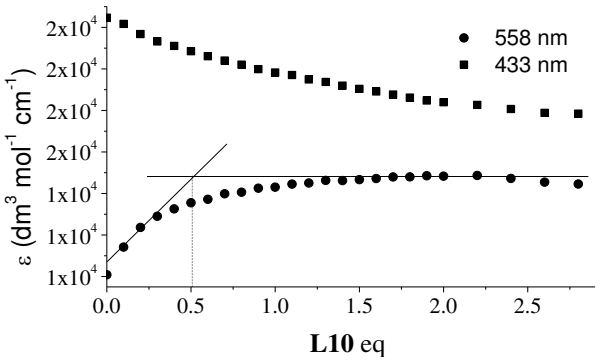

Figure 3.117 phenol red molar extinction coefficient at pH 7.5 in the presence of **L10** increasing amounts. [PR]= $4.97 \cdot 10^{-5}$ M.

3.3.2.4 Interaction with fluoresceine

Even in the case of fluorescein the absorption spectra were recorded in the presence of the receptor at different pH values. The spectra obtained, reported in figure 3.118, are similar to those of fluorescein recorded in the absence of receptor.

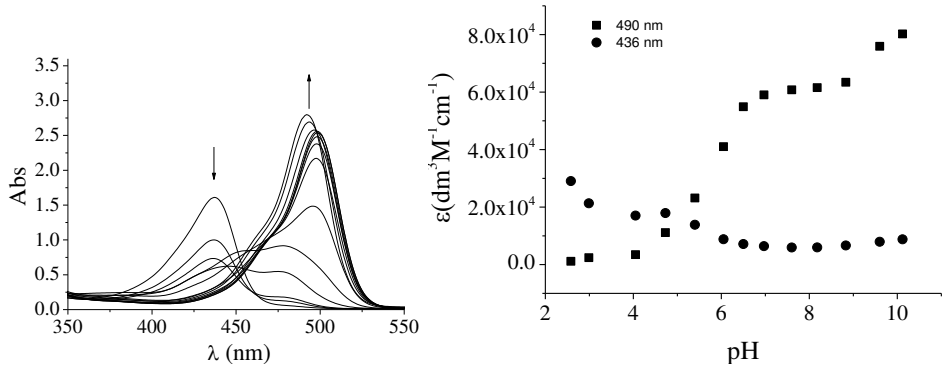

Figure 3.118 a) UV-visible absorption spectra of fluoresceine in water at different pH values in presence of one equivalent of **L10**. **b)** Trend of molar extinction coefficient of fluoresceine at 436 and 490 nm at different pH values with and without **L10**. ([F] = $1 \cdot 10^{-5}$ M)

At acidic pH, the absorption band at 436 nm, typical of the species H_3F^+, shows a marked intensity decrease from pH 1.87 to about pH 3, due to process $H_3F^+ \rightleftharpoons H_2F$. Further increasing pH we can initially observe a progressive red shift of the fluorescein absorption band at 490 nm, due to further fluorescein deprotonation to form HF^-, which that appears to be prevalent in solution already at pH 4. Finally, a further increase of pH induce a progressive absorbance increase at 490 nm, characteristic of the last deprotonation process which leads to the formation of F^{2-}. This suggests that the coordination of F by **L10** favors the deprotonation processes $H_2F \rightleftharpoons HF^- + H^+$ and $HF^- \rightleftharpoons F^{2-} + H^+$, which occur at more acidic pH values than those observed in case of free fluorescein. Once gain this can be attributed to the stabilization of the anionic species of the indicator as a consequence of their interaction with the highly protonated forms of the macrocyclic system.

The fluorescein acid-base and UV-visible absorption characteristics are more complex than the other indicators. This prompted us to study the interaction fluorescein-receptor through potentiometric measurements in aqueous solution, performing titrations at different ratios fluorescein-receptor. The species formed and the corresponding stability constants are reported in table 3.35.

Reazione	logK
$F^{2-} + H_2L^{2+} \rightleftharpoons (H_2L)F$	10.6(5)
$F^{2-} + (H_2L)H^{3+} \rightleftharpoons (H_2L)HF^{+}$	9.2(6)
$F^{2-} + (H_2L)H_2^{4+} \rightleftharpoons (H_2L)H_2F^{2+}$	9.4(2)
$F^{2-} + (H_2L)H_3^{5+} \rightleftharpoons (H_2L)H_3F^{3+}$	9.3(2)
$F^{2-} + (H_2L)H_4^{6+} \rightleftharpoons (H_2L)H_4F^{4+}$	8.2(2)
$F^{2-} + (H_2L)H_5^{7+} \rightleftharpoons (H_2L)H_5F^{5+}$	8.1(1)
$F^{2-} + (H_2L)H_6^{8+} \rightleftharpoons (H_2L)H_6F^{6+}$	7.1(1)
$F^{2-} + (H_2L)H_7^{9+} \rightleftharpoons (H_2L)H_7F^{7+}$	6.2(1)
$HF^{-} + (H_2L)H_7^{9+} \rightleftharpoons (H_2L)H_8F^{8+}$	5.1(1)
$H_3F^{-} + (H_2L)H_7^{9+} \rightleftharpoons (H_2L)H_{10}F^{10+}$	5.4(1)
$2\ F^{2-} + (H_2L)^{2+} \rightleftharpoons (H_2L)F_2^{2-}$	19.5(1)
$2\ F^{2-} + (H_2L)H_2^{4+} \rightleftharpoons (H_2L)H_2F_2$	18.3(1)
$2\ F^{2-} + (H_4L)H_2^{6+} \rightleftharpoons (H_2L)H_2F_2^{2+}$	16.3(1)
$2\ HF^{-} + (H_4L)H_2^{6+} \rightleftharpoons (H_2L)H_2F_2^{4+}$	15.1(1)

Table 3.35 Stability constants of **L10** with F, standard deviation in parentheses. (298.1 K, 0.1 M $N(CH_3)_4Cl$).

The data in table 3.35 highlight two important aspects:

- First, the addition constants of fluorescein to the receptor are remarkably high. In fact, they are more similar to the transition metal coordination constants with a polyamine rather than to those related to the complexation of anionic species. This is indicative of a strong interaction between the macrocyclic system and the anionic species, which can be due to the formation a large number of strong hydrogen bonding interactions and charge-charge between the polyammonium groups and the indicator anionic groups, perhaps in consequence of fluorescein encapsulation within the receptor cavity. Furthermore, an inclusive coordination involves a strong substrate desolvation (which viceversa is presumably much solvated in water, considering the presence of many hydrophilic groups) and therefore a high entropic energy gain.
- Second, **L10** can form complexes with receptor/substrate stoichiometry 1:1 and 1:2. For a same charge of the receptor, the addition constants of two units F^{2-} to the receptor are about twice compared to the addition constant of a single anion F^{2-}. This is unusual, since in general the coordination of a second anionic species is

generally made difficult due to the electrostatic repulsion between the two coordinated anions. In this case it seems likely that the simultaneous coordination of two anionic species is accompanied by interaction one another, that stabilizes the complex with 1:2 stoichiometry. In other words, the receptor appears to promote formation of a dimer between two fluorescein units, probably due to their encapsulation inside the macrocyclic cavity. The potentiometric data do not allow to infer conclusions about the interactions nature, but, given the structure of the indicator, it is likely that the two units fluorescein interact with each other by π-stacking between their aromatic units.

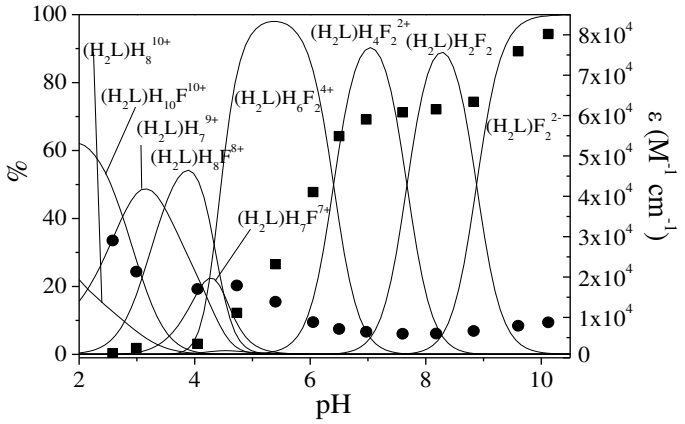

Figure 3.119 pH-dependence of the fluorescein molar extinction coefficient at 436 nm (●) and 490 nm (■), superimposed on the species distribution diagram formed in solution ([F] = $1 \cdot 10^{-5}$ M, [**L10**] = $5 \cdot 10^{-6}$ M).

It is possible to compare the species distribution diagrams obtained through potentiometric measurements with the absorbance values recorded at 436 nm and 490 nm, superimposing the values of the molar extinction coefficient measured at these wavelengths with the distribution curves calculated in the same experimental conditions. The results are shown in figure 3.119.

In general it can be observed that the molar extinction coefficient trend at 490 nm highlights as potentiometric and spectrophotometric measurements are in good agreement. The fluorescein is coordinated by the species H_2L^{2+}, $(H_4L)^{4+}$ and $(H_6L)^{6+}$ in its form completely deprotonated F^{2-}, while the molar extinction coefficient at 490 nm decrease between pH 6 and 4 implies the progressive F^{2-} protonation to give the species HF^-.

We have recorded fluorescein UV-visible absorption spectra at fixed pH in the presence increasing concentration of ligand. The experiments were carried out at pH = 5. At this pH, fluorescein is mainly in its HF^- form in absence of the receptor. The results are shown in figure 3.120.

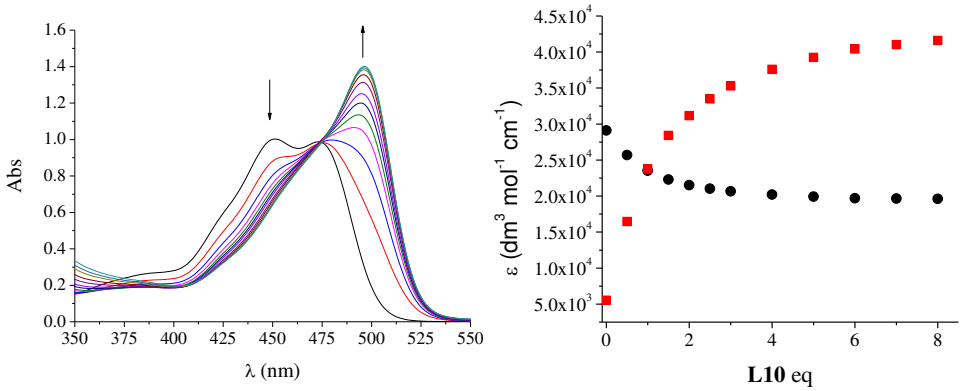

Figure 3.120 a) Fluorescein UV-visible absorption spectra in the presence of increasing ligand amounts at pH = 5 in acetate buffer. b) Fluorescein molar extinction coefficient trend in presence of ligand increasing amounts at pH = 5 in acetic buffer, 500 nm (■) and 450 nm (●). ([F]=$3.44 \cdot 10^{-5}$ M).

It can be observed that at pH 5 we note the progressive disappearance of the band at about 450 nm, typical of the species HF^- and appearance of the band at about 500 nm typical of the form F^{2-}. In other words, the addition of the receptor changes the spectrum from the typical form of the species HF^- to that of F^{2-}. This indicates that at pH=5 coordination also involves the HF^- deprotonation to form the doubly charged species F^{2-}. The fluorescein coordination by the receptor in its forms with higher protonation degree favors formation of the the dianionic species, capable of giving stronger electrostatic and hydrogen bonding interactions with the polyammonium receptor. These spectral changes are also observable at naked eye, with a gradual color change upon ligand addition to the solution buffered at pH 5 or 5.7, from yellow to orange (figure 3.121).

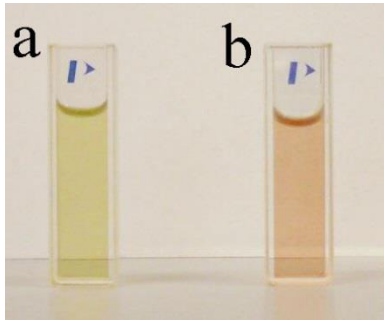

Figure 3.121 a) Free fluorescein at pH 5. **b)** fluorescein with 1 equivalent of **L10** at pH 5.

3.3.3 "Indicator displacement" technique for the anionic analytes detection

As already seen (point 1.4), is indicated with the term "chemosensor" a molecule capable of operating a molecular recognition on a specific substrate and to signal the coordination event through the change of a physical quantity. Among the various chemosensors types, colorimetric ones are of particular interest because

they allow the quantitative determination of the substrate coordinated through simple colorimeters, without the use of expensive equipment. In some cases it is also possible to appreciate qualitatively the presence of a particular analyte to the naked eye. To have a good colorimetric chemosensor two conditions are required:

- Appreciable variation in color upon the substrate coordination;
- Selectivity in the coordination of a target substrate.

The complexes formed by the xylyl-tetracyclam with different indicators can be promising as chemosensors of anionic species. In fact, the interaction of these preformed complexes with anionic analytes can lead to the indicator "displacement' from the the complex, with a consequent optical effect due to the indicator original color restoration at a given pH. Obviously, this is possible only in the presence of anionic species capable of interacting with the polyammonium receptor more strongly compared to the indicator, i.e. capable of forming complexes more stable than those formed by the indicator itself. Given the characteristics of our receptor, which has a large dimensions cavity and a high charge already at neutral pH, it is logical to expect that the indicator "displacement" takes place upon coordination of anions with high charge and large dimension. In particular, we looked at two substrates types: inorganic phosphates (mono-, di- and triphosphate) and nucleotide (ATP).

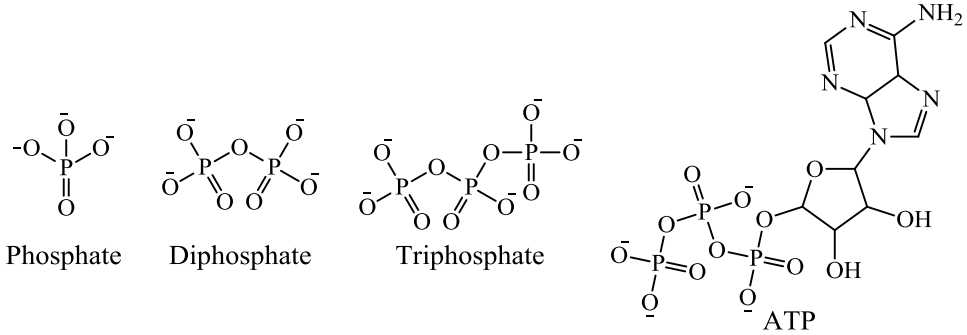

Figure 3.122 Anionic substrates studied.

The purpose of this preliminary study has been the assessment of the possible use of the technique of "indicator displacement" for the development of a new analytic device for the anionic species optical determination. For this purpose, we simply added increasing amounts of anions to solutions containing the complex between the receptor and substrate with 1:2stoichiometry, at the same values of pH use in the previously described experiments. Addition of phosphate anions to solutions of the complexes with phenol red at pH 7.5 and with phenolphthalein at pH 10 did not lead to change in the UV-visible spectra, as shown in figures 3.123 for the case of the phenol red complex in the presence of triphosphate.

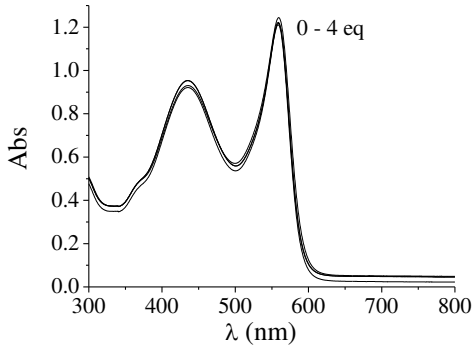

Figure 3.123 a) UV-visible absorption spectra of the complex between **L10** and phenol red in the presence of triphosphate increasing amounts at pH = 7.5. ([PR]= $4.97 \cdot 10^{-5}$ M).

Most likely, the complexes formed by these indicators are more stable than those complex from inorganic phosphates and ATP. The addition of these anionic substrates therefore do not lead to displacement of the indicators, which are tightly bound by the receptor.

On the contrary, the addition of triphosphate and ATP in a solution containing the complex with bromocresol purple at pH 5.5 leads to a net color change, while the addition of phosphate and diphosphate gives no colorimetric effect. We added increasing amounts of the anionic substrates used to a solution of the preformed 1:2 complex between **L10** and BCP and then we evaluated the spectral characteristics variation of the BCP/**L10** complex upon the additions of each anionic species, in order to verify if the anions under investigation are capable of replacing the coordinated indicator. In such a case, in fact, the bromocresol purple is replaced by the phosphate anion in its complex with the receptor, thus restoring the original spectrum of the free indicator. All the spectra were recorded at pH = 5.5. In fact, at this pH, there is the most marked difference between the absorption spectra of the free and complexed substrate. The spectra obtained upon addition of the anionic species triphosphate and ATP to a solution of the complex with BCP are given below (figures 3.127 to 3.128), together with the molar extinction coefficient change at 432 nm and 600 nm as function of equivalents added to the ligand solution.

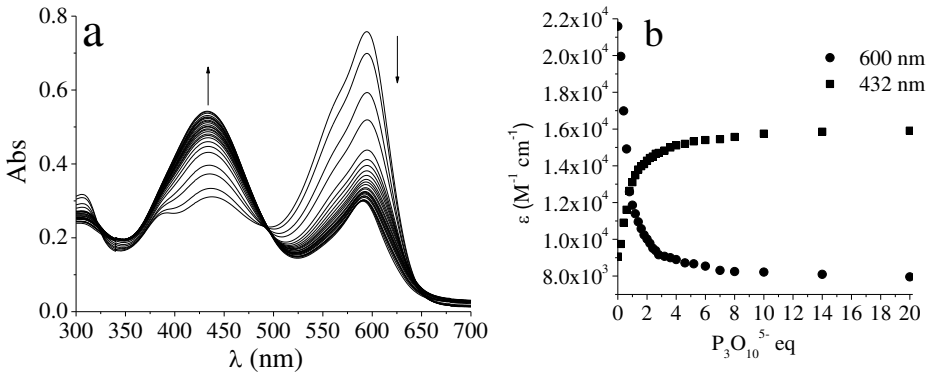

Figure 3.124 a) Complex between **L10** and BCP UV-visible absorption spectra obtained following the addition of $P_3O_{10}^{5-}$ increasing amounts to pH = 5.5. **b)** Complex between **L10** and BCP molar extinction coefficient at 600 nm (●) and 432 nm (■) obtained following the addition of $P_3O_{10}^{5-}$ increasing amounts to pH = 5.5. [BCP]= $3.41 \cdot 10^{-5}$ M.

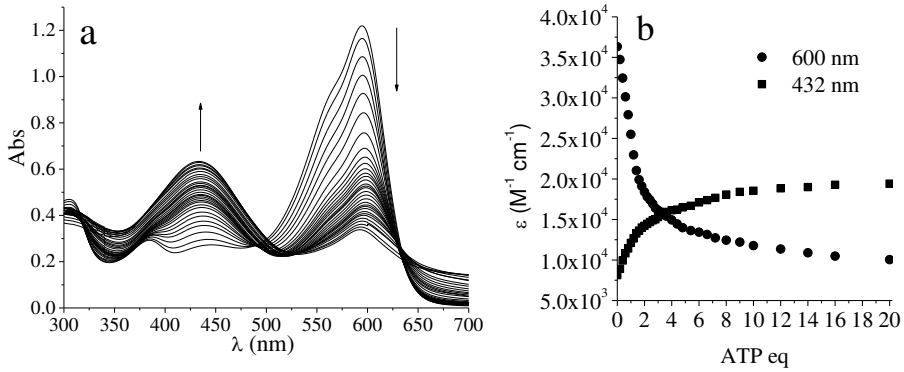

Figure 3.125 a) Complex between **L10** and BCP UV-visible absorption spectra obtained following the addition of ATP increasing amounts to pH = 5.5. **b)** Complex between **L10** and BCP molar extinction coefficient at 600 nm (blue) and 432 nm (red) obtained following the addition of ATP increasing amounts to pH = 5.5. [BCP]= $3.26 \cdot 10^{-5}$ M.

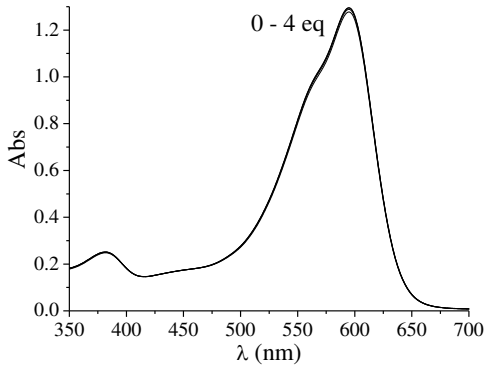

Figure 3.126 a) Complex between **L10** and BCP UV-visible absorption spectra obtained following the addition of PO_4^{2-} increasing amounts to pH = 5.5. [BCP]= $3.24 \cdot 10^{-5}$ M.

It is evident how the anionic species ATP (present in aqueous solution at pH 5.5 in its trianionic form $HATP^{3-}$ containing the terminal phosphate group of the triphosphoric chain protonated) and triphosphate (present at pH 5.5 in its form trianionic, $H_2P_3O_{10}^{3-}$) are able to "displace" the indicator from the macrocycle cavity, restoring the original BCP yellow at this pH. The data shown indicate also as this shift is almost complete after the addition of 2-3 equivalents of substrate in the case of triphosphate and ATP. Mono- and diphosphate (present in solution at this pH as a mixture of HPO_4^{2-} and $H_2PO_4^-$ the first, and as the second $H_2P_2O_7^{2-}$) fail instead to move the indicator.

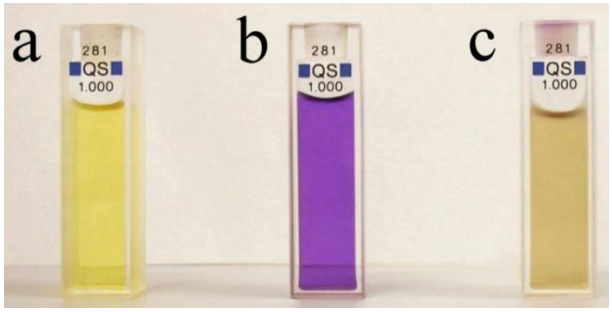

Figure 3.127 a) Free BCP pH 5.5 b) BCP+**L10** pH 5.5 c) BCP+**L10**+P_3O_{10} pH 5.5

Although this is a purely qualitative assessment, it is evident that more charged anions are more efficient in replacing the indicator from its interaction with the polyammonium receptor, as is to be expected considering that the interaction receptor-substrate interactions is mainly due to charges charge and via hydrogen bonding.

Other investigated anions do not alter the color of the solution, as we can see from the figures 3.128.

Figure 3.128 Color change of the solution of **L10** in the presence of two equivalents of BCP and five equivalents of the various investigated anions.

4 Conclusion

Two main approaches can be exploited for anion recognition and fluorescence sensing in aqueous solution, which differ in the receptor unit used. In the first approach, polyammonium cations recognize the anionic species mainly *via* charge-charge and hydrogen bonding interactions. Alternatively, metal complexes can be used as receptors. In this case, the metal acts as anchoring point for the anion and therefore, it should feature a coordination sphere not saturated by the ligand donors. In this context, we have developed new polyamine ligands capable to form highly charged polyammonium cations in aqueous solution and/or complexes with transition metal cations. To this purpose, in the course of my first year of my Ph.D. in Chemical Sciences, I have synthesized new polyamine-based ligands containing one or two fluorogenic unit(s) (**L1**-**L5**), with the purpose to use their metal complexes as anion receptors. These ligands are able to form stable complexes with transition metals and to selectively detect the Zn(II) ion.

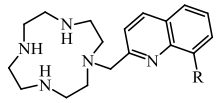

R=H, **L1**
R=OH, **L2**

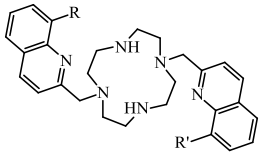

R'=OH R=H, **L3**
R=R'=OH **L4**
R=R'=H, **L5**

Nevertheless, their metal complexes showed a scarce ability in anion binding. Therefore, we developed ligands **L6** and **L7,** which contain two (**L6**) or even three (**L7**) metal binding sites (the two 1,4,7-triazacyclononane units and in the case of **L7** the terpyridine unit). Their Zn(II) complexes showed selectivity in phosphate anion binding and fluorescence sensing. In particular the Zn(II) complexes with **L6** resulted to selectively detect with triphosphate, while the corresponding complexes with **L7** recognizes and senses the diphosphate anion.

While **L6** and **L7** display separated binding sites for metal cations, **L8** contains an unique macrocyclic cavity where two metals can be lodged at short distance. In this case we analyzed not only their binding ability for inorganic anions but also for nucleosides and dinucleotides. In particular, the dizinc complex with **L8** is able to detect uracil-containing substrates, which are bound by the metal centers *via* the imide nitrogen. The signal, in this case, is constituted by an exciplex emission, due to the formation of a complex in

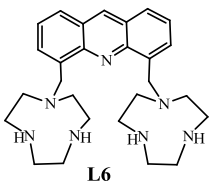

L6

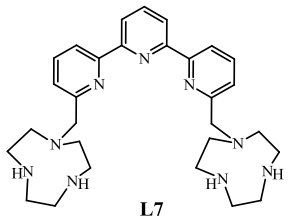

L7

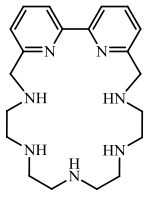

L8

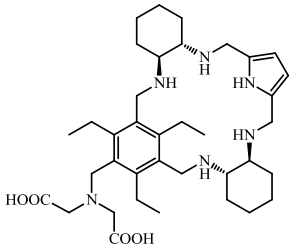

H_2L9

the excited state where the two metal-bound uracil units and the dipyridine fluorophore interact one another.

Ligand **H_2L9** represents a further development to this approach. In fact, this receptor is composed by an iminodiacetic (IDA) fragment, as a Zn(II) binding site, and a polyamine macrocyclic portion containing two trans-1,2-diaminocyclohexane (DAC) units as proton binding sites. Therefore, **H_2L9** forms stable protonated Zn(II) complexes where the metal ion and the ammonium groups cooperatively work in anion binding. Among inorganic anions, this metal base receptor result selective for triphosphate.

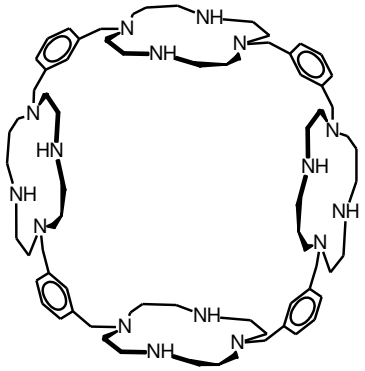

L10

Beside fluorescence sensing, colorimetric recognition represents an attractive method for anion sensing. However, the absorption spectra of chromogenic units are often scarcely influenced by anion coordination. To overcome this limit, we can use the indicator displacement approach, consisting in the use of an indicator, normally a pH-indicator, whose colour changes upon coordination by the receptor. Addition of a targeted anion to the indicator-receptor complex may result in the displacement of the indicator from the complex and to the consequent restoration of the original colour of the indicator. This approach was used in the case of ligand **L10**, which resulted to strongly bind different pH-indicators as phenolphthalein (**PP**), bromocresol purple (**BCP**), phenol red (**PR**) and fluorescein (**F**), whose colour is strongly affected by coordination. The most interesting finding was selective signalling of triphosphate the **L10** complex with **BCP**. In fact, among inorganic anions, only triphosphate was able to replace **BCP** in its complex with **L10**.